The biological basis for Sculptra®-induced augmentation

Dissertation

Presented to the department of Human Sciences, University of Osnabrück

in partial fulfillment of the requirements for the degree of

"*Doctor Rerum Naturalium*"

Philipp Stein

born in Münster

Osnabrück

August 2014

Summary

The dermal filler Sculptra® has been employed to treat facial volume loss and age-related wrinkles in Europe since 1999. Sculptra® injections were administered 87,946 times (increase of 25.7% to 2012) in the USA in 2013. Except for histological analysis and clinical reports, data based on molecular biology or biochemistry, enlightening the mechanisms of action, do not exist to date. In contrast, such data are available for cross-linked hyaluronic acid, which is also administered for facial augmentation. To overcome this gap of knowledge, a comprehensive study about macroscopic to microscopic events occurring after Sculptra® injections was conducted.

The augmentation of facial tissue with Sculptra® is approved; however, as the required repetitive biopsies could not be taken from the face, Sculptra® was injected to the inner side of the upper arms of 21 volunteers. Furthermore, this "off label use" was documented: The effect of the injections on the volunteer's subjective quality of life was investigated using a questionnaire. For objective evaluation, the upper arms were photographed and sonographic measurements were applied.

Photos of the treated upper arms revealed no changes in their shape during the study course. The amount of Sculptra® administered was not sufficient to augment the upper arms of postmenopausal women. Furthermore, these applied Sculptra® treatments of the upper arm did not improve the volunteers' quality of life significantly. Upon sonographic measurement, however, a highly significant decrease in echogenicity was retrieved by comparing baseline subepidermal tissue values (t0) with 20 month (t2) values from either arm. Upon comparison of both treated sides, echogenicity was comparable; therefore 22 MHz sonography is an objective non-invasive measure to document the subcutaneous effect of Sculptra®.

Immunofluorescence staining of sections from biopsies characterised the cell infiltrate and collagen type. $CD68^+$ macrophages were found in direct proximity to PLLA, $CD90^+$ fibroblasts aligned adjacently, while αSMA positive structures indicated myofibroblasts and neovascularisation. Substantial collagen type III deposition was detected right next to PLLA particles and collagen type I in the periphery of a given PLLA encapsulation. mRNA expression was strongly up-regulated for collagen type I and III transcripts, as well as for TGFß1 and TIMP1. PLLA particles were still retrievable 28 months after subcutaneous application.

The augmenting effect of Sculptra® is generated by a complex reaction, comprised of various cells, chemokines and cytokines, leading to the proliferation of fibroblasts and their differentiation into myofibroblasts, synthesising a substantial amount of collagen in order to restore subcutaneous volume deficiencies. Degradation of facial and extra facial PLLA particles is considerably slower than described previously. The augmenting effect of Sculptra® diminishes over a period of 18-20 months in the face, but the degradation of PLLA particles seems to be much slower. Whether Sculptra® stimulates the synthesis of other ECM components, such as HA, or rationalises a continuous stimulus for collagen production, at least as long as it is not synthesised, should be analysed in further studies.

Index

1. Introduction

1.1 Anatomy and physiology of human skin

As a separating layer between the body and its environment, the skin protects against external influences. The skin's architecture, composed of the epidermis, dermis and subcutaneous tissue, provides the prerequisites for this interaction [1].

Epidermis

The epidermis is composed of cells, their desmosomal connections and an intercellular lipid seal, providing a protective barrier against pathogens, chemicals, allergens, radiation and excessive evaporation.

The epidermis is a multi-layered, keratinised squamous epithelium, derived from the ectoderm. The dominant epidermal cell type is keratinocytes (90-95%) producing keratin and lipids. The epidermis is subdivided into four further layers, named by the phenotype of the differentiating keratinocyte. The most proximal layer is monocellular (*stratum basale*). Proliferating keratinocytes migrate through different differentiation states to the uppermost layer, where they finally shed. Basal keratinocytes are characterised by poor cytoplasm and mitotically active nuclei. After division, keratinocytes differentiate into synthetically more active, cytoplasm-enriched cells, forming the *stratum spinosum.* Upon formaldehyde fixation for histological examination, desmosomal connections to adjacent cells are visible and give that layer its name. The most differentiated keratinocyte, with highest synthetic activity and flattened nuclei, resides within the *stratum granulosum.* When keratinocytes have lost their nuclei, they are called corneocytes, justifying the *stratum corneum*.

Further cells of the epidermis are Langerhans cells, melanocytes and Merkel cells. Langerhans cells, representing 3-6% of all epidermal cells, are mobile in all epidermal layers. The dendritic Langerhans cells take up antigens and process and present them to T-cells. The dendritic melanocytes, located in the *stratum basale*, synthesise and store melanin within melanosomes. Melanocytes transfer melanosomes to surrounding keratinocytes *via* dendritic connections; one melanocyte supplies 36 keratinocytes. Melanosomes cap the nuclei of keratinocytes and protect them against DNA damaging UV light. Merkel cells are mechanoreceptors for tactile perception and are localised in the s*tratum basale*. Furthermore, the epidermis is penetrated by sweat glands as well by pilosebaceous follicles.

The epidermis and dermis are intertwined through an epidermal-dermal junction zone. Hence, the epidermis is not vascularised; the epidermal-dermal junction zone serves as a diffusion filter for nutrients and metabolic products between the epidermis and dermis.

Dermis

The dermis supports the epidermis and gives the skin its structure and resilience. This is enabled by a dense network of collagen and elastic fibres. This fibre network is embedded into an amorphous, hydrophilic matrix, creating the extracellular matrix (ECM). Furthermore, the dermis is vascularised and innervated and hosts appendages like hair follicles, sweat glands, sebaceous glands and apocrine glands. Blood vessel endothelium expresses CD31 antigens, whereas lymph vessel endothelium expresses podoplanin, allowing differential recognition by specific antibodies. Nerve cells and receptors for the sense of pain and temperature are found in the dermis as to the skin appendages belonging to sweat, sebaceous glands and hair follicles. Sweat glands serve for thermoregulation, while sebaceous glands are responsible for lubricating the skin.

The dermis is divided into a cell-enriched *stratum papillare*, possessing a fine collagen structure, and a more proximal *stratum reticulare*.

Most of the dermis is made up of a network of collagen fibres (type I 50-80%; type III 10-15% of the dermal dry weight), which provide its mechanical stability. Collagen type I and III have an estimated half-life of 15 years [2]. Additional elastic fibres (elastin 2% of dermal dry weight) enable the skin's flexibility. Elastic fibres are composed of elastin and fibrillin microfibrils. As for collagen, elastin possess a calculated half-life of many decades [3]. Elastin synthesis is predominantly confined to foetal and early postnatal development. In adults, a posttranscriptional mechanism mediates rapid decay of the elastin mRNA, which regulates the expression and maintains protein production at undetectable levels [4]. This intact fibre network, where cells may attach, is essential for dermal integrity und function [5].

The dermal ECM is composed of structural proteins as well as proteoglycans and glycosaminoglycans, which are able to bind water to a thousand-fold their own volume. Dermal hydration contributes crucially to the skin's tightness. A prominent glycosaminoglycan is hyaluronic acid (HA).

The major dermal cells are mesenchymal-derived fibroblasts, which are responsible for the ECM-turnover. Fibroblasts synthesise precursors of collagens and elastins, which are subsequently released into the ECM, where procollagen is cleaved, assembled to fibrils and cross-linked to form mature collagen bundles. Fibroblasts also synthesise enzymes, i.e. matrix metalloproteinases (MMPs), which are responsible for the degradation of these fibrous structures, balancing regeneration or healing of the tissue. MMP-1 is involved in the turnover of skin collagen. In healthy young skin, MMP-1 expression is exceedingly low, near the limit of detection [6]. Additionally fibroblasts can release tissue inhibitors of matrix metalloproteinases (TIMPs) to control MMP activity. Matrix remodelling is required for cellular migration [7].

The spindle-shaped fibroblasts can be identified by antibodies recognising CD90 (Thy-1). Fibroblasts are an extremely heterogeneous multifunctional cell population, which exhibit

functional differences depending on where they reside. Cultured dermal fibroblasts from deeper layers are morphologically larger than those of superficial layers: they proliferate slower and produce less collagenase and decorin, but more collagen. Cultured facial dermal fibroblasts exhibit lower mRNA expression and the production of TGFß1 and CTGF at the protein level. Moreover, cells from deeper layers produce more TGFß1 and αSMA compared to cells from more superficial layers [8]. Superficial dermal fibroblasts obtained from the face showed lower expression and production of ECMs than dermal fibroblasts obtained from the trunk. Facial and trunk dermal fibroblasts of superficial and deep dermis possess identical proliferative capacity, but facial dermal fibroblasts express lower fibrotic activity in mRNA and protein expression [9].

Fibroblasts in a less active state are called fibrocytes. During wound healing, fibroblasts can differentiate into myofibroblasts, which are characterised by myofilaments and the expression of alpha smooth actin (αSMA), also found in endothelial cells. This enables myofibroblasts to contract in order to close a wound. Myofibroblasts are characteristic of fibrotic tissue.

Common to the ECM of the dermis are freely moving cells of the immune system. This group of cells includes macrophages, which is detectable by antibodies against CD68; these cells recognise foreign bodies and phagocytise and degrade them, as well as mast cells, which mediate allergic and inflammatory reactions.

Subcutis

The subcutis is located beneath the dermis and is separated from the muscles through the fascia. The subcutis consists of fat (triglyceride enriched adipocytes), fixed by connective tissue septa to the dermis and to the *periosteum,* respectively, to the *aponeurosis.* The adipose tissue is subdivided into fat lobes, which consist of fat lobules. Fat lobules consist of lipid vacuoles possessing adipocytes. Between the fat lobes in the connective tissue septa, blood vessels and nerve pathways meander, trekking from there into the dermis. Special receptors, *Vater pacini* corpuscles, are distributed in the subcutis for the purpose of mediating vibration sentiency.

The lipidaceous subcutis provides energy (storage) and mechanical protection. Generally, the distribution of fat pads is gender-specific and their shape is related to the nutritional condition of a given individual. From an aesthetic point of view, the subcutis fulfils a modulating function. Aging correlates with a regression of connective tissue, loss of volume and supportive function. With age especially, the subcutaneous fat pads follow gravity.

1.2 Pathophysiology of aging

Skin aging is a complex process influenced by many different factors (Figure 1.1).

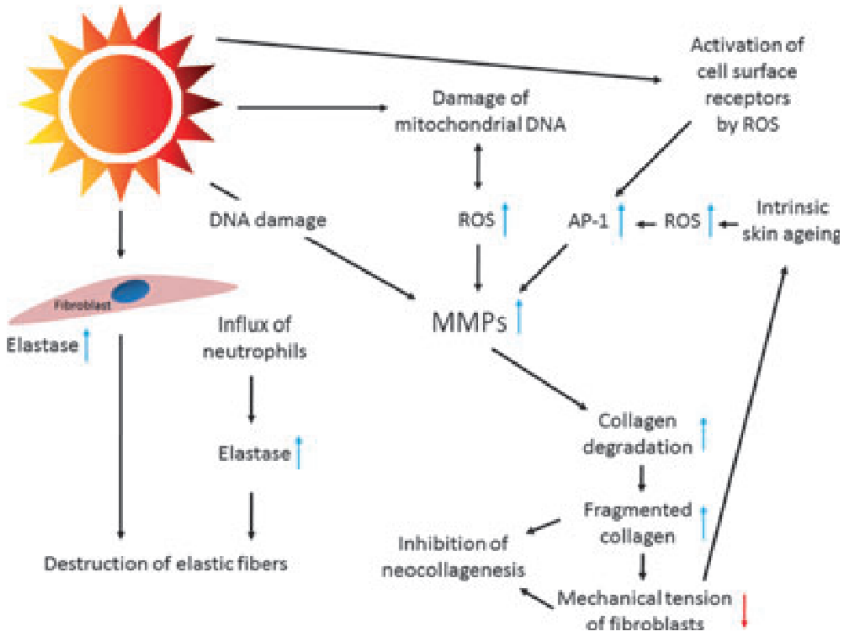

Figure 1.1 This model schematically depicts factors of pathogenic relevance for skin aging. The induction of MMP is for particular importance as they degrade collagen and other components of the ECM. Mainly UV-induced reactive oxygen species (ROS) and DNA damage lead to the increased induction of MMPs in keratinocytes and fibroblasts. Proteolytic enzymes such as elastases and MMPs derived from neutrophil granulocytes contribute to degradation of the ECM. Also, UV-exposure directly stimulates the production of elastase in fibroblasts. As a result, partially degraded collagen and reduced mechanical tension of fibroblasts inhibit neocollagenesis. Reduced mechanical tension leads to the further production of ROS, which again results in the increased expression of MMPs. Reprint of Kohl *et al.* [10].

The genetically predetermined form of skin aging is called intrinsic or endogenous skin aging [11]. Exogenous factors are superimposed on the process of intrinsic skin aging [12]. The dominating exogenous factor is UV radiation. Sun-protected skin areas reflect intrinsic skin aging and sun exposed skin areas extrinsic aged skin.

There are different explanatory approaches of intrinsic skin aging. At first, cellular senescence observed by Hayflick (1965) *in vitro* was thought to cause intrinsic skin aging [13]. Cultured cells lose their potential to proliferate and pass only through a limited number of divisions. Indicating experiments on keratinocytes [14], fibroblast [15-16] and melanocytes [17] showed an age-related reduction of cell division.

Telomeres consist of 1000-fold repetitive TTAGGG sequences and build up a 7000-12000 base pairs on the end of every human chromosome. The 3´end of DNA consists of a 100-400 base pair overhanging single strand, attached to the double strand, forming a t-loop. In combination with DNA binding proteins, this structure constitutes a complex, so-called cap, protecting the DNA, which recognises double-strand breaks. During DNA replication, DNA polymerase is not able to replicate the complete 3´ end. Therefore, a telomere shortening of

about 100 base pairs occurs per cell division [18]. Once the telomere is shortened over a critical threshold, the telomere loop can no longer form. The result is that the 3‘ overhang is exposed. The induced DNA damage results in apoptosis or senescence. Telomerase is a ribonucleoprotein enzyme with reverse transcriptase activity, extending the chromosomal end with telomere DNA sequences. Telomerase is active in germ line cells, embryo- and adult stem and cancer cells, but only in a few somatic cells. Proliferating keratinocytes reveal telomerase activity with a loss of ~25 base pairs per year. Whereas slowly proliferating fibroblasts expose no telomerase activity, proliferating fibroblasts incur a loss of ~25 base pairs per year [19]. Compared to fibroblasts of younger donors, fibroblasts of older ones show shortened telomeres [18]. However immunohistochemical staining revealed telomerase-positive fibroblasts [20]. How far these ambiguous findings about telomere shortening are relevant remain to be further investigated.

Oxidative stress has a substantial impact on skin aging and contributes to the mutation of mitochondrial DNA [21]. The respiratory chain generates reactive oxygen species (ROS) as by-products during oxidative phosphorylation and is its main endogen source [22]. If protective mechanisms fail, ROS lead to oxidative stress and pose a menace in proximity to mitochondrial DNA. Mitochondrial DNA shows a more substantial mutation rate then nuclear DNA [23]. If mitochondrial ROS leak into the cytoplasm and/or extracellular space, oxidative damage of lipids (membranes), proteins (enzymes) and nucleic acids (DNA) is the consequence [24-25]. Skin cells possess anti-oxidative mechanisms diminishing ROS. Enzymes, like superoxide dismutase, catalase, glutathione peroxidase, glutathione transferases, peroxidases and thiol-specific antioxidant enzymes, are able to convert ROS and thus prevent oxidative damage [26]. Furthermore, anti-oxidative molecules, like glutathione, vitamin A, C and E and flavonoids support protection. During the process of skin aging, the effectiveness of those protective mechanisms is diminished [27-28].

Even though oxidative phosphorylation and therefore ROS generation occurs during intrinsic as well as extrinsic skin aging, the ROS generation rate is enhanced when UV-irradiated. In particular, UVA radiation penetrates deep into the dermis. Cellular chromophores, urocanic acid, melanin precursors and riboflavin absorb UVA radiation and thereby generate ROS, which in turn leads to lipid, protein and DNA damage. Sander *et al.* (2002) found oxidative modified proteins in the upper dermis of photo-aged and acute radiated healthy skin [29]. Furthermore, these authors detected UV dose-dependent protein oxidation in keratinocytes and fibroblasts *in vitro*, supporting the *in vivo* results.

The UV-induced release of ROS activates surface receptors of keratinocytes and fibroblasts, stimulating signal transduction pathways, influencing growth, differentiation, senescence and tissue degeneration. For example, receptor activation stimulates the MAP-kinases p38, JNK (c-Jun amino-terminal kinase) and ERK (extracellular signal-regulated kinase) and expression of the transcriptional factor activator protein 1 (AP-1). AP-1 induces the up-regulation of MMPs, MMP-1 (collagenase-1), MMP-2 (gelatinase A), MMP-3 (stromelysin-1) and MMP-9 (gelatinase B) [30-31], degrading ECM proteins, like collagen type I, III, IV and

elastin. AP-1 negatively regulates the synthesis of procollagen type I [32]. Furthermore AP-1 inhibits the effect of TGFß, a cytokine promoting collagen production in fibroblasts, while AP-1 induces the expression of the intracellular signalling protein SMA7, antagonising TGFß [33]. Application of the anti-oxidant N-acetylcysteine can normalise TGFß signalling [34]. TIMP1 expression decreases in human skin and contributes to ECM degradation [35]. UV irradiation induces the activation of nuclear factor (NF)-κB transcription factor, which in turn stimulates the expression of MMPs [30]. Catalytic cleavage of collagen fibres changes the mechanical environment of cells situated within the dermis.

Through transmembranous integrin receptors, fibroblasts attach to proteins of the ECM and connect to the intracellular actin cytoskeleton. This linkage is called focal adhesion [36-37]. The tension generated by the cytoskeleton is transferred *via* integrins to the ECM. The mechanical tension between the fibroblasts and the three-dimensional structures of the ECM stretches the fibroblasts. Focal adhesions are able to activate intracellular signalling transduction cascades, thus regulating fibroblast metabolism [38-39]. Fibroblasts under tension produce more collagen and less MMP. The accumulation of fragmented collagen correlates with decreased mechanical tension on fibroblasts (Figure 1.2), which in turn collapse and produce less collagen and more MMP [6, 40].

Xia *et al.* (2013) constructed constitutive active MMP-1 fibroblast mutants and cultured them in three-dimensional collagen lattices [41]. These fibroblast mutants reflected alterations of aged fibroblasts: reduced plasma area, disassembled cytoskeleton, impaired TGFß pathway and reduced collagen production. Exactly those effects are prominent in intrinsic and extrinsic photoaged skin and enhance the above-mentioned ROS-induced degenerative processes in a self-perpetuating manner.

Upon UVB exposure, keratinocytes express cytokines stimulating fibroblasts to express elastase [42]. Low dose UVB radiation alters the quaternary structure of fibrillin-rich microfilaments and of the major adhesive glycoprotein fibronectin. Furthermore, elastic fibres are associated with proteins that are susceptible to UV radiation. The susceptibility of those proteins may be based on their chromophore-rich amino acids (Cys, His, Phe, Trp and Tyr) [43]. UVB-absorbed amino acid residues occur in glycoproteins and proteoglycans [44] and collagen, elastin and laminin fragments induce an immunological reaction [45]. Neutrophils are indeed stimulated by UV radiation to infiltrate the tissue and to release MMP-1, 8, 9 and elastase [46].

The predominant dermal proteoglycan Decorin binds to collagen type I and protects it against proteolytic degradation by MMP-1. UV radiation degrades decorin, and polymorphonuclear (PMN) cells simultaneously infiltrate. PMN cells release neutrophilic elastase, which degrades decorin to render collagen fibrils more susceptible to MMP-1 [47].

It is most likely that all of the above-mentioned degenerative damage is comparable to the process of wound healing; imperfect repair is the consequence and solar damage the result [30, 48].

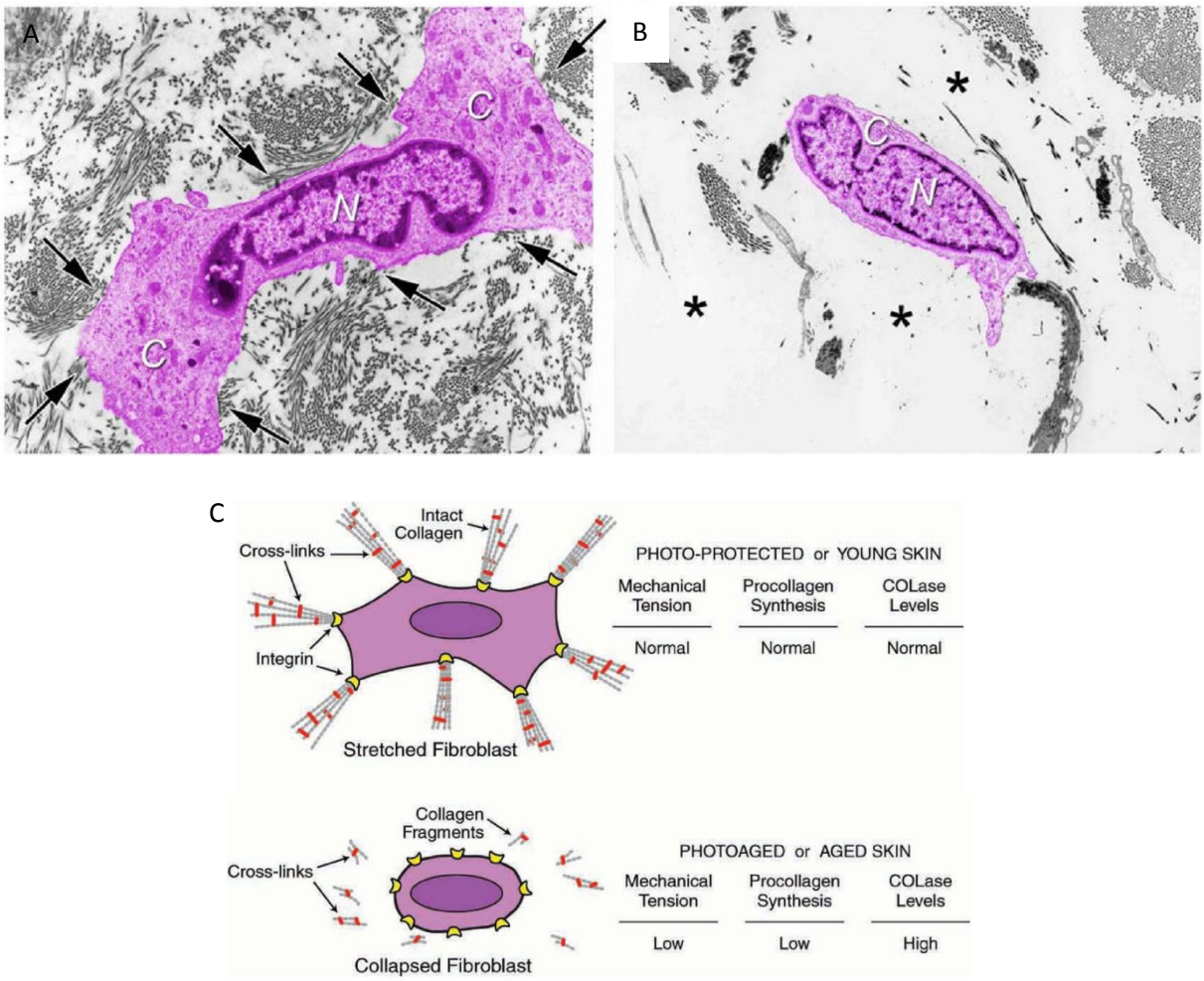

Figure 1.2 Fragmentation of collagen fibrils within dermis of aged/photoaged skin causes collapse of fibroblasts. A) Transmission electron micrograph of fibroblast (artificially coloured pink for clarity) within the dermis of young adult, sun-protected human skin. Note the elongated, stretched appearance, and extended cytoplasm (C) away from the nucleus (N) of the fibroblast, which is in close proximity to abundant collagen fibrils (arrows, original magnification x2000). B) Transmission electron micrograph of fibroblast (artificial coloured for clarity) within dermis of photodamaged human skin. Note the collapse of the cytoplasm inwards nucleus (N), and lack of adjacent collagen fibrils compared to (A). Fibroblast is surrounded by amorphous material (*). C) Model depicting relationship between mechanical tension, and collagen production and fragmentation in human skin. In sun-protected young adult human skin, intact type I collagen fibrils in the dermis provide mechanical stability and attachment sites for fibroblasts. Receptors (integrins) on the surface of fibroblasts attach to collagen (and other proteins in the dermal extracellular matrix). Cytoskeletal machinery (actin-myosin microfilaments, not shown) within fibroblasts pulls on the intact collagen matrix, which in turn offers mechanical resistance. Dynamic mechanical tension that is created promotes the assembly of intracellular scaffolding (microtubules/intermediate filaments, not shown), which pushes outward to cause fibroblast stretch. This stretch is required for fibroblasts to produce normal levels of collagen and MMPs. In photodamaged/aged human skin, attachments of fibroblasts to integrins are lost, and fragmented collagen fibrils fail to provide sufficient mechanical stability to maintain normal mechanical tension. Reduced mechanical tension causes fibroblasts to collapse, and collapsed fibroblasts produce less procollagen and more collagenases (COLase). Reduced collagen production and increased collagenase-catalysed collagen fragmentation results in the further reduction of mechanical tension, thereby causing continual loss of collagen. Reprint of Fisher *et al*. [6].

UV radiation evokes DNA mutations and UVB radiation, in particular photocarcinogenic cyclobutane pyrimidine dimers and 6,4 photoproducts. UVA radiation generates phosphodiester bond breaks in DNA. To repair DNA damage, skin cells possess different mechanisms: DNA double-strand breaks are repaired *via* the non-homologous end-joining (NHEJ) and homologous recombination (HR) pathways. Lesions on single-stranded DNA are repaired *via* nucleotide excision repair (NER) and base excision repair (BER). However, the efficiency of cellular DNA repair machinery may decline with age [49].

Aging is also accompanied by altered dermal vascularisation. The dermis of intrinsic aged skin exhibits a significant decrease in vessel size, but no change in the vascular density when compared to young skin. However, the papillary dermis of photoaged skin exhibits a significant decrease in both vessel size and vascular number [50].

1.2.1 Clinical aging

Above-mentioned, age-dependent cellular and structural alterations reflect the clinical complexity. Skin collagen fibres provide tensile strength, elastic fibres resilience and proteoglycans hydration in young skin. Intrinsic aged skin is thin, characterised by fine wrinkles, dryness and reduced elasticity. This appearance results from the degradation of the fibrous ECM components collagen type I, III, IV and elastin [51]. Furthermore, the amount of glycosaminoglycans, like HA, decreases with age. HA plays an important role in cellular adhesion, cellular motility and other biological functions, as well as binding water [52-53]. Depletion of ECM components leads to atrophy and dermal shrinkage.

The epidermis protects the skin against excessive dehydration. Intrinsic aged skin exhibits epidermal atrophy, i.e. thinning of up to 10-50% between the ages of 30-80, correlated with normal barrier function; however, barrier repair properties are diminished [11].

Extrinsic, especially photoaged skin, exhibits deep wrinkles and a more distinct loss of elasticity. The additional fragmentation of collagen type I and III and VII, rationalises the destruction of forming anchor fibrils to the DEJ [54]. Furthermore, more glycosaminoglycans and poorly functional elastin are deposited [55]. However, glycosaminoglycans co-localised in a degenerated elastin fibre network possess no hydrating properties [56]. Therefore, skin thickening, known as solar elastosis, manifests.

Besides the described epidermal and dermal alterations, the subcutaneous tissue atrophies with age. The smooth contour of a young face is based upon an elevated, finely distributed fat volume, hence the subcutaneous fat of the face is partitioned into multiple, independent anatomical compartments [57]. There are superficial and deep fat compartments, separated by septa ascending from the underlying fascia and inserting into the dermis. This framework provides a “retaining system” for the human face. Implicit in this concept is the suggestion that the face ages three-dimensionally, with separate compartments changing relative to one another by both position and volume [58]. Additional alterations in muscular structure and bone resorption add to the appearance of the aging face [59-60]. All of this contributes to the appearance of folds and changes the facial contour.

While studies on facial aging and methods to intervene are numerous, only a few on the integumental aging processes are retrievable from the literature. Recently, there has been some interest on the aging hand, neck and décolleté being noticeable. However, especially in postmenopausal women, the upper arm changes rapidly. This aging process will eventually lead to a change in clothing habits and quality of life. In summary, the aesthetic aspect of the female upper arm is influenced by three genetically determined factors: 1. Disposition to being overweight, 2. Lipoedema, and 3. fat cell hyperplasia expressed in a dysmorphic upper arm. In particular, the inactivity atrophy of arm and shoulder girdle musculature and atrophy of *facia brachialis* and lateral positioned *retinacula cutis* are responsible for sagging of the upper arm. Furthermore, the atrophy of triceptical fat body contributes to the arm deformity [61].

1.3 Augmentation for clinical rejuvenation

Age-related atrophy of subcutaneous fat correlates with a decline of facial volume and an altered facial contour. To counteract this volume loss, dermal fillers are applied. However, the application of dermal fillers can be accompanied by adverse reactions [62].

Currently, these dermal fillers are divided into “resorbable” and “permanent”. Facial fat loss can be compensated by autologous fat injections. The utilisation of autologous fat is reasonable, if simultaneous liposuction is requested [63]. Otherwise the procedure for tissue harvest and implantation is laborious and the longevity of a fat transplantation is controversial. Thus this method, when compared to minimally invasive injectable fillers, seems to have gone out of fashion [64]. Minimally invasive treatments are cost efficient and considerably more pleasant, and are accompanied by a minimal down-time.

Currently, the most frequently used filler is cross-linked HA. In the USA, 1,872,172 procedures were performed in 2013 (Cosmetic Surgery National Data Bank 2013). Cross-linked HA is principally extracted from a non-pathogenic bacterium *Streptococcus equi*, but may also originate from animals. Native HA is an essential component of the ECM with a high degree of water binding capacity. Molecular biological and biochemical studies have partially revealed the mechanism of action of cross-linked HAs [65-66]. When cross-linked HA, compared to physiological saline solution, is injected into the skin of 70 year-old individuals, stretched, proliferating fibroblasts with enhanced collagen type I expression evolve in the micro environment of cross-linked HA. Further, proliferation of endothelial cells and keratinocytes is enhanced, reflecting an increase in epidermal thickness. Stretching of fibroblasts seems to depend on the interaction between these cells and their environment. Stretched fibroblasts are stimulated to synthesise appropriate amounts of collagen and fewer MMPs.

Hence, collagen is the main dermal component; it is also applied as dermal filler. Bovine collagen and human collagen, derived from human fibroblast cell lines, have previously been employed. Prior to the application of bovine collagen, hypersensitivity needs to be checked. First generation injectable collagens were quickly degraded, which led to the development of glutaraldehyde cross-linked collagens, with longer durability. Further, a porcine-derived

collagen-based filler has been employed [64], which is cross-linked by ribose-induced glycation, mimicking the natural *in vivo* cross-links [67].

Calcium hydroxyapatite occurs in teeth and bones. It is available as a dermal filler in the form of microspheres, suspended in carboxymethylcellulose, glycerin and water [68]. In the USA, 160,926 procedures were implemented in 2013 (Cosmetic Surgery National Data Bank 2013). This slow resorbable filler may stimulate collagen neo synthesis. Most likely, calcium hydroxyapatite spheres are degraded *in vivo* compared to smaller bone fragments *via* phagotycing macrophages. Histological examination reveals calcium hydroxyapatite microspheres surrounded by foreign body giant cells and fibroelastic fibres 6 months after injection. At this time, these microspheres exhibit alterations in shape, but no migration within the tissue [69]. Drobeck *et al.* (1984) and Misiek *et al.* (1984) conducted animal tests, including subcutaneous hydroxyapatite discs and particle implantations: Drobeck *et al.* (1984) observed a few macrophages and proliferating fibroblasts within a collagen capsule [70], while Misiek *et al.* (1984) noticed mild inflammation, granulation tissue with foreign body giant cells and collagen deposition [71].

The poly-L-lactic acid (PLLA)-based product Sculptra® also belongs to the group of slow resorbable dermal fillers, and will be described in the next subchapter in detail.

One of the permanent fillers is polymethylmethacrylate microspheres (20%), suspended in 80% bovine collagen and lidocaine. Due to the presence of bovine collagen, hypersensitivity must be checked prior to application. Histological examination reveals capsules composed of collagen, fibroblasts, macrophages and foreign body giant cells around each single microsphere [72]. Those non-phagocytisable and not enzymatically degradable microspheres may maintain lifelong stimulation of collagen synthesis. The advantage of these microspheres is seen in their smooth surface, which is responsible for a low incidence of granulomatous reactions. Bovine collagen prevents clumping of microspheres and seems to maintain separation between them [73].

1.3.1 Sculptra®

Sculptra® has been used for the restoration of facial volume loss and age-related wrinkle flattening in Europe since 1999 (Figure 1.3). Initially, Sculptra® was employed to minimise facial lipoathrophy of HIV-positive patients on anti-retroviral therapy. In the USA, Sculptra® was approved for the treatment of lipoathrophy by the FDA in 2004 and subsequently for its aesthetic use in 2009. Current literature provide information referring to its augmenting effect, and discuss injection techniques and product dilutions, in order to optimise the aesthetic benefit and minimise adverse reactions [74-77].

Figure 1.3 Prae (left) and post (right) 4 Sculptra® injections into the naso-labial folds (Schürer, unpublished)

The augmenting effect of Sculptra® can last for more than 2 years [78] and late-onset nodules are possible when the immune status changes [79-80]. Besides injection-related local short-term reactions like oedema and swelling, adverse reactions like nodules could be limited by 1. Using higher dilutions, 2. Avoiding superficial injections, 3. Massaging the treated area and 4. Optimising the injection techniques.

While the employment of Sculptra® for facial treatment is approved, few publications focus on its off label use [81]. Three successful cases for rejuvenation of the dorsal hand, the intercostal space and *stria distensae* with highly diluted Sculptra® (150 mg/10 ml PLLA) have been described by Schell (2006) [82]. Furthermore Schulmann *et al.* (2008) published a case report where a chest wall deformity appeared after breast reconstruction; implanting PLLA significantly improved the aesthetic appearance (150 mg/5.5 ml PLLA) [83]. Also, 36 patients with different degrees of cutaneous flaccidity, atrophy and wrinkles in the neck and chest were treated by Mazzuco and Hexsel (2009) with PLLA (150 mg/10 ml) [84]. They reached a patient satisfaction score of 91.6% by questionnaire evaluation, while three independent evaluators attested to an improvement of 81-100% using photos of 21 patients. Significantly reduced scar size and severity of acne patients were achieved by Sculptra® (150 mg/5 ml PLLA) treatments [85].

In addition to photo-documentation, the augmenting effect of Sculptra® can be non-invasively objectified by sonography. Schelke *et al.* (2010) measured the distance between the skin's surface and bone and described an increased distance in the temple area of one individual [86]. Valantin *et al.* (2003) documented a significant increase of total cutaneous thickness during a 96 week time span in HIV positive patients with facial lipoathrophy [87].

The lyophilisate of one vial of Sculptra® comprises 150 mg poly-L-lactic acid, 90 mg sodium carboxymethylcellulose and 127.5 mg mannitol.

Poly-L-lactic acid (PLLA) is attributed to be the active ingredient. The tissue response to polylactic acid (PLA), used since the late 1960s as a surgical material, was initially examined in rodents [88-91]. They reported inflammatory reactions, infiltrating lymphocytes and macrophages forming giant cells. Furthermore, activated fibroblasts were observed. Examination with C^{14}-marked PLA showed that PLA is metabolised to CO_2 and H_2O. Additionally, PLA could be found neither in lymph nodes nor in other organs after *in situ* application.

Lemperle *et al.* (2003) examined the PLLA-injected human forearm tissue of one individual [92]. Histological examination revealed fine capsules surrounding the PLLA-based microspheres, as well as macrophages and lymphocytes three months after implantation. Six months after implantation, the porous surface of PLLA microspheres was surrounded by macrophages and giant cells and the degradation of PLLA was completed in month nine. A nasolabial tissue biopsy of a 55 year-old woman, taken 12 months after the last Sculptra® treatment, revealed aggregation of giant cells, histiocytes and collagen fibres. Repeated biopsies after 30 months of implantation showed PLLA-free and collagen-enriched tissue [93]. These authors concluded a progressive dissolution of PLLA-microparticles and an association with a gradual ingrowth of type I collagen. Goldberg *et al.* (2013) analysed picro Sirius red-stained PLLA-treated tissue sections by digital microscopy and quantitatively assessed collagen I and III: compared to baseline, the mean level of type I collagen - and not type III collagen – increased significantly [94].

In summary, the augmenting effect seems to be achieved by capsule formation as a tissue response to foreign biomaterial [95-98].

1.4 Foreign body reaction

The foreign body reaction (FBR) is an innate host response to protect the tissue from foreign incorporated, potentially toxic material by forming a delimitative impermeable tissue capsule. Incorporated foreign material evokes a complex, dynamic inflammatory and wound healing response including cell infiltration, i.e. macrophages and fibroblasts orchestrated by cell signalling mechanisms *via* chemokines and cytokines, eventually resulting in FBR.

The cascade of the host response is initialised *via* opsonisation of the foreign body surface by blood and interstitial proteins. Immune cells recognise absorbed proteins by receptors and produce cytokine and chemokines, recruiting and activating further cells (Figure 1.4).

Considering implantology, this host reaction may impair the function of implants. For example, fibrotic encapsulated blood vessel substitutes or heart valves are useless and biosensors are only able to fulfil function when the analyte reaches the sensor unimpeded. Thus, prevention or at least reduction of FBR is an object of research in biomaterial engineering. The point of vantage is the surface property of the material, because chemical and physical properties of a foreign body determine the extent of the immune reaction. Biocompatible materials, respectively biocompatible surfaces or coatings, are required. A further attempt might be the employment of nanofibre-mediated siRNA gene silencing, reducing the collagen capsule [99].

After the insertion of a foreign body, two events trigger an inflammatory response: On the one hand, the immediate, above-mentioned opsonisation, and on the other hand, the injury of the micro-vasculature and tissue releasing histamine by local mast cells [95]. Opsonisation is a dynamic process known as “Vroman effect” with smaller mobile proteins absorbing first and being replaced by larger, more immobile proteins with higher affinity. The combination and concentration of these adsorbed proteins, as well as their conformational changes, determine the attachment and survival of cells [100]. Host proteins absorbing to the surface of biomaterial are albumin, complement fragments, fibrinogen, fibronectin, Immunoglobulin G and vitronectin [101-103]. Fibrinogen, complement fragments and vitronectin are recognised by integrin receptors of macrophages and neutrophils [104]. In particular, fibrinogen is essential for initiating the inflammatory response [103]. Absorption and denaturation of fibrinogen leads to exposure of normally occult P1 (γ190-202) and P2 (γ377-395) epitopes, comparable to fibrin after the thrombin-mediated conversion of fibrinogen. Macrophages recognise those epitopes by Mac-1 (Macrophage-1 antigen), adhere and become activated [105].

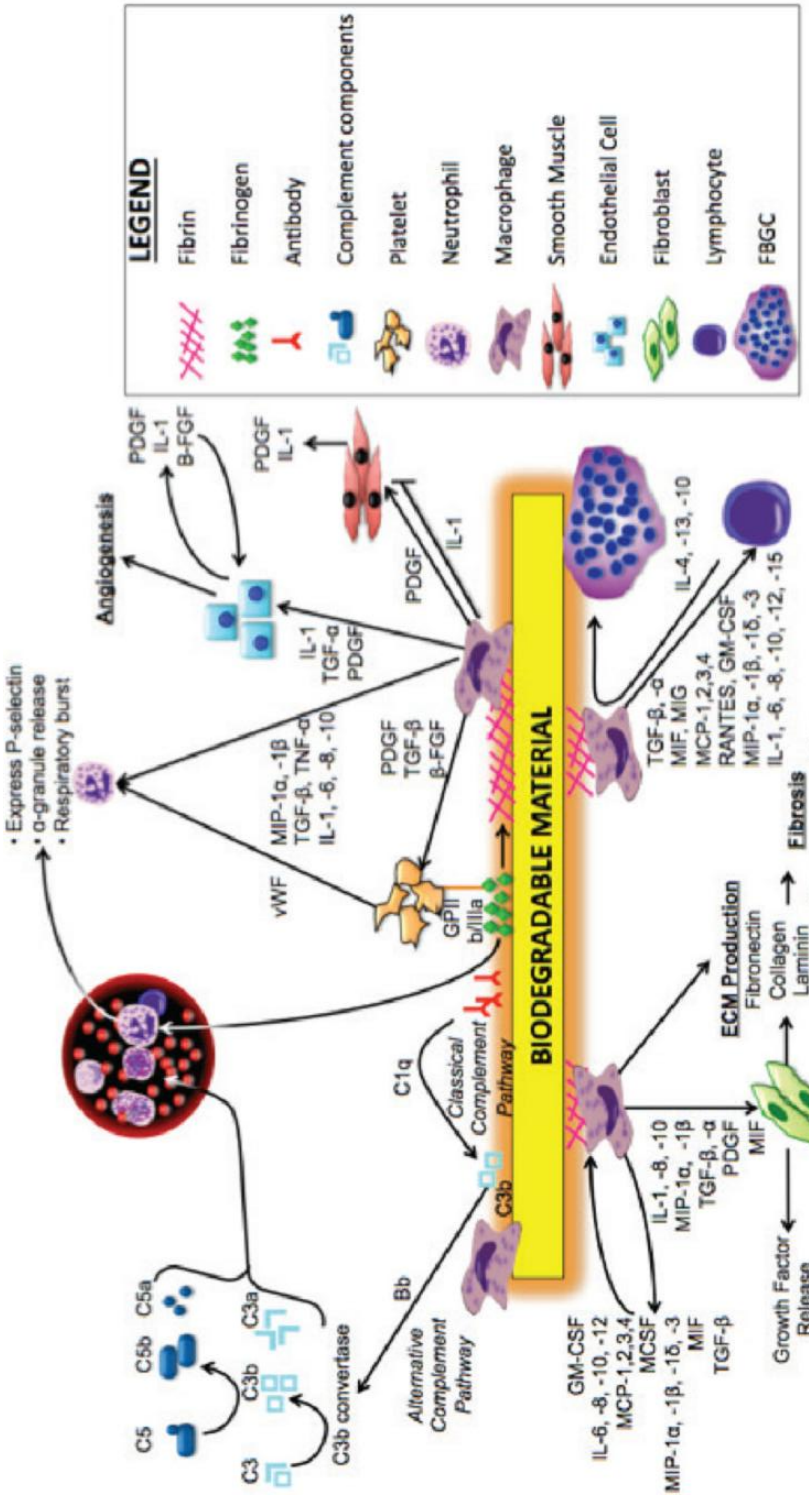

Figure 1.4 "Schematic illustration of biodegradable material-induced inflammation." Consecutive steps occurring after the implantation of biodegradable material. Reprint of Amini *et al.* [95].

Parallel to opsonisation, mast cell degranulation mediates the inflammatory response. When H1 and H2 histamine receptors are inhibited, the recruitment of macrophages/monocytes and neutrophils is significantly reduced (80%) [106-107]. This underlines the importance of histamine and pro-inflammatory cytokines, like IL-1ß and TNFα, to activate neutrophils as well as endothelial cells, expressing vascular cell adhesion molecule (VCAM)-1, intercellular adhesion molecule (ICAM)-1 and E-selectin [108-109]. These adhesion molecules enable neutrophils and other leukocytes to extravasate into the blood stream. Leukocytes are guided by a gradient of chemokines to the foreign material. Neutrophils granulate by releasing further inflammatory factors and additionally producing vascular endothelial growth factor (VEGF). Histamine [110] and VEGF are initiators and stimulators of angiogenesis [111-113].

Extravasated platelets release further chemoattractants like transforming growth factor (TGF-ß) and platelet-derived growth factor (PDGF). *Via* diapedesis, enabled by histamine release and the versatile chemokine gradient of TGF-ß, PDGF, leukotriene (LTB4), interleukin (IL-1), IL-6 generated by aforementioned cells, monocytes and macrophages are attracted to the foreign body, replacing neutrophils.

Upon receptor-mediated adhesion to host proteins, monocytes/macrophages by themselves release chemokines like PDGF, tumour necrosis factor (TNFα), IL6, granulocyte-colony stimulating factor (G-CSF), granulocyte macrophage colony stimulating factor (GM-CSF) [114], and monocyte chemotactic protein (MCP-1) [115], attracting more monocytes/macrophages. Macrophages are further attracted by RANTES**,** macrophage inflammatory protein, MIP-1α, MIP-1ß, MCP-2, MCP-3 and MCP-4 [116].

In general, the responsiveness of cells to chemokines seems to be different from subpopulation to subpopulation. Weber *et al.* (2000) examined monocyte subpopulations $CD14^{+}CD16^{+}$ and $CD14^{++}$ and found that CCR2 is virtually not expressed on the $CD14^{+}CD16^{+}$ surface [117]. This would impair transendothelial chemotaxis and MCP-1-induced up-regulation of CD11b. On the other hand, $CD14^{+}CD16^{+}$ is expressed more than CCR5 and is thus more responsive to MIP-1α then $CD14^{++}$.

Leucocytes adsorb *via* different receptors to opsonised host proteins, covering foreign body surfaces. Several receptor families with overlapping ligand distribution have been revealed. There are families of integrins, FC receptors, toll-like receptors, and scavenger receptors [118]. Hence, integrin- and FC-receptors bind to host proteins and play the primary role in FBR, while toll-like- and scavenger-receptors play the secondary role. However, direct binding ability of toll-like receptor and scavenger receptors to charged materials have been described [119-120], while they may play a minor part in FBR.

Integrin receptors enable the cell to migrate through the ECM and interact through signal transduction with the environment [121]. Monocytes and macrophages express integrins with three different types of ß-chains in order to bind fibrinogen, fibronectin, ICAMs, complement fragments and vitronectin, leading to measuring (monocytes) and activation of

cytokine production, enabling phagocytosis, mobility or just survival [104]. Luttikhuizen *et al.* (2006) precisely described the complement receptors CR1, CR3 and CR4, binding to complement fragments and belonging to the family of integrins, expressed by macrophages [98]. CR1 recognises C3b, C4b and Cbi and is involved in particle binding. CR3 and CR4 bind to C3bi and facilitate phagocytosis.

Integrin binding induces a rearrangement of the cell's cytoskeleton and the formation of podosome-like adhesion structure adhesion structures [122]. This enables macrophages to engulf the surface of the foreign body.

FC receptors, FcγRI, FcγRII and FcγRIII-detected particles, which are opsonised with IgG and complement fragments, stimulate phagocytes in order to release pro-inflammatory cytokines like IL-1, Il-6 and TNFα [98].

Macrophages are specialised phagocytes, maturing from monocytes, originating from myeloid progenitor cells in the bone marrow. Myeloid progenitor cells develop into monoblasts, pro-monocytes and eventually into monocytes, which are released into the blood stream. When initiated, monocytes migrate into the tissue, mature under the influence of macrophage colony-stimulating factor (M-CSF), granulocyte macrophage colony-stimulating factor (GM-CSF) and interleukin 3 (IL-3) to macrophages [123]. Macrophages phagocytise cell debris arising during tissue remodelling and cells undergone by apoptosis. Further, macrophages try to phagocyte entities, process them intracellularly, or, if this fails, to engulf and process them extracellularly.

Besides their classification referring to surface receptor expression, macrophages are classified with respect to their activation (Figure 1.5). Classically activated macrophages (M1) are activated by microbial components like lipopolysaccharides (LPS) *via* toll-like receptor 4 [124] or Th1 cytokine interferon-γ (IFN-γ). These macrophages try to phagocytise pathogens and to destroy them due to the secretion of reactive nitrogen- (NO, $ONOO^-$) and oxygen-species (H_2O_2, O_2^-) [125-126]. Furthermore, they secrete pro-inflammatory cytokines like TNFα, IL-1, IL-6, IL-12 and IL-23 and initiate thereby a Th1-response.

M1 is faced by a more heterogeneous group of immune-modulating and tissue-remodelling M2 macrophages, recently divided into three subpopulations (M2a, M2b, and M2c) [127]. The current literature reveals an inconsistent nomenclature concerning the term "alternative activated macrophages", standing on the one hand for all M2 macrophages, and on the other hand only for the M2a macrophage subpopulation [128].

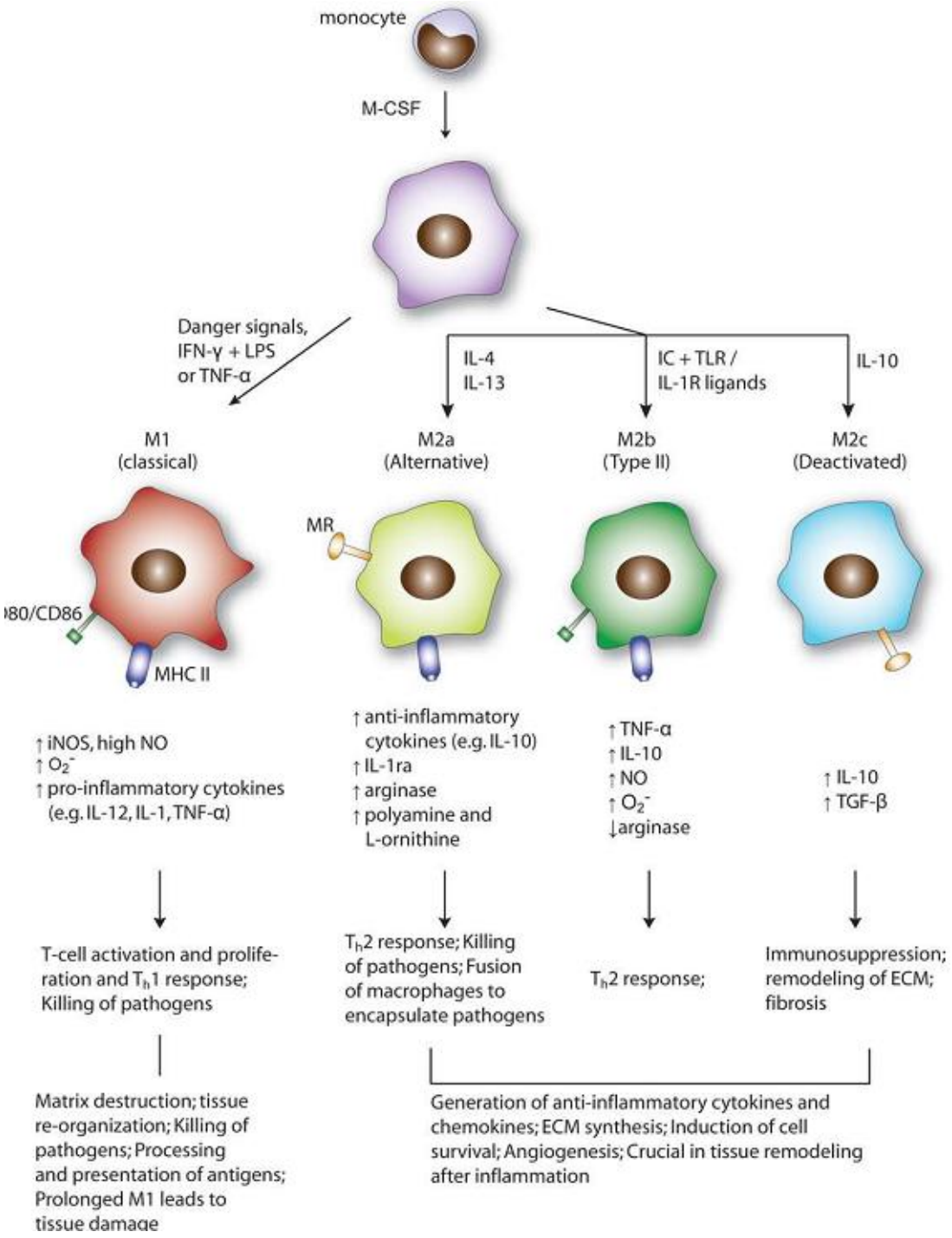

Figure 1.5 An illustration of different subsets of macrophages, their inducers, phenotype, and functions. The plasticity of macrophages allows them to polarise into populations with different phenotypes and functions in response to stimuli. Macrophages can be differentiated from monocytes in the presence of M-CSF. Upon stimulation of danger signals, IFN-γ+LPS or TNF-α, macrophages can acquire the M1 phenotype, which is associated with high microbicidal and anti-tumour activity, the production of pro-inflammatory cytokines and activation of Th1 responses. Macrophages can also be alternatively activated into various M2 phenotypes, including M2a, M2b, and M2c. M2a (induced by Il-4 and IL-13) and M2b (induced by immune complex +TLR or IL-1R ligands) secrete higher amounts of IL-10 but reduced IL-12 and are associated with Th2 responses. M2c (induced by IL-10) produce elevated levels of IL-10 and TGFß and is associated with immune suppression and tissue remodelling. These activation states of macrophages are hypothetical ends of the spectrum of the macrophage phenotype with the actual macrophage phenotype viewed as within a continuum of functional sates. Reprint of Kou and Babensee [129].

M1 macrophages express higher amounts of IL-12, IL-23 and less IL-10, underlining Th1 relation. M2 express lower amounts of IL-12 and Il-23, but higher amounts of anti-inflammatory IL-10 [127]. M1 macrophages up-regulate inducible nitric oxide synthase, catabolising L-arginine to nitric oxide and citrulline; this is in contrast to M2 macrophages, except M2b, which induce arginase 1 converting L-arginine to ornithine a precursor of polyamines and prolines necessary for collagen synthesis [130].

M2a, alternative activated macrophages, are stimulated by Th2 cytokines IL-4 and IL-13. M2a produce lower levels of NO due to higher arginase activity. Mannose receptor expression is up regulated by IL-4 [131]. M2b are induced to bind to immune complexes. In common with M1, they initially show strong NO production, and consequently a lower arginase activity, followed by the expression of pro-inflammatory cytokines like TNFα, IL-1, IL-6. In contrast to M1, M2b produce IL-10, effecting Th2, whereas M1 produce IL-12, effecting TH1. M2c are induced by IL-10 and produce higher level IL-10 and TGFß [127].

Macrophages cannot strictly be divided into categories, because there are fluent transitions between their subtypes. Macrophages possess plasticity and can switch between classically activated and alternatively activated variants. There seems to be a progress in plasticity. First, classical activated macrophages clear pathogens and destroy ECM *via* MMP, collagenase, elastase and hyraluronidase release, to reach the place of action in time. Subsequently, they switch in response to cytokines to the alternative modus to contribute to tissue remodelling.

Macrophages are key cells in the FBR. If the foreign body is too large or not conventional phagocytisable, single macrophages fuse to foreign body giant cells (FBGC), also called multinucleated giant cells. This process is also known as “frustrated phagocytosis”. Fusion of FBGC is initiated by IL-4 and/or IL-13 [132-134]. Furthermore, vitronectin and the expression of mannose receptors support fusion [135-136] and IL-4 and IL-13 enhance the expression of mannose receptors [134]. Further receptors, such as $P2X_7$ and DC-STAMP, seem to be essential for fusion. Macrophage clones, displaying elevated $P2X_7$ expression, were able to fuse in contrast to clones with low $P2X_7$ expression *in vitro*. Moreover, a $P2X_7$ blocker inhibited fusion [137]. Fusion of FBGC in DC-STAMP-deficient mice was abrogated [138]. Further receptors like MFR and CD47 might also participate in fusion [139-141]. CLL2 is involved in FBGC-fusion; hence, it is reduced in CCL2-null mice as well as upon CCL2-antibody and/or CCL2-inhibitor application *in vitro* [142]. Furthermore, the surface composition of a foreign body is crucial for macrophage fusion and cytokine/chemokine expression of FBGC. Thus, the material surface is determining whether adequate host proteins are able to bind and promote fusion [143-144]. Hernandez-Pando *et al.* (2000) examined the cytokine production of murine FBGC by means of immunohistochemistry and mRNA expression analysis [145]. After the first 4 weeks, IL-1α and TNFα were abundant, but TGFß was negative. After 55-60 days, IL-1α and TNFα were barely detectable, but TGFß expression was very strong. In contrast, Luttikhuizen *et al.* (2007) reported low TGFß mRNA expression in the FBGC of rats compared to the surrounding tissue [146].

Macrophages secrete various compounds, like proteolytic active enzymes, free radicals and reactive oxygen species, with the intent to degrade the foreign material. Furthermore, they can secrete MMPs and TIMPs, influencing tissue modulation.

FBGC generate *via* the release of reactive intermediates and degrading enzymes a damaging milieu for the foreign body. Absorbable polymers, like poly-lactic acid or poly-glycolic acid primarily underlie degradation, i.e. polymer chains are broken up. Subsequently, resorption to monomers and eventually metabolism in the Krebs´ cycle follow.

Foreign body absorption takes time, alongside its fibrotic encapsulation and separation from the surrounding tissue. Granulation tissue consists of macrophages, infiltrated fibroblasts and neo-vascularisation. It is a precursor of the fibrotic capsule [96].

Macrophages and FBGC are both mediators of the FBR, communicating *via* cytokines with monocytes, neutrophils, fibroblasts, T-and B-cells and influencing those. Macrophages are involved in ECM deposition and remodelling. IL-4 activated macrophages express fibronectin mRNA and protein and ßIG-H3 (TGFß1 induced cell adhesion molecule), relevant for cell attachment in the wound healing phase. Song *et al.* (2000) employed macrophage-fibroblast co-cultures to study the effect of classically and alternatively (IL-4) activated macrophages on fibroblasts [147]. Alternatively activated macrophages enhance collagen synthesis, whereas classically activated macrophages suppress collagen synthesis. Coincidently, alternatively activated macrophages increasingly express mRNA of pro-fibrotic TGFß1 and PDGFAA and PDGFBB. In contrast, mRNA of TNFα and MMP7 was increased in classically activated macrophages. TNFα stimulates the collagenase production in fibroblasts [148-149] and reduces collagen type I production [150], leading to ECM degradation.

TGFß is the key cytokine during fibrosis and leads to fibrotic diseases in several organs, like lungs [151], kidneys [152], liver [153], and heart [154]. Encapsulation comprises chronic fibrosis and thus TGFß represents the leading actor during this tissue reaction. There are three TGFß isoforms (TGß1, ß2, ß3) that have been identified in mammals, which are secreted as inactive precursors along with TGFß binding protein in order to attach to the ECM. The activated form of TGFß is generated by proteolytic cleavage, removing TGF binding protein *via* MMP-2 and MMP-9 activity [155]. Active TGFß binds to the TGFß type III receptor, presenting in turn TGFß to the signal transducing TGFß type I and II receptors. Signal transduction is ensured by phosphorylation of Smad2 and Smad3, mediating fibrotic responses [156-157]. Li *et al.* (2007) investigated the role of TGFß in foreign body capsules (FBC) in rats at different time points [156]. mRNA and protein levels of TGFß1 was significantly increased in FBC at all of the time points compared to the control. Furthermore, immunohistochemistry of FBC revealed a high number of stained cells for phosphorylated Smad2 and presence of TGFß1 compared to the control tissue. Besides TGFß1, the connective tissue growth factor (CTGF) might be an important cytokine for FBC. Mazaheri *et al*. (2003) reported on reduced capsule formation around an implant using antisense CTGF in a rat model [158]. Moreover, according to the corporate work by Ward *et al.* (2008) and Li *et al.* (2007) [133, 156], CTGF mRNA expression in FBC is substantially higher at all of the time

points compared to control tissue. Further, IL-13 mRNA expression was increased, accompanied by an increased T-cell abundance at all of the time points [133]. Th2 cell product IL-13 is known to stimulate fibroblast-dependent collagen formation [159-160], even in a TGFß-independent manner [161].

TGFß1 and PDGF are initially secreted by platelets [162] and serve as chemoattractants for fibroblasts [163-164]. Subsequently, macrophages produce TGFß, stimulating fibroblasts to produce CTGF [165]. TGFß appeals an anti-inflammatory effect and inhibits macrophage production and secretion of chemoattractants CCL2 and CCL3, reducing the infiltration of further phagocytes [166]. PDGF, TGFß and CTGF are mitogens for fibroblasts [167]. Moreover, TGFß archives reduced the production of MMP and enhanced the production of TIMP [168]. mRNA expression of collagen and TIMP is increased by TGFß, while that of MMPs is decreased [169].

TGFß leads to an increased production of collagen type I and III, fibronectin and proteoglycans by fibroblasts and myofibroblasts [170-172]. Fibroblasts differentiate under the influence of TGFß1 into myofibroblasts, while PDGF promotes myofibroblast proliferation [173-174]. Myofibroblasts are characteristic of granulation tissue, synthesise more collagen type III than type I [175] and are featured through αSMA expression, which enables their contraction. During wound healing, they are involved in wound closure. Fibroblasts are Thy-1 positive; as soon as they are activated by TGFß, they differentiate into myofibroblasts, which are Thy-1 negative [176]. Thy-1 negative cells have a significantly higher myofibroblast gene and protein expression compared to Thy-1 positive cells. Moreover, Thy-1 negative cells show significantly greater collagen contraction compared to Thy-1 positive cells, indicating more fully differentiated myofibroblasts. Myofibroblast resist apoptosis, consequently leading to an accumulation in fibrotic tissue [177].

Fibrocytes were characterised as collagen^{+}/vimentin^{+}/CD34^{+}/bone marrow-derived circulating cells [178]. They migrate from the blood rapidly to injured tissue. *In vitro,* those fibrocytes express αSMA when activated by TGFß1 and contract collagen gels. Therefore, they exhibit two important properties of myofibroblasts and complete the population of granulation tissue [179]. Moreover, during fibrosis, further cell types, like endothelial, epithelial mesenchymal stem cells are also capable to form myofibroblast cells [180].

The following observations indicate that specific properties of a foreign body determine whether it is capsulated by collagen type I and/or Type III: von Recum *et al.* (1993) examined the capsule of silastic, hydroxyapatite and polished titanium implants by immune histochemistry [181]. For all materials, a collagen type III positive staining was found, only the capsule around polished titanium was additionally collagen type I positive and even more prominent than collagen type III. Shannon *et al.* (1997) repeated the immune staining of capsule tissue around titanium and examined further capsule tissue around stainless steel [182]. Contrary to the previous study, they found an equal amount of collagen type I and III in the capsule around the titanium implant as well as around the stainless steel implant.

Tan *et al.* (2012) examined the tissue response to titanium oxide and hydroxyapatite implants in rabbits [183]. Therein, immune histological approaches of titanium oxide and hydroxyapatite tissue capsules first revealed collagen type III, decreasing over time, which was finally replaced by collagen type I. Li *et al.* (2007) and Ward *et al.* (2008) analysed the capsule tissue around amphiphilic polyurethane covered mock biosensors: Li *et al.* (2007) reported increased mRNA expression of collagen type I in capsule tissue with the highest expression after 21 days compared to control tissue [156]. Immunofluorescence staining showed elevated collagen type I content and αSMA positive structures at day 7 and 21, indicating vasculature and myofibroblasts. During days 48-55, collagen type I staining dominated entirely and αSMA was almost non-detectable, suggesting less pronounced vasculature and fewer myofibroblasts. Immunofluorescence staining performed by Ward *et al.* (2008) revealed capsule tissue with an increased amount of collagen type I, decorin and a slightly elevated amount of fibronectin comparing to control tissue [133].

During wound healing, collagen type III is initially expressed and is later replaced by collagen type I. Higgins *et al.* (2009) investigated FBR concerning its cell surface markers and soluble mediators [184]. Therefore, they implanted nylon meshes subcutaneously into mice and analysed the tissue 2, 4 and 10 weeks after implantation by immunohistochemistry. The implant was principally surrounded by F4/80 and CD11c positive macrophages and FBGC in a first cell layer. None of the cells were CD11c positive, which is an established marker for dendritic cells. T- and B-cells ($CD3^+$; $B220^+$) were not retrieved in close proximity to the implant site, but in the periphery. IL-13, Il-4, IL-10 and TGFß were present in the tissue at all of the time points. In detail, IL-4 was found in small macrophages and FBGCs close to the implant, but not in the periphery. IL-13 was found in FBGCs and macrophages distributed throughout the wound. IL-10 was present in direct proximity to the implant in FBGCs and macrophages. TGFß-positive staining was apparent in FBGCs, macrophages, fibroblasts and throughout regions of fibrosis. Additionally, Th1-associated IL-6, TNFα, IFN-γ and MCP-1 were tested. IL-6 was retrieved at all of the analysed time points in fibroblasts and macrophages in the periphery. TNFα und IFN-γ were not detected at any time point. At least MCP-1 was expressed at every time point in macrophages and FBGCs surrounding the lesion. Klinge *et al.* (2014) characterised the inflammatory cell infiltrate of granuloma of human explanted meshes [185]. More than 80% of the cells expressed CD68, CD8, CD45R0 as well as vimentin. CD4 and desmin were expressed in 30-80% of the cells. Altogether, this indicates that the cell infiltrate of an FBR does not comprise macrophages exclusively, but rather of a variety of cells in different transitions.

In summary, current data on skin aging reveal dermal and subcutaneous structural changes. Age-related lipoatrophy is prominent. To counteract this visible loss of tissue, minimally-invasive procedures, such as the injection of augmenting material have evolved. Hence, the focus lies on its clinical effect; biochemical studies have been neglected in the long-term. Side effects, such as granulomatous reactions to dermal filler, have been described. Only recently have biochemical studies on the effect of cross-linked HA been performed in order to elucidate fibroblast physiology and the mechanism responsible for the augmenting effect. Such studies on Sculptra®, hydroxyapatite and other fillers are still missing. Hence, dermal implantation of a filler is comparable to the implantation of a foreign body; the current literature on FBR has been reflected in detail. If a study on the tissue response of Sculptra® is planned, detailed knowledge of FBR in general is required to plan the required experiments.

Here, the study was performed with human volunteers; hence, it is human tissue that is of concern. Murine studies were not considered, since Sculptra® is applied and approved for the augmentation of rhytides and volume loss in humans. However, performing human studies requires special consideration compared to murine studies. For example, volunteers have to feel that they are in good hands to agree on procedures like injections and punch biopsies. Care-taking and communication was as essential as the layout of a long-term study.

2. Study design

The present study was approved by the ethical committee of the University of Osnabrück 11th November 2009 (reference number 4/71040/06) and conducted according to the ethical principles of the declaration of Helsinki. Participating volunteers were insured.

Included were twenty-one healthy, 50-65-year-old, Fitzpatrick skin type I-III volunteers. Excluded were individuals I) with connective tissue diseases, II) on oestrogen [186], thyroid or corticosteroid therapies [187], III) consuming nicotine [188] or vast amounts of green tea [189], IV) exposed to intensive UV-radiation [189], hence these factors may influence the expression of MMPs and consequently cutaneous collagen metabolism.

Prior to the study every volunteer was instructed in oral and written form about the investigational product and risks of participating in the study. Participants could resign from the study at any time without assigning a reason. Every volunteer gave their informed consent (cf. 7.4).

The clinical course of the study was documented by photography and sonography in three-monthly visits. Volunteer's qualities of life were evaluated by a questionnaire prior to and at the end of the study phase. In total, four visits, receiving Sculptra® subcutaneous, were carried out at three monthly intervals. To ensure molecular biological and histological examinations of skin biopsies over the 20 months time phase, 21 volunteers were randomised into three groups (A, B, C). A base line punch biopsy was taken from every volunteer. Two further biopsies were taken two weeks after injections # 1 and # 4 (group A), two weeks after injection # 2 and 8 months after the last injection (group B) and two weeks after injection # 3 and 10 month after the last injection (group C) (Figure 2.1;Table 2.1). Volunteer # 9 permitted a fourth biopsy in month 38.

	2010						2011			
month	0		3		6		10		18	20
date	8-22March	29-31March	7-16 June	14-28 June	14.09-11.10	27.09-12.10	10-17January	25.01-1.02	September	November
PLLA injection	all		all		all		all			
biopsy	all	group A		group B		group C		group A	group B	group C

Figure 2.1 Time line of events

Table 2.1 Study procedure

month	0	3	6	9	12	15	18	20	38
visit	1	2	3	4	5	6	7	8	9
patient history, information, agreement	X								
questionnaire	X							X	
Photo documentation	X	X	X	X	X	X	X	X	
sonography	X	X	X	X	X	X	X	X	
biopsy group	A,B,C Group A two weeks after injection	B two weeks after injection	C two weeks after injection	A two weeks after injection			B	C	Volunteer #9
Sculptra® injection	X	X	X	X					

3. Material and Methods

3.1 Material

If not mentioned specifically, plastic ware was purchased from Sarstedt (Nümbrecht) and Eppendorf (Hamburg).

3.1.1 Chemicals

Table 3.1 Chemicals and manufacturers.

chemicals	**manufacturer**
agarose	Bioline
disodiumhydrogenphosphate	Merck
dNTP Mix	Roche
BSA, Tween 20, Triton-X 100, glycerine, calcium acetate, citric acid	Sigma-Aldrich
potassium chloride, EDTA, TRIS, sodium chloride, potassium hydrogen phosphate , sodium acetate, ethidium bromide, bromphenol blue	Serva

3.1.2 Oligonucleotides

Oligonucleotides were purchased from Eurofins MWG Operon, Ebersberg. Applied as lyophilisate primers were dissolved in H_2O to a stock dilution of 100 pmol/µl and stored at - 20°C. Primer solutions of 10 pmol/µl were used for PCR.

Table 3.2 Primers for real-time PCR.

gene	**forward primer**	**reverse primer**	**Product (bp)**
RPLP0	GCGACCTGGAAGTCCAACTA	TCCTTGGTGAACACAAAGCC	260
Col1A1	CAAAGTCTTCTGCAACATGG	TCTGCTGGTCCATGTAGG	261
Col3A1	AAGGGGAGCTGGCTACTTC	GAGTAGGAGCAGTTGGAGG	271
ACTA2	ACAATGAGCTTCGTGTTGCC	AGGTAGTCAGTGAGATCTCG	295
TGFB1	GACATCAACGGGTTCACTAC	GTCCAGGCTCCAAATGTAGG	298
TIMP1	AAAGGGTTCCAAGCCTTAGG	AGGGAAACACTGTGCATTCC	256
DN	AGCAAAGTTAGTCCTGGAGC	GCAATGCGGATGTAGGA	272
PDGFB	TGTCCAGGTGAGAAAGATCG	TGCGTGTGCTTGAATTTCCG	240
CTGF	AGTTTGAGCTTTCTGGCTGC	CATGTCTCCGTACATCTTCC	245

Coding sequences for primer design were retrieved from NCBI (http://www.ncbi.nlm.nih.gov/ nucleotide/) (10th July 2012). Primer design was implemented with the help of www.primerfox.com (Fuchs, 10th July 2012). Specificity of the suggested primers was checked by the nucleotide blast of NCBI (http://blast.ncbi.nlm.nih.gov/Blast.cgi?PROGRAM=blastn&BLAST_PROGRAMS=megaBlast&PAGE_TYPE=BlastSearch&SHOW_DEFAULTS=on&LINK_LOC=blasthome) (10th July 2012).

3.1.3 Antibodies

Primary and secondary antibodies listed in table 3.3 and 3.4 were used for immunofluorescence staining of human skin cross sections.

Table 3.3 Primary antibodies

primary antibody	clonality/host	Company/catalog no.	dilution
anti human collagen type I	monoclonal IgG1 mouse	abcam (ab90395)	1:500
anti human collagen type III	polyclonal IgG rabbit	abcam (ab7778)	1:400
anti human CD90/Thy1	polyclonal IgG sheep	R&D Systems (AF2067)	1:10
anti human CD68	Monoclonal IgG1 mouse	abcam (ab955)	1:100
anti human αSMA	monoclonal IgG2a mouse	abcam (ab7817)	1:100
anti human CD31	polyclonal IgG rabbit	abcam (ab28364)	1:10
anti human podoplanin	Monoclonal IgG1 mouse	abcam (ab10288)	1:1400

Table 3.4 Secondary antibodies

secondary antibody	host	Company/catalog no.	dilution
anti mouse IgG Cy3	sheep	Sigma Aldrich (C2181)	1:500
anti sheep IgG Alexa Fluor 647	donkey	Invitrogen (A21448)	1:125
anti rabbit IgG Alexa Fluor 647	donkey	abcam (ab150075)	1:125

3.2 Clinical methods

3.2.1 Photo documentation

Upper arms of the volunteers were photographed (Nikon D 70; objective Sigma DC 18-200 mm 1:3,5-6,3 D, ring flash Sigma EM- 140 DG) at a distance of one meter in ventral and dorsal position. Photos were arranged employing Adobe Photoshop elements 7.0.

3.2.2 Sonography

The treatment course was monitored by sonography. Hence Sculptra® was injected subcutaneously a 22 MHz ultrasonic probe was selected. The sonography unit type DUB-USB (taberna pro medicum, Lüneburg) was attached to a Sony Vaio notebook with installed DUB SkinScanner 3.95 software. Penetration depth was 10 mm and intensification was 48 dB.

Sonography is a non-invasive imaging method using ultrasonic waves to visualise tissue structures. Ultrasonic waves permeating tissues are reflected differently, depending on the sound conduction properties of the tissue structures. The intensity of reflections and the time span between impulse and echo are detected and composted to a picture with more or less echogenic structures. The program illustrates the data in an A-scan and a B-scan. A-scan (amplitude modulation) shows the intensity of the echo and its penetration depth in form of amplitudes. B-scan (brightness modulation) is a two dimensional illustration of the skin cross section.

The DUB SkinScanner software possesses a tool for measuring the echo density of a freely selectable rectangle in sectors of a B-scan. Upon the clinical visits sonographic scans of both

upper arms of each volunteer were collected in terms of a loop (succeeding pictures). Three scans of one loop were chosen and analysed as follows: B-scan was phase adjusted. The first vertical measuring line was set to the entry echo of the epidermis. The second vertical measuring line was set 0.7 cm into the depth of the scanned tissue. Than the first measuring line was set under the echo of the epidermis. Now both horizontal measure lines were spanned up to an area of 20 mm^2. This procedure gave standardized depths and areas, minimized inter- and intraspecific differences and allowed evaluation of scans. Echo density of three B-scans per upper arm where calculated to an arithmetic average. Differences between left and right arm (Mann-Whitney U test) and changes between baseline measures and at months 20 (Wilcoxon test) were analysed using SPSS® (Version 19; IBM Corporation, Somers, NY, USA).

3.2.3 Tissue sampling

Following thoroughly disinfection an 1 cm^2 area of the left inside of the upper arm skin was anaesthetised by 1 ml of local anaesthetic Xylonest 1% (AstraZeneca, Wedel). 3 mm Ø, deep punch biopsies (kai Europe, Solingen) of skin and subcutis were taken and the defect closed. Stiches were removed two weeks later. Punch biopsies were divided, one half was transferred for molecular biological examination into a sterile Eppendorf tube and was immediately snap frozen and stored in liquid nitrogen, the second half was fixed in formalin 4% and sent to the dermatohistopatholocic laboratory of P. Kind, MD (Offenbach).

3.2.4 Injection of Sculptra®

Sculptra® (Sanofi Aventis, Berlin), available in its lyophilised form (vial à 150 mg poly-l-lactic acid microspheres (Ø 40-63 µm), 90 mg carboxymethylcellulose and 127.5 mg pyrogen free mannitol) was reconstructed with 8 ml of sterile water, plus 2 ml of Xylocaine (1%) (AstraZeneca, Wedel) to the final volume of 10 ml/vial.

To allow slow and complete water absorption of PLLA microspheres, the lyophilisate was reconstructed with 5 ml sterile water at least 24 hours prior to the injections. Remaining above mentioned 3 ml sterile water and 2 ml of Xylocaine was added to the suspension a few minute prior to application. It is recommended to take up resuspended Sculptra® at body temperature into 1 ml luer lock syringes (DB, Franklin Lakes, NJ; USA). Prior to the injection, treated skin areas were disinfected with octenisept (Schülke & Mayr, Norderstedt). Resuspended Sculptra® was injected subcutaneously (26 G needles), employing a tunnelling technique during slow retraction (Figure 3.1). Per injection site 0.2 ml of the suspension was applied. A total of one vial Sculptra® was injected per upper arm every three months. During the study course 4 vials per upper arm/ volunteer were employed. Injections were carried out by the head of the clinical trial, N. Y. Schürer, MD (Osnabrück). After the last injection treated area was massaged with the aim to distribute the applied material.

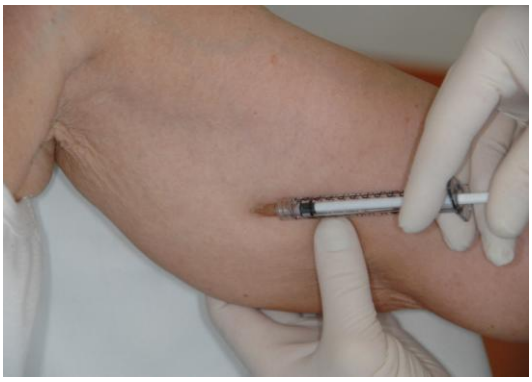

Figure 3.1 Sculptra® injection into the ventral aspect of the upper arm

3.2.5 Quality of Life

In cooperation with Prof. Augustin (Institut für Versorgungsforschung in der Dermatologie und bei Pflegeberufen, Universitätsklinikum Hamburg-Eppendorf) the questionnaire **F**reiburg **L**ife **Q**uality **A**ssessment-k (Fragebogen zur Lebensqualität, Haut und Kosmetik) (cf. 7.5) was employed to evaluate the volunteers quality of life status prior to and after the study. 44 questions and five respective answers inquired I) the general wellbeing, II) the mindset to the skin and III) to the outer appearance in general. Each answer was valued and classified into 5 topics namely hiding of the body, dissatisfaction of the outer appearance, avoiding contact, aiming for cosmetics, and dissatisfaction with the skins appearance. Values of each topic were averaged and expressed in a diagram. The questionnaire is modified to the core questionnaire referred in Augustin *et al.* (2004)[190].

3.3 Molecular biological methods

Gene expression analysis regarding the influence of Sculptra® on the human dermis and subcutis were carried out by realtime PCR [191]. Therefore, total RNA was prepared from the tissue samples and mRNA was transcribed by reverse transcriptase, dNTPs and oligo$(dT)_{20}$ primer into cDNA. cDNA represents the unity of all expressed genes to the time point of tissue collection and serves as a template for real-time PCR.

3.3.1 Total RNA isolation from skin tissue samples

Total RNA from skin tissue samples was isolated using the RNeasy Fibrous Tissue Mini Kit (Qiagen, Hilden) following manufacturer´s recommendation. Tissue samples were homogenized with the Ultra-Turrax T25 (IKA, Staufen) at 18000 rpm for 30 s in 300 µl RLT buffer. RLT buffer contains chaotropic guanidinium isothiocyanat, which lyses cells and inactivates RNases. Lysates were dissolved with 590 µl RNase free water and incubated with 6 U proteinase K at 55°C for 10 minutes. During the following centrifugation step, cell debris was pelleted by 10000 *x*g for 3 minutes. Supernatants were mixed with 450 µl 96% ethanol and centrifuged through a silica membrane (RNeasy mini column) at 8000 *x*g for 15 s. The silica membrane was washed with 350 µl RW1 buffer by a further centrifugation step at 8000 *x*g for 15 s. To remove bound DNA from this membrane, a 15 minute digestion was performed *via* the incubation of 27 units DNase I in 80 µl RDD buffer at room temperature. Digested DNA was washed off with 350 µl RW1 buffer at 800 *x*g for 15 s followed by two

more washing steps with 500 µl RPE buffer at 8000 *x*g. Finally isolated total RNA was eluted twice with 40 µl RNase free H_2O.

Purity and concentration of isolated total RNA was analysed photometrically using a NanoPhotometer (IMPLEN, Munich). Concentration was determined by the absorption at 260 nm and calculated according to the absorption of 1 correlating with the RNA concentration of 40 ng/µl. Nucleic acids absorb ultraviolet light by a wave-length of 260 nm, whereas aromatic amino acids of proteins absorb ultraviolet light at 280 nm. The quotient of RNA-/protein-content reflects the purity of the sample. The sample was used when the quotient was higher than 1.8. Isolated RNA was immediately used for synthesis of cDNA.

3.3.2 Polymerase chain reaction (PCR)

PCR enables the enzymatic exponential duplication of desired DNA segments [192]. PCR was required to examine the binding ability and annealing temperature of gene specific primers for the real-time PCR. Therefore different PCR assays of current primer pairs were incubated in gradient PCR cycler (Eppendorf, Hamburg) enabling different temperatures for each assay during the annealing phase. Amplification was carried out by DreamTaq DNA polymerase (Fermentas, St. Leon-Roth). A 25 µl sample containing 100 ng cDNA, gene specific primers (forward and reverse á 0.6 µM), 0.2 µM dNTPs, 2.5 µl 10x DreamTaq buffer, 2.5 U DreamTaq DNA polymerase, was incubated as follows: 60 s at 94°C; 35x [30 s at 94°C; 30 s at 56°C or 58°C or 60°C; 30 s at 72°C] 10 min at 72°C. Resulting PCR fragments were further processed like described in 3.3.5 Agarose gel electrophoresis.

3.3.3 Reverse transcription

For cDNA-synthesis from isolated total RNA ThermoScript PCR System (Invitrogen, Darmstadt) was used following manufacturer´s recommendations. For first strand synthesis 20 µl sample containing 15 U reverse transciptase, 2.5 µM oligo$(dt)_{20}$ primer, 5 µM dNTP mix and 200 ng RNA were incubated at 55°C for 1 h. The reaction was terminated by incubating at 85°C for 5 minutes. Finally 2 U RNAse H was added and incubated by 37°C for 20 min, in order to remove the RNA. Synthesized cDNA was stored at -80°C until it was used as template in real-time PCR.

3.3.4 Real-time PCR

Real-time PCR is a variant of PCR to detect the accumulating amount of specific DNA fragments *via* fluorescence measuring. Thereby fluorescence dye Sybr Green (Fermentas, St. Leon-Rot) intercalates into double stranded DNA and the fluorescence signal increases proportional to the PCR product amount. During the experiment the cycle number (quantification cycle (C_q) or threshold cycle (C_t)) is recorded when reaching a certain DNA amount. For standardization ribosomal phosphoprotein large P0 (RPLP0) was used as a housekeeping gene [193]. Housekeeping genes are expressed in the same strength to every time point in every cell and a comparison of C_qs ratios enables a conclusion on the examined genes. Examinations were carried out by the iCylcler real-time PCR system (BioRad, Munich) in triplicates, according to manufacturer´s recommendations. Briefly, 25 µl sample containing 75 ng cDNA, gene specific primers (forward and reverse á 1µM) and Maxima SYBR

Green/Fluorescein qPCR Master Mix were incubated as follows: 10 min at 95°C; 35x [30 s at 95°C; 30 s at 58°C; 30 s at 72°C] 3 min at 72°C. Specificity of current PCR products was controlled by melting curve analysis (cf. 7.3). Finally data were analysed by the q-gene approach according to Simon (2003) [194].

3.3.5 Agarose gel electrophoresis

To analyse PCR products according to their size 0.8% agarose matrix in TAE buffer (40 mM TRIS, pH 8, 10 mM NaAC, 1 mM EDTA) was accomplished according to Sambrook *et al.* (1989) [195]. To enhance the density of the sample and to obtain an indication about the position of the DNA sample by a dye, DNA samples were mixed in a ratio 1:5 with gel loading buffer (5x TAE, 30% glycerin, 0.25% bromphenol blue). Separation ensued by a tension of 80 V over 65 minutes at a distance of electrodes of 13 cm. Separated DNA fragments were stained by ethidium bromide (2 µg/ml) for 20 minutes, washed in H_2O, visualized and documented by VersaDoc (BioRad, Munich). DNA fragment sizes were estimated in relation to the SmartLadder (Eurogentec) standard. Under UV-Light prominent bands were excised and DNA fragments were purified employing the QIAquick Gel Extraction Kit (Qiagen, Hilden) according to the manufacture´s recommendations. DNA fragments were sequenced by Seqlab (Göttingen).

3.4 Histological examinations

3.4.1 Haematoxylin eosin staining

Embedding formalin fixed tissue in paraffin, manufacturing 3 µm thick serial cross-sections on Superfrost slides (Menzel, Braunschweig), and staining with haematoxylin and eosin (H&E) according to Böhmer (1865) was ensured by the dermatohistopatholocic laboratory of P. Kind, MD (Offenbach) [196].

Haematoxylin stains acidic structures, like nuclei and endoplasmatic reticula blue. Eosin stains basic structures, like cell plasma proteins, mitochondria and collagen in red colour. Documentation of H&E-stained tissue was ensured by Olympus microscope (BX60) and by Cellp software. For detection of birefringent PLLA-particles polarized light was employed.

3.4.2 Immunofluorescence staining

Paraffin embedded cross-sections were initially dewaxed (deparaffinized) and rehydrated. Dewaxing of sections ensued by 3 times 5 minutes incubation in xylene (Sigma-Aldrich, Taufkirchen) and rehydration in an ethanol dilution series. Therefore sections incubated twice in 100% ethanol for three minutes and currently once in 95%, 90%, 80% and 70% ethanol for 3 minutes. A three-minute rinse off with water followed.

For antigen retrieval the cross-sections were incubated for 15 minutes in boiling sodium citrate buffer (10 mM sodium citrate, 0.05% Tween 20, pH 6.0) or in Tris-EDTA buffer (10 mM Tris, 1 mM EDTA, 0.05 Tween 20, pH 9.0). Than the heat was switched off and cross-sections were left for further 30 minutes within the buffer. After two washing steps with H_2O for two minutes, cross-sections were blocked with 2% bovine serum albumin (BSA) in

phosphate buffered saline with triton (PBS-T) (137 mM sodium chloride, 10 mM phosphate, 2.7 mM potassium chloride, pH 7.3 and 0.1% Triton X-100). This blocking step was carried out in a humidified chamber at room temperature. Cross-sections were incubated with the primary antibody (cf. table 3.3) diluted in PBS-T + 2% BSA over night at 4°C. Two washing steps for 3 minutes, each with PBS-T, followed by one with PBS (137 mM sodium chloride, 10mM phosphate, 2.7 mM potassium chloride, pH 7.3) preceded a 1 h incubation period with the secondary antibody, diluted in PBS-T + 2% BSA (cf. table 3.4) and 4´,6-Diamidino-2-phenylindole dihydrochloride (10 µg/ml) (DAPI) (Sigma, Taufkirchen) at room temperature. Two wash steps with PBS-T and finally with PBS (137 mM sodium chloride, 10 mM phosphate, 2.7 mM potassium chloride, pH 7.3) (three minutes each) followed. Mounting was ensued by a drop of Vectashield mounting medium (Vector Laboratories, Burlingame, CA, USA), the gap between the slide and covers lip was sealed by nail polish. Microscopy of the specimens followed by application of the fluorescence microscope Olympus IX70 and the metamorph software (Molecular Devices, Sunnyvale, USA). Furthermore, the microscope Olympus IX881 with confocal laser scanning unit fluoview FV1000, equipped with a multi argon laser (458/488/515 nm), laser diodes (405, 559, 635 nm), objective UPLSAPO 20x NA 0.75 air, LUCCPLFLN 40x NA air, UPLSAPO 60x NA 1.2 water and acquiring software FV10-ASW Version 3.0 was employed. Raw data was analysed with the software Image J.

3.5 Biochemical methods

3.5.1 Collagenase test

A collagenase test was performed using the substrate kit for quantitative collagenase determination (Sigma-Aldrich, Taufkirchen) according to the manufacture´s recommendation based on Grassmann and Nordwig [197]. Besides the test approaches, blanks and standards were carried out with and without Sculptra® to be aware of an influence of Sculptra® on the absorption measurement. For each relevant approach 50 µl Sculptra® solution (vial diluted in 8 ml water and 2 ml Xylocaine) was washed in citrate buffer (0.1 M citric acid, 0.01 M calcium acetate, pH 6.3) to exclude Xylocaine. Solids were sedimented and resuspended in the I) collagenase, II) standard and III) blank solution. Collagenase incubation at 37°C for 5 minutes was ensured in a Thermomixer comfort (Eppendorf, Hamburg) by 500 rpm to avoid subsidence of Sculptra® particles. The reaction was stopped *via* incubation at 99°C for 15 minutes. Absorption was determined by SpectraMax Plus (Molecular Devices, Biberach an der Riss). Volume activity (U/ml) and specific activity (U/mg) were calculated like follows.

$$\frac{U}{ml} = \frac{(\mathrm{A}_{565}\ \text{test-}\mathrm{A}_{565}\ \text{blank}) * 0.123\ \mu mol * 0{,}6ml}{(\mathrm{A}_{565}\ standard - \mathrm{A}_{565}\ blank) * 0.1ml * 0.15ml * 5min}$$

$$\frac{U}{mg} = \frac{U * 1\ ml}{ml * 2.5\ mg}$$

4. Results

4.1 Clinical monitoring

The upper arm as treatment area was selected for the following reasons: for biological examinations tissue harvesting by punch biopsies was necessary. Hence small scars remain, biopsies were taken at the less visible inner site of the upper arm. Furthermore, women suffer at a certain age from the loss of tissue elasticity of the upper arms. Hence employment of Sculptra® for extra facial augmentation is documented successfully in the literature, Sculptra® was applied to the inner site of the upper arm. The development of nodules is described in literature. Therefore, in case of the development of late onset nodules, unsightly appearances would be less visible on the inner site of the upper arm.

During this 20 months-study no dropouts were recorded. Palpable patches of small nodules had developed by 2 of the 21 volunteers in the Sculptra® treated upper arms. Four more volunteers reported about the development of palpable nodules 10-28 months after the last injection in a follow-up telephone interview.

Figure 4.1A Left upper arm of volunteer #21 before the treatment (at baseline)

Figure 4.1B Left upper arm of volunteer #21 after 20 months of treatment (after 4 Sculptra® injections at 3 months intervals)

Figure 4.2A Right upper arm of volunteer #9 before the treatment (at baseline)

Figure 4.2B Right upper arm of volunteer #9 after 20 months of treatment (after 4 Sculptra® injections at 3 months intervals)

Direct visual comparison of Sculptra®-untreated and -treated (after four injections) upper arm photo documentation revealed no objective changes in shape and / or structure (Figure 4.1A, B and Figure 4.2A, B: exemplary before and after pictures of two volunteers).

4.2 “Quality of Life” questionnaires

To document the volunteers’ opinion on the augmenting effect of Sculptra® to the inner site of the upper arm, their quality of life was questioned prior to and after 4 Sculptra® injections, i. e. before and 20 months after the first injection. Questions and answers were assigned to 5 topics: 1) “hiding the body”, 2) “dissatisfaction of outer appearance”, 3) “avoiding contact”, 4) “effort to maintain attractiveness”, and 5) “skin problems”. Figure 4.3 represents the 5 topics in bars accordingly, prior to (prae, yellow bar) and 20 months after the first injection (post, blue bar).

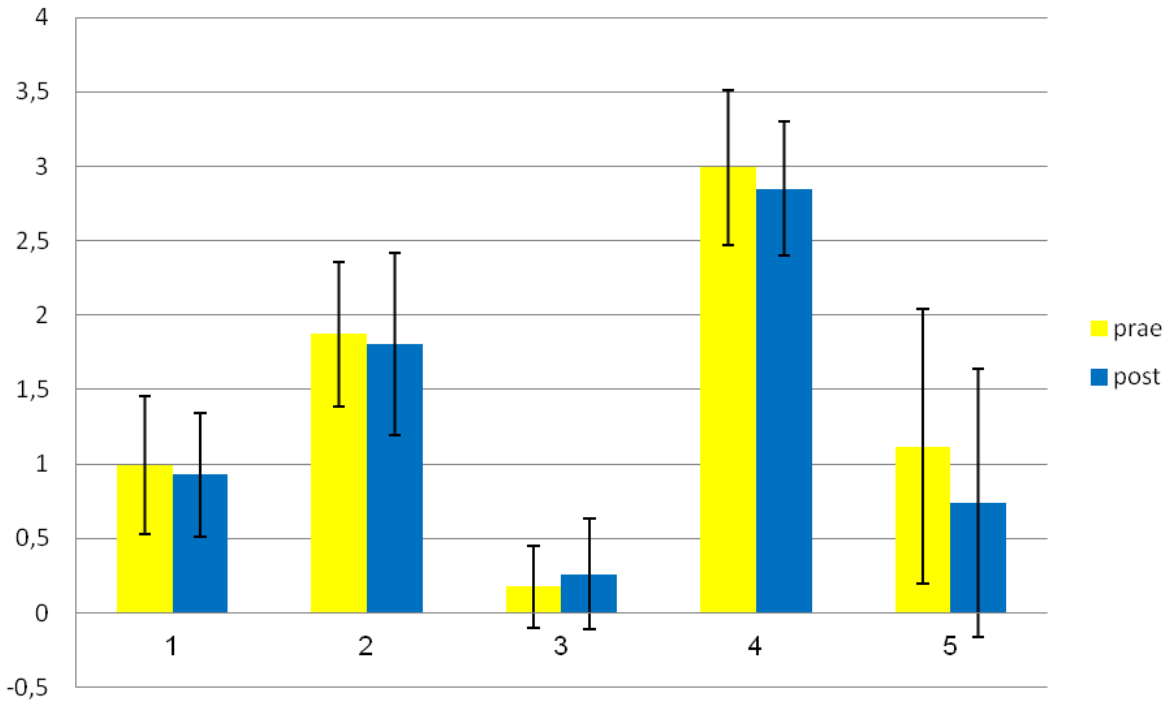

Figure 4.3 Comparison of volunteers’ quality of life prae (yellow bar) and after 4 Sculptra® injections, i.e. 20 months after the first injection (blue bar). Five double bars refer to 5 topics: 1) “hiding the body”, 2) “outer appearance dissatisfaction”, 3) “avoiding contact”, 4) “effort to maintain attractiveness”, and 5) “skin problems”. Degrees of topics are given in numbers (y-axis): 0 = not at all; 1 = slightly; 2 = moderate, 3 = considerably; 4 = very much / a lot.

The values for “hiding the body” (bar 1) and “outer appearance dissatisfaction” (bar 2) drop from 1.0 and 1.9 to 0.9 and 1.8, however without significance. Degree of “avoiding contact” (bar 3) increased from 0.2 to 0.3 and that of “to maintain aesthetic attractiveness” (bar 4) decreased from 3.0 to 2.9. The degree of “skin problems” (bar 5) decreased from 1.1 to 0.7. None of these changes were statistically significant. **“Quality of life” did not chance in the present study.**

4.3 Sonography of subcutaneous tissue

Present sonography set up was applied to monitor the treatment progress and to objectively document subcutaneous tissue changes after Sculptra® injections. The DUB SkinScanner Software possesses a tool for measuring the echo density in a spanned of rectangle in a standardised way (cf. 3.2.2). Here two representative pictures of the sonographic status are presented: recorded at baseline, prior to any Sculptra® injection (Figure 4.4A) and 20 months later after 4 Sculptra® injections (Figure 4.4B).

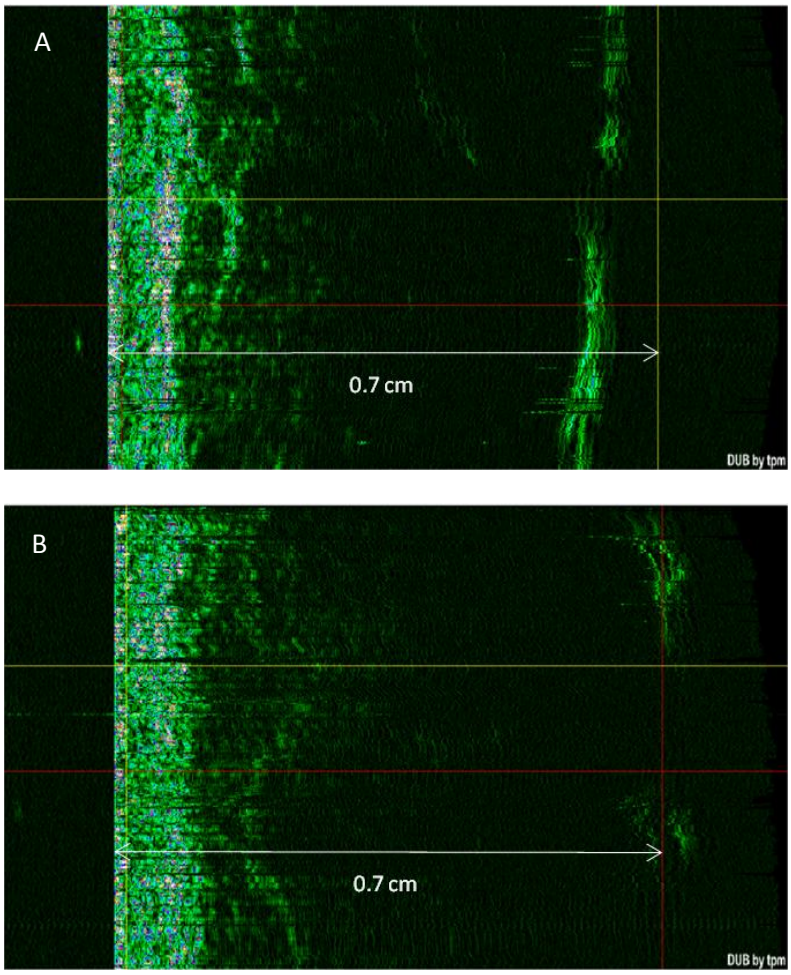

Figure 4.4A-B Comparison of 22 MHz sonography scans from the ventral aspect of the upper arm from volunteer #9 of Sculptra® untreated (A) tissue and Sculptra® treated tissue (four injections over a 20 months time period; B). Echo density decreases from 16 (A) to 13 (B).

Echo densities of three B-Scans per upper arm, visit and volunteer were averaged and statistically analysed by SPSS. The echogenicities of the left and right upper arms at time points t0 (first day of study prior to any injection of Sculptra®), t1 (13 months after the first and 2.5 months after the last injection) and t2 (20 months after the first and 10 months after the last injection) are presented in Figure 4.5. Statistical significance of differences between the left and the right arm (Mann-Whitney U test) and between t0 and t1, respectively t2 (Wilcoxon test) was determined. For the left upper arm (blue bar) the echogenicity was calculated at t0 to a mean of 16.03+-2.86 (SD) and for the right arm (red bar) to 17.18 (mean)+-2.54 (SD). At t1 the echogenicity declined to 13.07 (mean) +-2.58(SD) (blue bar, the

left arm) and to 13.86 (mean) +- 2.91 (SD) (red bar, right arm). At t2 the echogenicity declined further to 12.60 (mean) +-1.90 (SD) (blue bar, the left arm) and to 12.75 (mean) +-2.38 (SD) (red bar, right arm). There were no significant differences between the left and the right arm at time points t0 (p ≤0,116), t1 (p≤0,489) and t2 (p≤0,956). Highly significant changes (p≤0.000) took place when the time course of either arm was compared from t0 to t2 and further in the right arm from t0 to t1. Significant change of echogenicity was revealed in the left arm (p≤0.007) when t0 and t1 was compared. No change was observed when t1 was compared with t2, neither for the left (p≤0.140) nor for the right arm (p≤0.147).

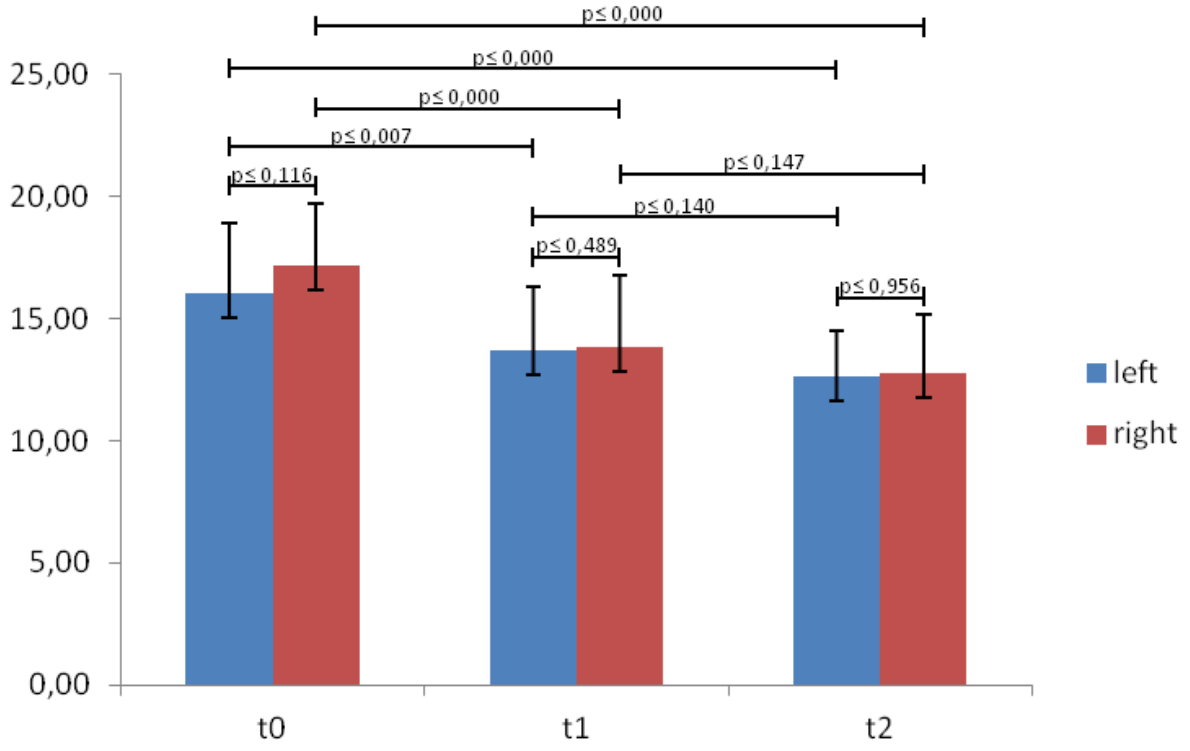

Figure 4.5 Comparison of the mean echo densities of the tissues during the study course. The three double bars represent mean echo densities (y-axis/no defined unit) of left (blue) and right (red) arms prior to Sculptra® treatment (t0), 13 months after the first and 2.5 months after the last injection (t1) and 20 months after the first and 10 months after the last injection (t2).

A highly significant decrease in echogenicity was retrieved comparing baseline tissue values (t0) with 20 month (t2) values from either arm and tissue value (t0) with 13 month (t1) value from the right arm. A significant decrease in echogenicity was retrieved comparing baseline tissue value (t0) with 13 month (t1) value from the left arm.

4.4 Histopatholoy of skin biopsies

Figure 4.6 illustrates a human skin histology of an untreated tissue section from epidermis *via* dermis to subcutis.

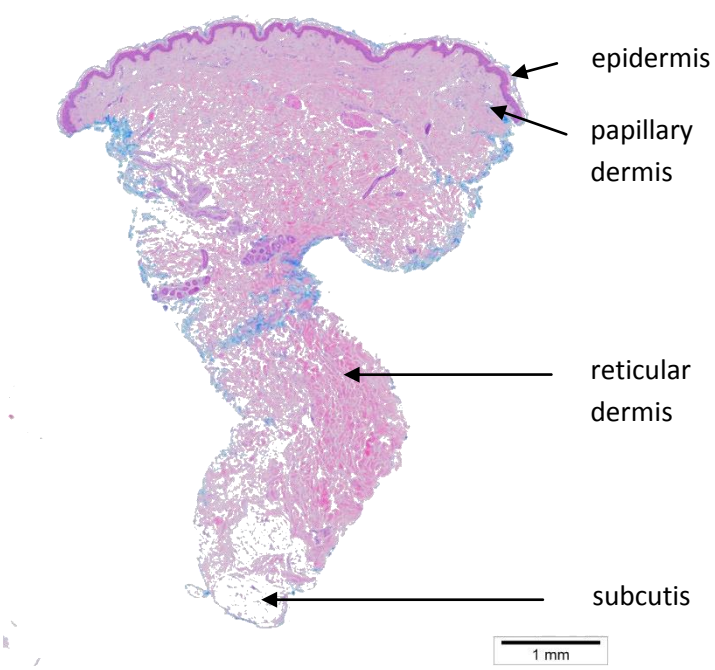

Figure 4.6 Histology of human skin. H&E stained cross-section of untreated tissue in bright field view.

After Sculptra® injection, microscopy of H&E stained tissue cross-sections revealed birefringent PLLA particles under polarized light in tissues from 8 of the 21 volunteers. All Sculptra® treated sections presented with a massive invasion of lymphocytes and macrophages, latter forming foreign body giant cells (Figure 4.7A-D).

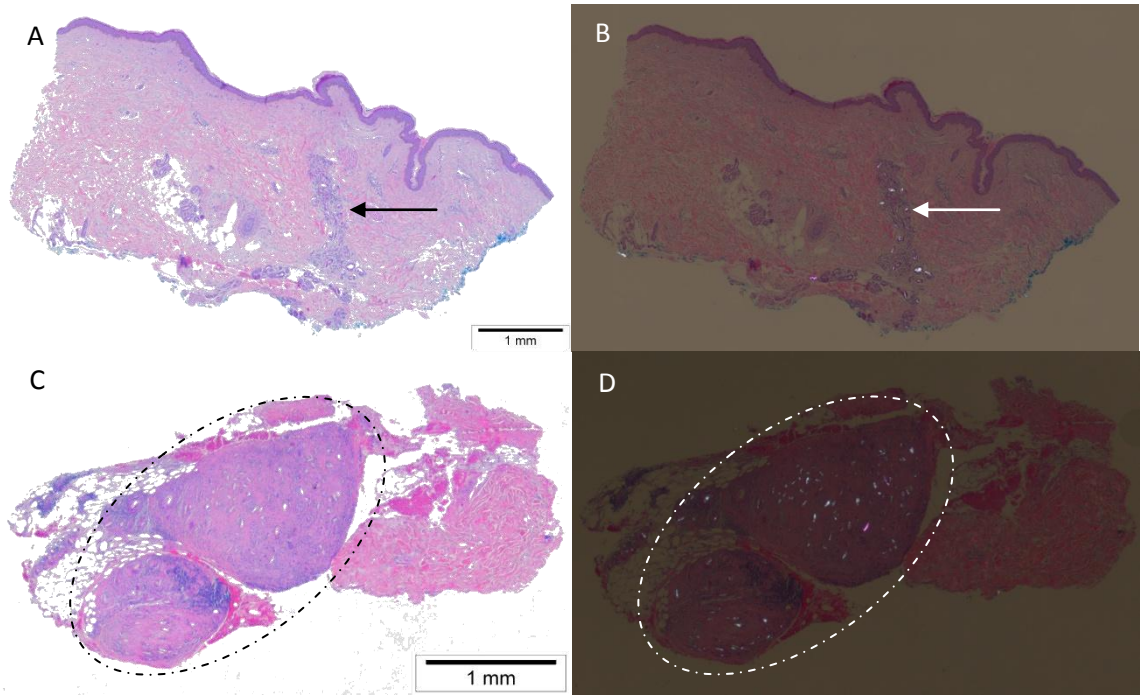

Figure 4.7A-D Histology of Sculptra® treated human skin. H&E stained cross-section of Sculptra® treated tissue in bright field (left) and polarized view (right). (A, B) illustrates an overview of the epidermal and dermal section; (C, D) an overview of the dermal and subcutaneous section. Sculptra® is injected subcutaneously under slow retraction. Thus blue stained channel-like structure within Sculptra® particles might demonstrate an injection channel in a superficial dermal layer (A, B) (arrows) and in the subcutaneous layer Sculptra® particle depots evoke granulomas (C, D) (oval). Haematoxylin stains acidic structures, like nuclei blue, implying a massive cell infiltrate around birefringent Sculptra® particles.

Apart from the study protocol, a fourth biopsy was taken 28 months after the last injection of one volunteer. Birefringent Sculptra® particles along with the above described cellular reaction were observed even 28 months after the last injection (Figure 4.8A-H).

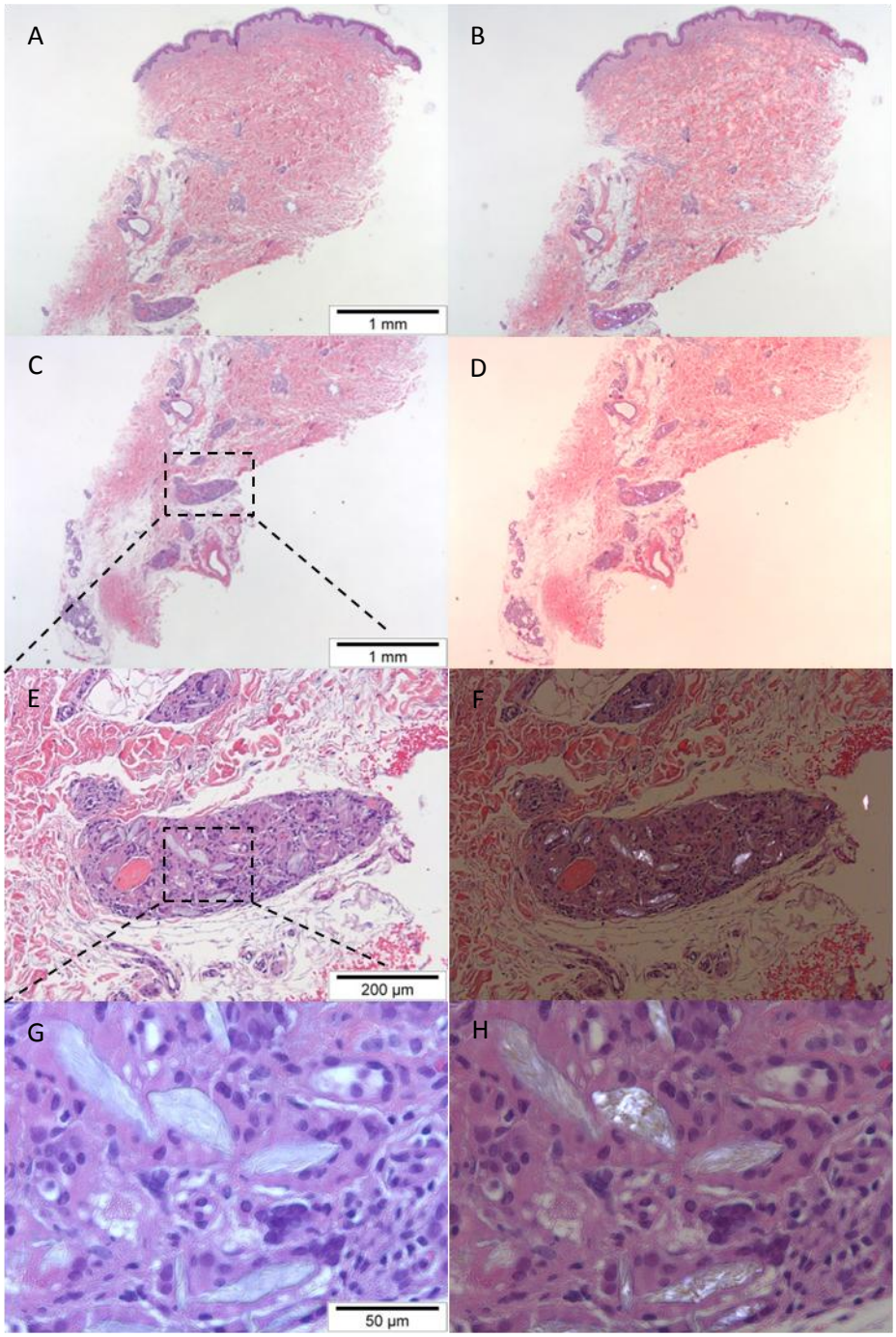

Figure 4.8A-H Sculptra® particles are still present 28 months after the last injection. H&E stained cross-section of Sculptra®-treated tissue in bright field (left) and polarized view (right). (A, B) illustrates an overview of the epidermal and dermal section; (C, D) an overview of the dermal and subcutaneous section. (E, F) focuses on a granuloma. (G, H) presents a closer view on Sculptra® particles surrounded by haematoxylin stained nuclei (blue), represent most likely macrophages, lymphocytes and foreign body giant cells.

Under polarized light birefringent Sculptra® particles along with foreign body reactions are visible in H&E stained tissue cross-sections of a biopsy from the inner arm, taken 28 months after the last Sculptra® injection.

4.5 Characterization of the cell infiltrate

In further experiments antibodies against human CD68, CD90 (Tyr-1) and αSMA should detect macrophages, fibroblasts and myofibroblasts/endothelia cells by immunofluorescence microscopy. For positive control studies the CD68 antibody was tested on spleen tissue (Figure 4.9), the CD90 antibody on fresh scar tissue (Figure 4.12) and αSMA antibody on untreated skin tissue (Figure 4.17.)

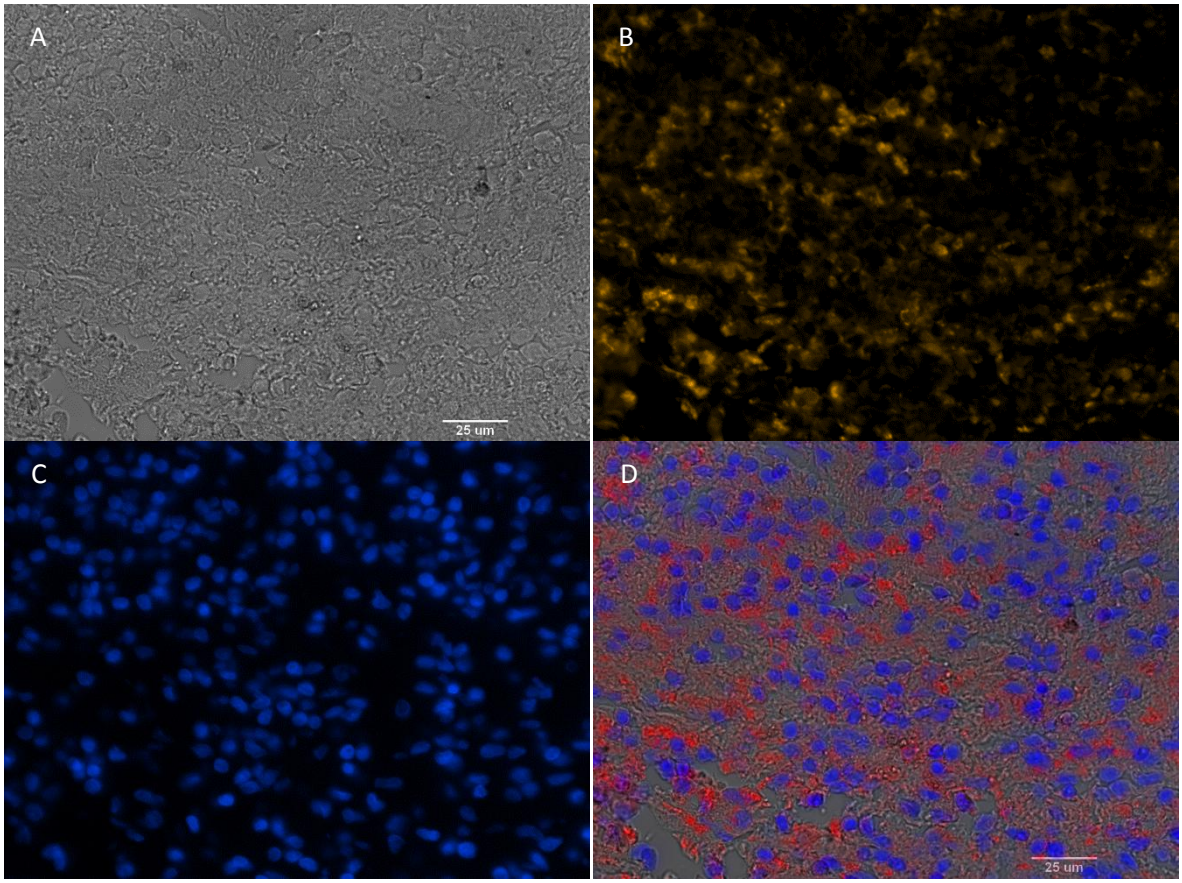

Figure 4.9A-D Positive control immunofluorescence staining of human spleen tissue employing human CD68 antibody. Human spleen tissue is visualised in DIC (A) view. Immunofluorescence staining revealed $CD68^{+}$ macrophages (B, orange). Nuclei (C, blue) were visualised by 4´,6-diamidino-2-phenylindole (DAPI). A, B and C were merged in D (here: red represents CD68 positive signal).

Human spleen tissue was used as positive control for macrophage detection. **CD68 staining of spleen tissue confirmed competency of the antibody to recognise macrophages (Figure 4.9A-D).** Staining pattern of untreated dermal and subcutaneous tissue employing the CD68 antibody is illustrated in Figure 4.10A-C.

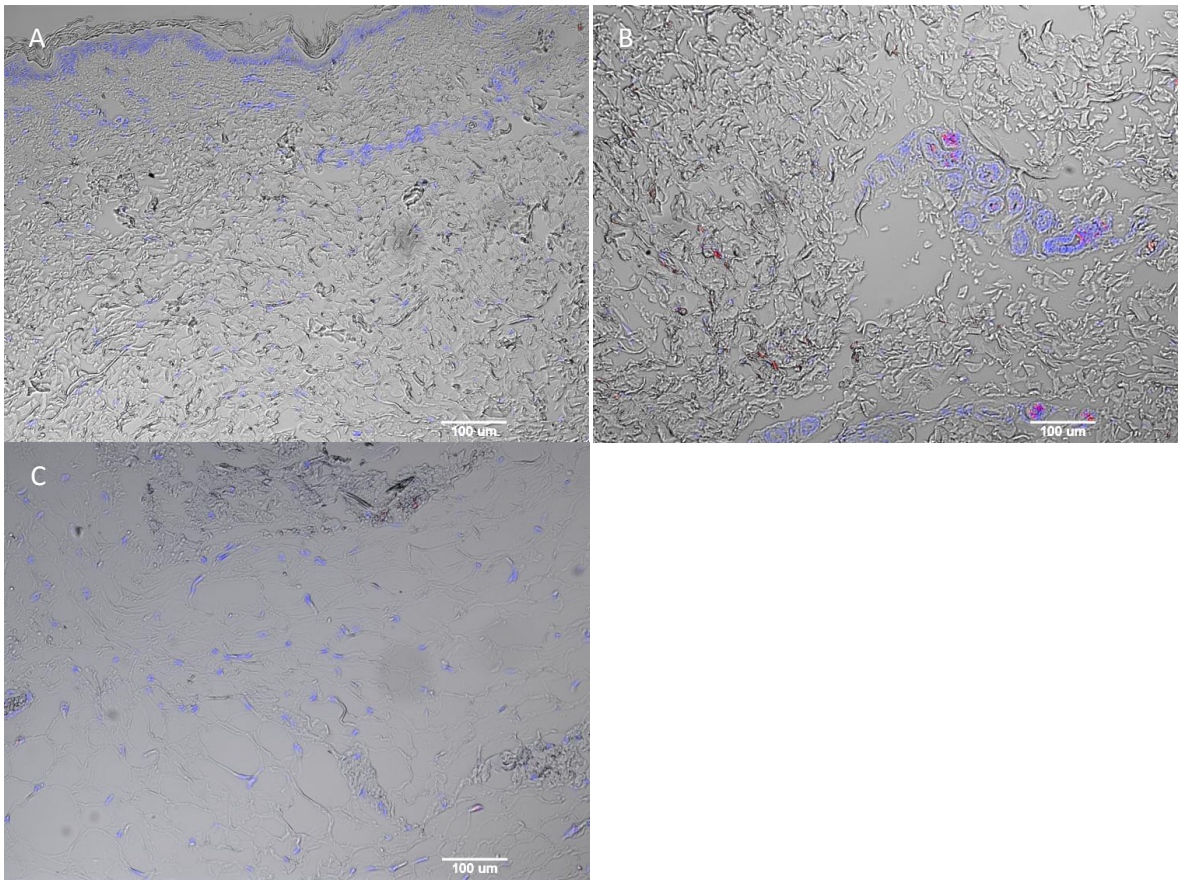

Figure 4.10A-C CD68 staining pattern of human skin. Immunofluorescence staining against CD68 (red) of epidermal/dermal (A), dermal (B) and subcutaneous (C) tissue. Nuclei (blue) were visualised by 4´,6-diamidino-2-phenylindole (DAPI).

CD68-positive signals are not abundant in untreated epidermal, dermal and subcutaneous tissue (Figure 4.10A-C).

To further detect $CD68^+$ cells in Sculptra® treated tissues, immunofluorescence staining was performed employing the previously worked out conditions (Figure 4.9-4.10).

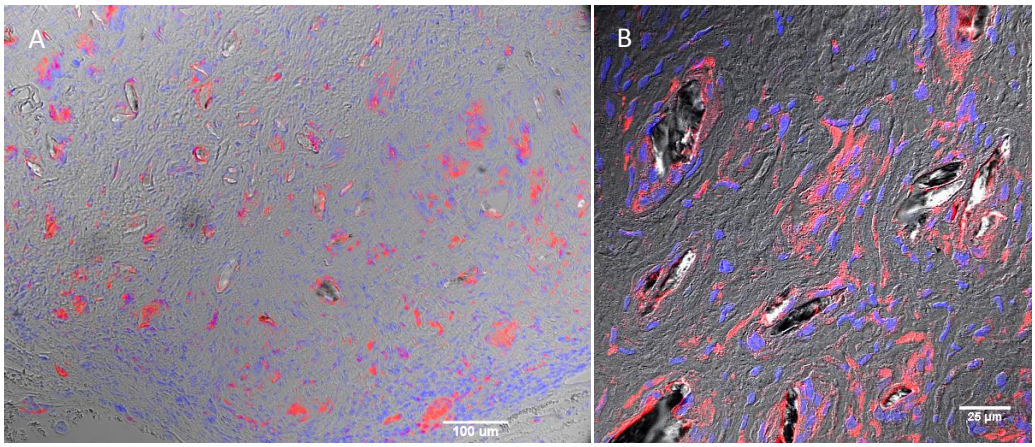

Figure 4.11A-B $CD68^+$ cells were found in direct proximity of Sculptra® particles. Immunofluorescence staining of Sculptra® particle-surrounding capsule tissue revealed $CD68^+$ macrophages (red) in close proximity to Sculptra®. Nuclei (blue) were visualised by 4´,6-diamidino-2-phenylindole (DAPI). (A) represents an overview of capsule tissue, (B) a close up on particles.

Cells in direct proximity of Sculptra® particles were CD68$^+$ (Figure 4.11).

Moreover the ability of CD90 antibody to recognise fibroblasts was tested on fresh scar tissue.

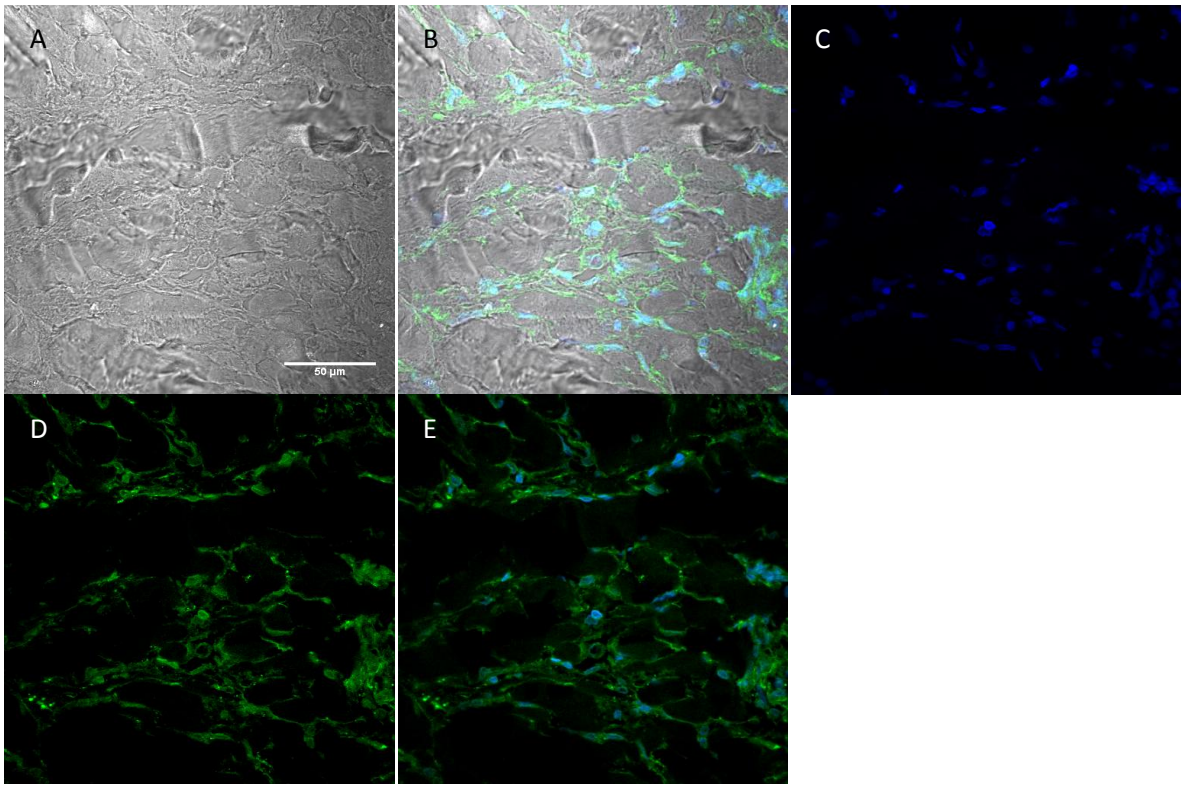

Figure 4.12A-E Positive control immunofluorescence staining of fresh human scar tissue employing human CD90 antibody. Human scar tissue is visualised in DIC (A) view. Immunofluorescence staining revealed CD90$^+$ fibroblasts (D, green). Nuclei (C, blue) were visualised by 4´,6-diamidino-2-phenylindole (DAPI). Channels A, C and D were merged in B. Channels C and D were merged in E.

Human scar tissue was used as positive control for fibroblasts detection. **CD90-staining of scar tissue confirmed competency of the antibody to recognise fibroblasts (Figure 4.12).** Staining pattern of untreated dermal and subcutaneous tissue employing the CD90 antibody is illustrated in Figure 4.13.

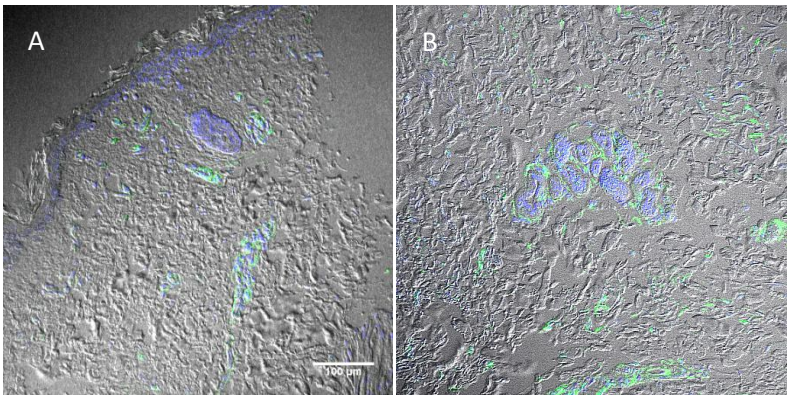

Figure 4.13A-B CD90 staining pattern of human skin. Immunofluorescence staining of epidermal/dermal (A), dermal (B) tissue revealed CD90 (green) positive signals. Nuclei (blue) were visualised by 4´,6-diamidino-2-phenylindole (DAPI).

CD90-positive signals were detected in a scattered fashion in proximity to vessels and appendages (Figure 4.13A-B).

Double immunofluorescence staining of macrophages and fibroblasts, employing antibodies against CD68 and CD90, should elucidate the cell formation in response to Sculptra® particles. Figure 3.14 gives an overview of Sculptra® treated tissue. $CD68^+$ cells are abundant in proximity to Sculptra® particles, whereas $CD90^+$ cells are abundant in a greater distance to the particles (Figure 4.14A-F).

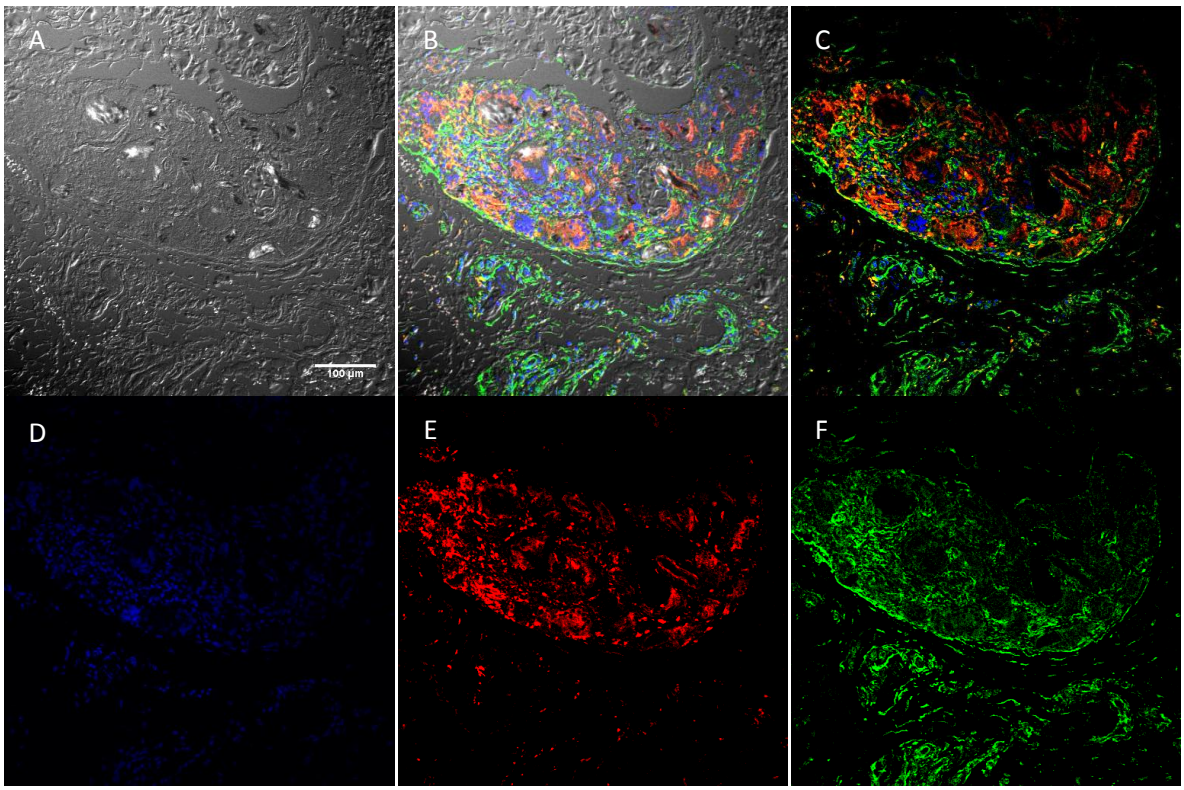

Figure 4.14A-F Characterisation of inflammatory cell infiltrate. Sculptra® particles are surrounded by capsule tissue visualised in DIC (A) view. Double immunofluorescence staining of capsule tissue revealed in close proximity to Sculptra® particles $CD68^+$ macrophages (red, E) and $CD90^+$ fibroblasts (green, F) in the periphery. Nuclei (D, blue) were visualised by 4´,6-diamidino-2-phenylindole (DAPI). All channels were merged in B, without DIC in C.

After illustrating an overview of Sculptra® treated tissue and the $CD68^+$ and $CD90^+$ cell infiltrate a closer view on a few particles was generated (Figure 4.15A-F).

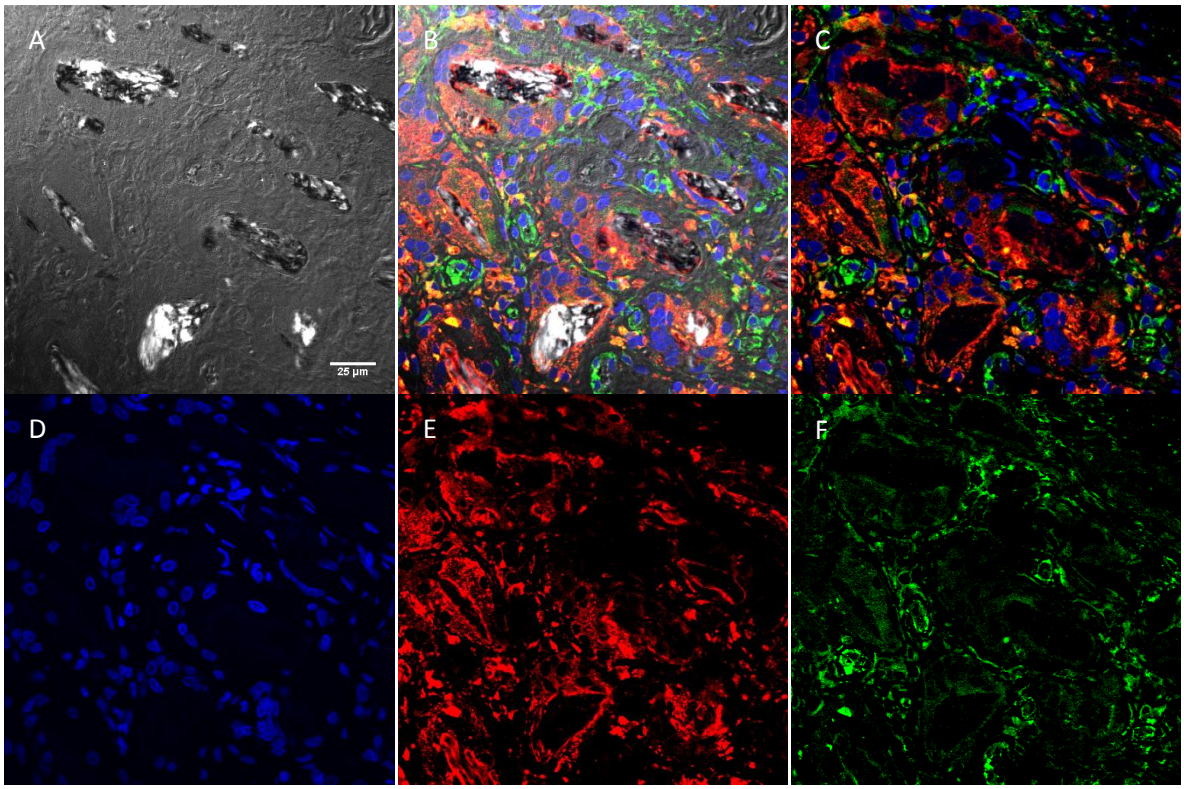

Figure 4.15A-F Characterisation of inflammatory cell infiltrate. Sculptra® particles are surrounded by capsule tissue visualised in DIC (A) view. Double immunofluorescence staining of capsule tissue revealed in close proximity to Sculptra® particles $CD68^+$ macrophages (red, E) and $CD90^+$ fibroblasts (green, F). Nuclei (D, blue) were visualised by 4´,6-diamidino-2-phenylindole (DAPI). All channels were merged in B, without DIC in C.

Zooming directly on a Sculptra® particle an inner cell layer of $CD68^+$ cells and in an outer layer $CD90^+$ cells is presented (Figure 4.16A-F).

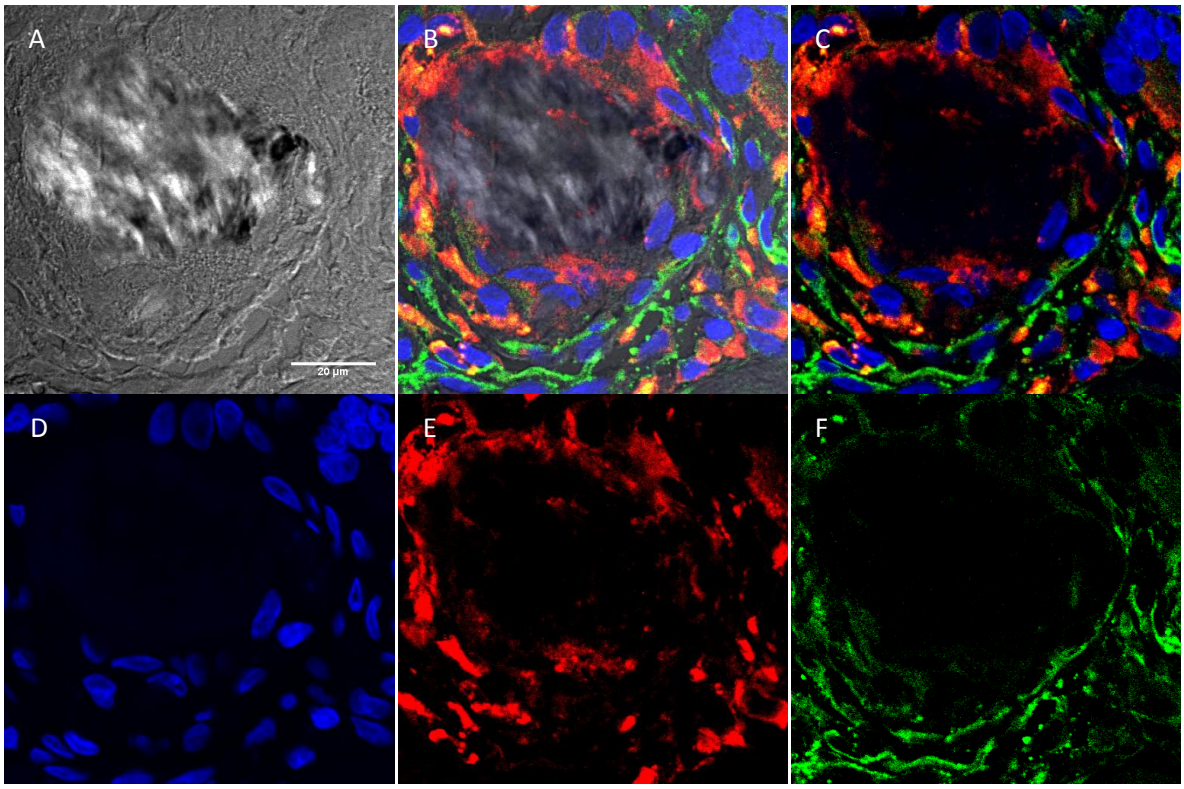

Figure 4.16A-F Characterisation of inflammatory cell infiltrate. A Sculptra® particle is surrounded by capsule tissue visualized in DIC (A) view. Double immunofluorescence staining revealed in close proximity to the Sculptra® particle $CD68^+$ macrophages (red, E) in a first cell row and $CD90^+$ fibroblasts (green, F) in a second cell row. Nuclei (D, blue) were visualised by 4´,6-diamidino-2-phenylindole (DAPI). All channels were merged in B, without DIC in C.

αSMA is expressed in endothelial cells and myofibroblasts. The competency of the antibody to mark αSMA expressing cell types was tested on untreated dermal tissue.

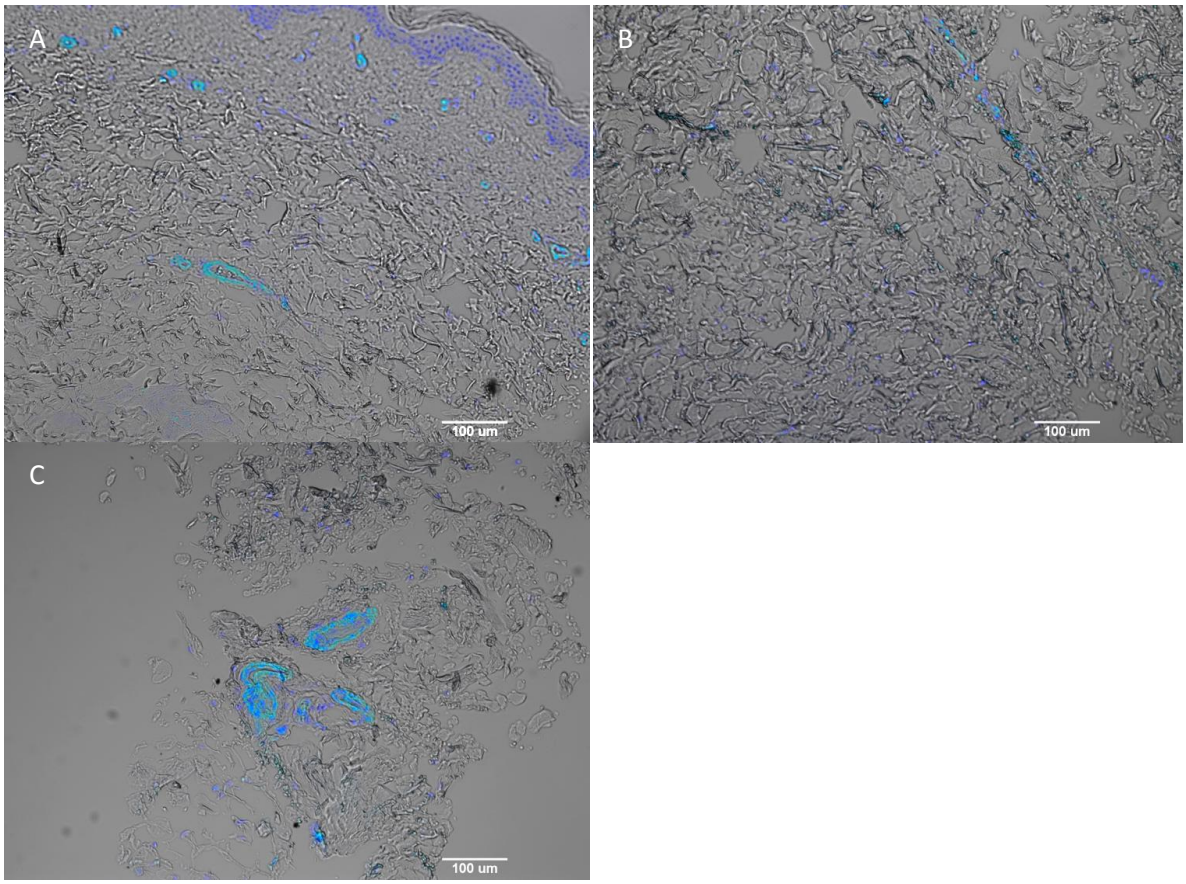

Figure 4.17A-C αSMA staining pattern of human skin. Immunofluorescence staining of epidermal/dermal (A), dermal (B) and subcutaneous (C) tissue revealed αSMA^{+} endothelial cells (light blue). Nuclei (blue) were visualised by 4´,6-diamidino-2-phenylindole (DAPI).

αSMA staining shows the typical pattern of papillary and subcutaneous plexi, vascularised subcutaneous tissue and confirmed competency of the antibody to recognise αSMA expressing cells (Figure 4.17).

To examine Sculptra® treated tissue on the abundance of myofibroblasts and vessel formation it was stained with a αSMA antibody.

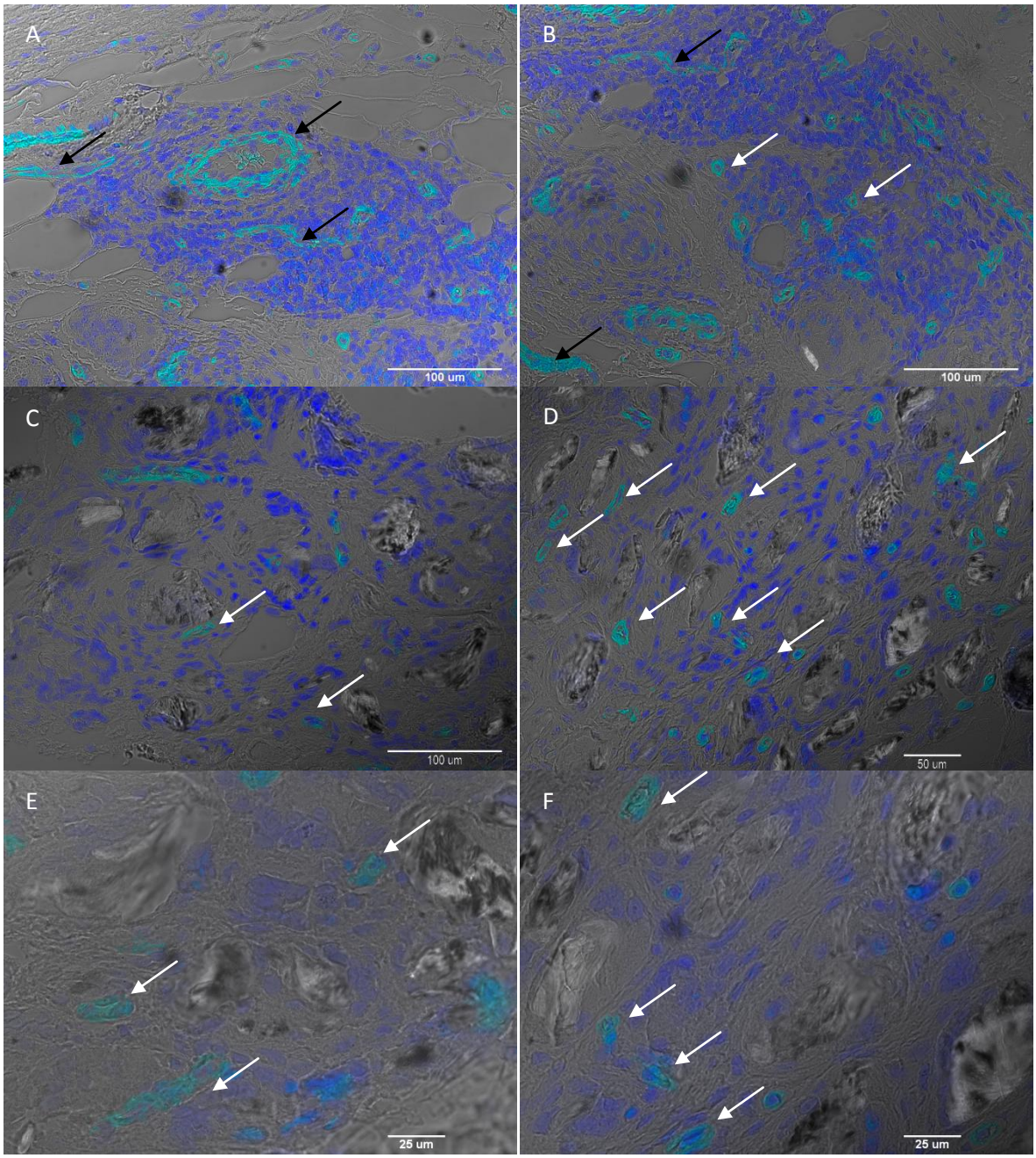

Figure 4.18A-F Sculptra® particle surrounding tissue revealed positive αSMA structures. Immunofluorescence staining of Sculptra® particle surrounding capsule tissue revealed αSMA positive vessel- (black arrow) and myofibroblast-like (white arrow) structures (light blue). Nuclei (blue) were visualised by 4´,6-diamidino-2-phenylindole (DAPI). (A-D) presents an overview of Sculptra® particle surrounding granulation tissue. (E-F) focuses on a few Sculptra® particles and surrounding cells.

αSMA staining of Sculptra® treated tissue shows stonger staining pattern in the granulation tissue. **Neovascularisation takes place and on a closer view myofibroblasts are differentiating in proximity to the Sculptra® particles (Figure 4.18).**

Additionally αSMA mRNA expression was tested (Figure 4.19).

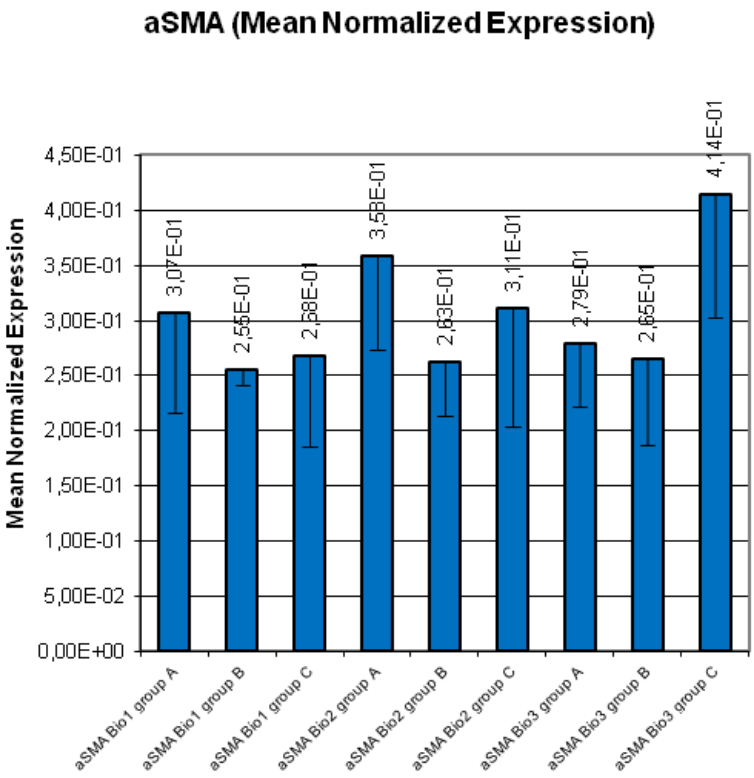

Figure 4.19 αSMA mRNA expression during course of study. The expression of αSMA mRNA is illustrated during different time points. The first three bars represent the mRNA expression of group A, B and C prior to any Sculptra® injection. Following four bars represent mRNA expressions two weeks after each Sculptra® injections for indicated groups. The second last bar represents mRNA expression 8 months and the last bar for 10 months after the last Sculptra® injection.

The first three bars represent αSMA mRNA expression of untreated tissue from group A, B and C. The expression varied between 0.26 and 0.31. Two weeks after the first Sculptra® injection the mRNA expression level increased up to 0.36 in group A. The following three biopsy time points were exactly two weeks after the next three Sculptra® injections at three months intervals. The expression varied between 0.26 and 0.31. For long term observation biopsies were taken 8 months (group B) 0.27 and 10 months (group C) 0.41 after the last Sculptra® injection. **In comparison to untreated tissue the αSMA mRNA expression was up-regulated two weeks after the first injection and fell immediately on the baseline level and stayed at the same level, until it rose 10 months after the last injection.**

αSMA staining indicated a new formation of vessel structures. For differentiation between blood- and lymph vessel endothelial cells commonly used markers CD31 and podoplain were applied for immunofluorescence staining. For testing the antibodies they were used on untreated dermal tissue.

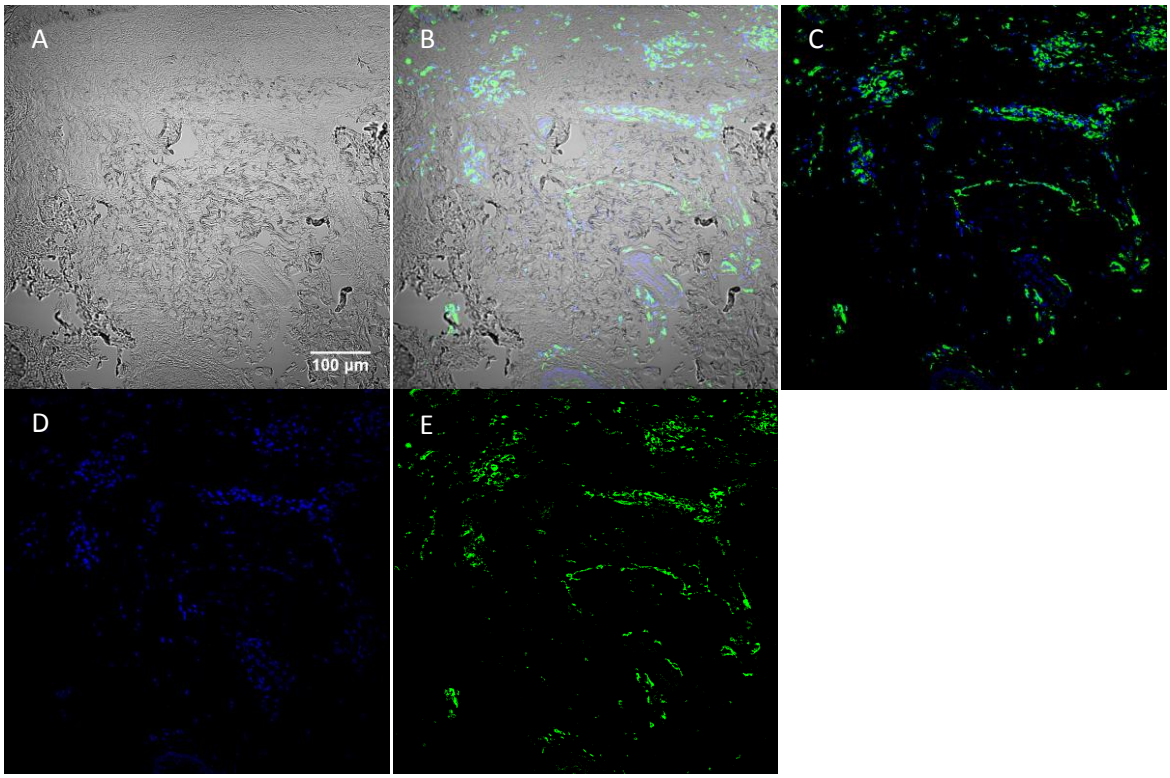

Figure 4.20A-E CD31 staining patern of untreated dermal tissue. Dermal tissue was visualised in DIC (A) view. Immunofluorescence staining of dermal tissue revealed CD31 positive structures (E, green). Nuclei (D, blue) were visualised by 4´,6-diamidino-2-phenylindole (DAPI). All channels were merged in B, without DIC in C.

CD31 antibody marks vessels structures und shows additionally a low scatterned staining pattern (Figure 4.20).

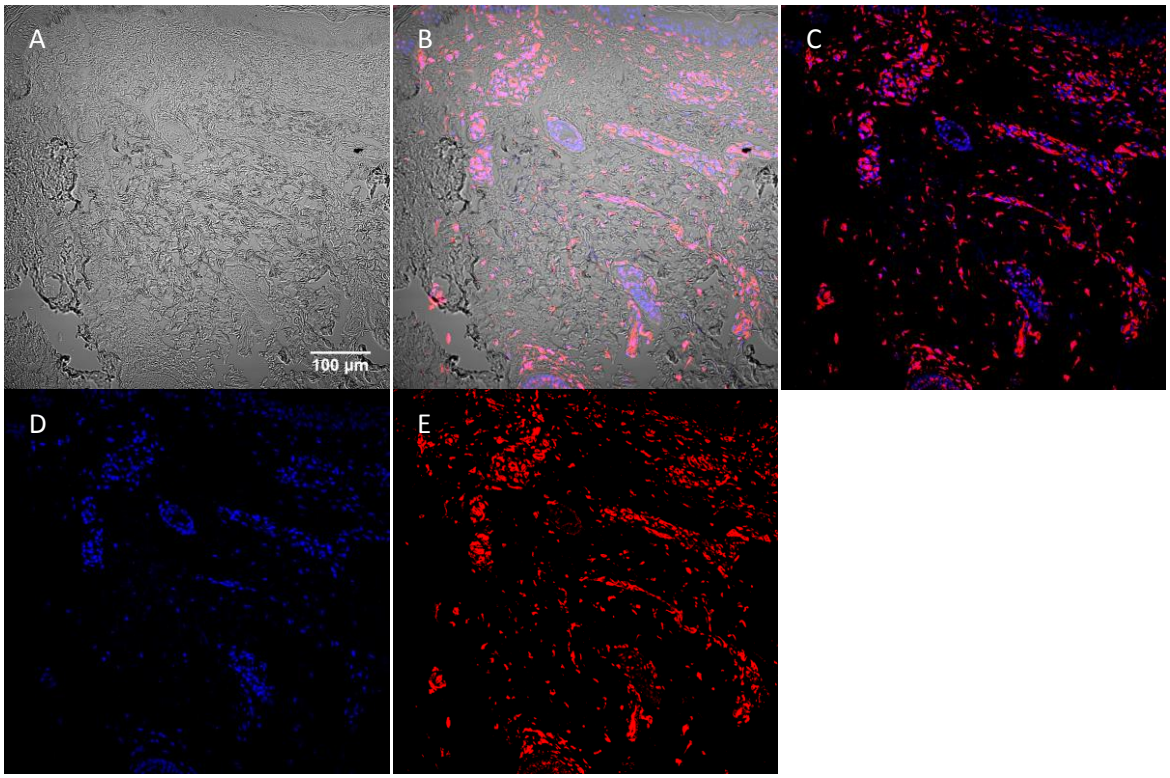

Figure 4.21A-E Podoplanin staining pattern of untreated dermal tissue. Dermal tissue was visualised in DIC (A) view. Immunofluorescence staining of dermal tissue revealed podoplanin positive structures (E, red). Nuclei (D, blue) were visualised by 4´,6-diamidino-2-phenylindole (DAPI). All channels were merged in B, without DIC in C.

Podoplanin marks vessel structures und shows additionally a remarkable scatterned staining pattern (Figure 4.21). Interestingly CD31 positve (Figure 4.20) and podoplanin positive (Figure 4.21) vessel structures resemble in consecutively sectioned tissue samples.

Sculptra® particle evoked granulation tissue was stained against CD31 and podoplanin to differentiate between blood- and lymphatic vessels.

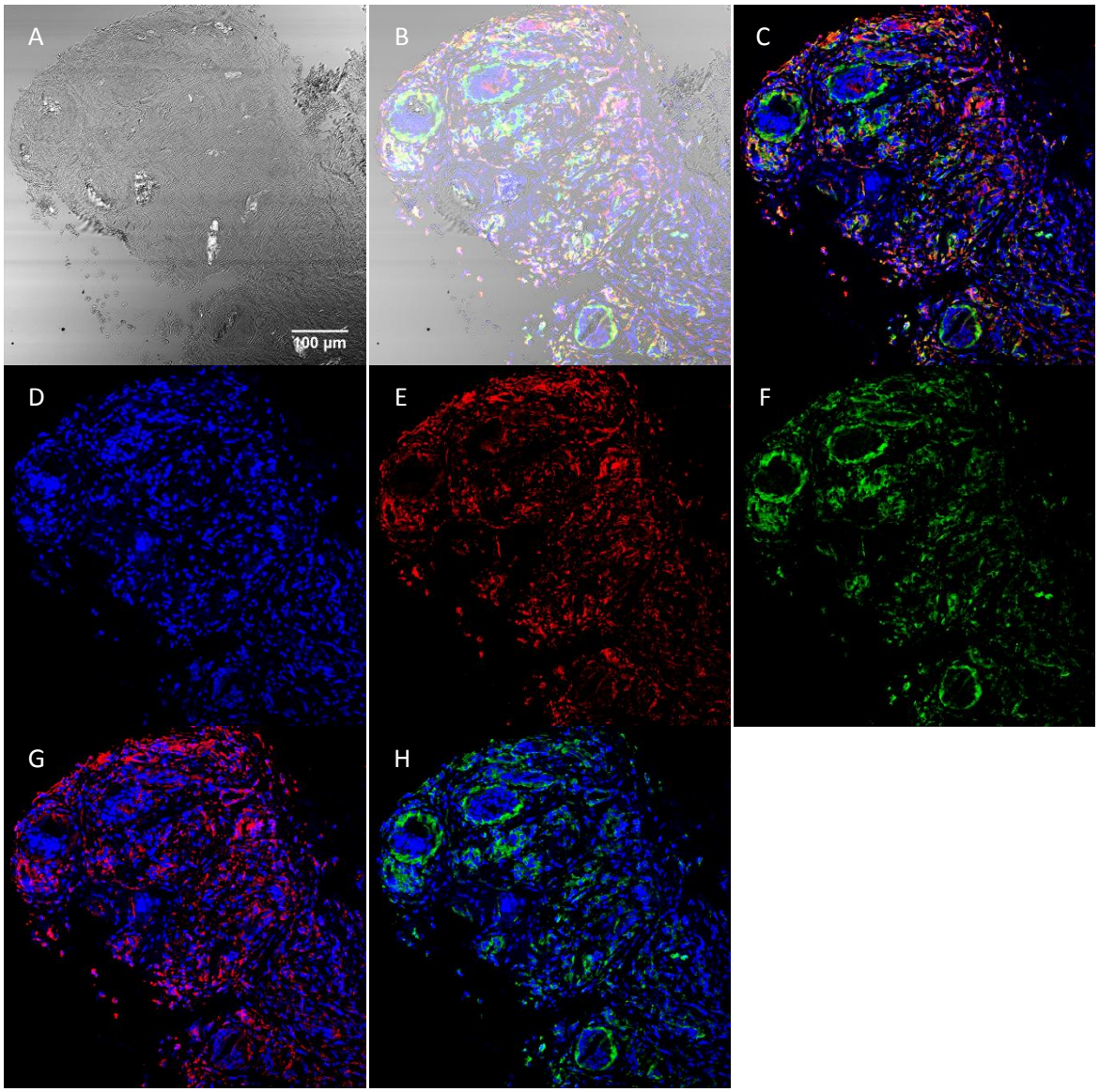

Figure 4.22A-I Attempt for differential illustration of blood- and lymph vessel structures in Sculptra® particle surrounding tissue. Sculptra® particles are surrounded by capsule tissue visualised in DIC (A) view. Immunofluorescence staining revealed in close proximity to Sculptra® particles CD31 (green, F) and podoplanin (red, E) positive structures. Nuclei (D, blue) were visualised by 4´,6-diamidino-2-phenylindole (DAPI). All channels were merged in B, without DIC in C. For differential consideration Channels E and D were merged in G; Channels F and D were merged in H.

Obviously CD31 staining was remakable around Sculptra® particles (Figure 4.22F). Podoplainin staining was more diffuse (Figure 4.22E). CD31 and podoplain staining did not reveal vessel like structures.

4.6 Fibroblasts encapsulate Sculptra® particles

The ideal dermal filler stimulates collagen neosynthesis in the injected tissue to correct volume loss changing tissue properties. (Myo-) fibroblasts were observed in the Sculptra®-treated tissue (cf. Figure 4.14; 4.18). Further, it is of interest to examine whether they produce collagen.

To test anti-human collagen type I and anti-human collagen type III antibodies, Sculptra® untreated tissue was stained by immunofluorescence. In figure 4.23 the distribution of collagen-type I and -type III is illustrated in the dermis.

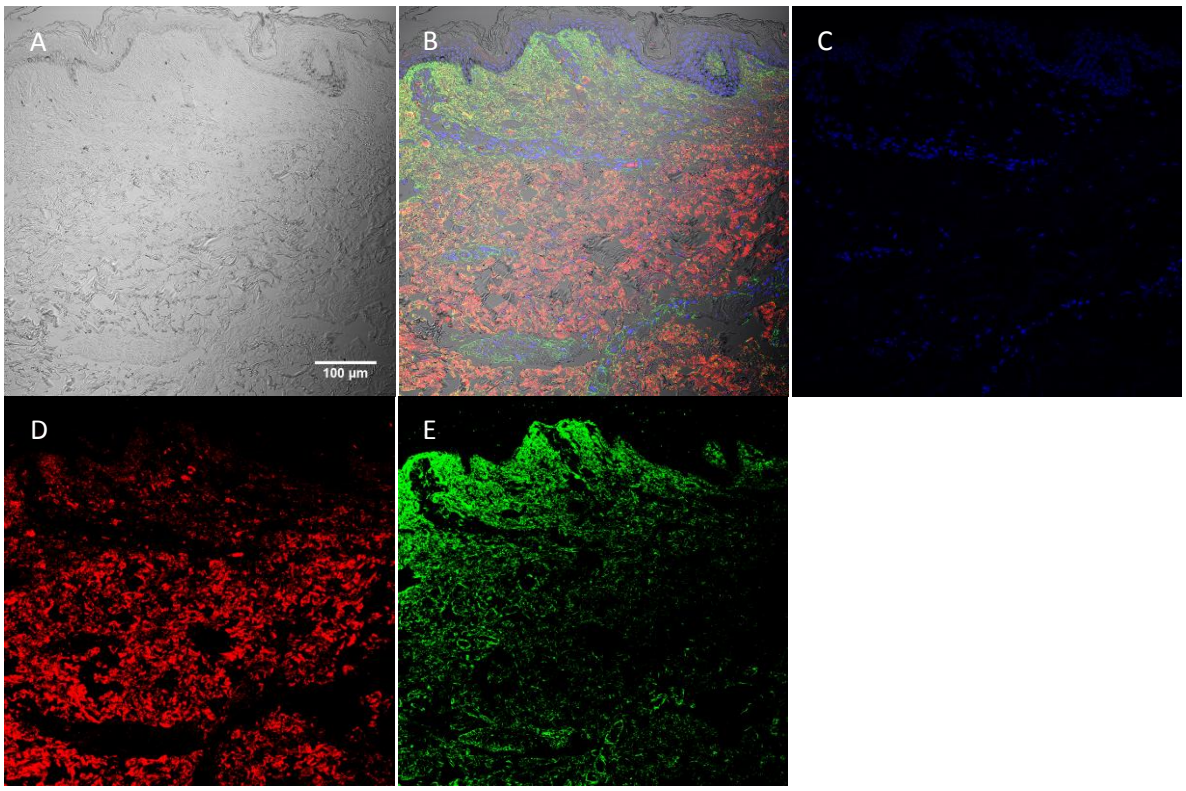

Figure 4.23A-E Collagen type I and collagen type III distribution of untreated human dermal tissue. Epidermal and dermal skin layers are visualised in DIC (A) view. Immunofluorescence staining of dermal tissue revealed collagen type I (D, red) and type III (E, green) distribution. Nuclei (C, blue) were visualised by 4´,6-diamidino-2-phenylindole (DAPI). B represents a merge of A, C, D and E.

Furthermore, Sculptra® treated tissue was stained against collagen type I and III.

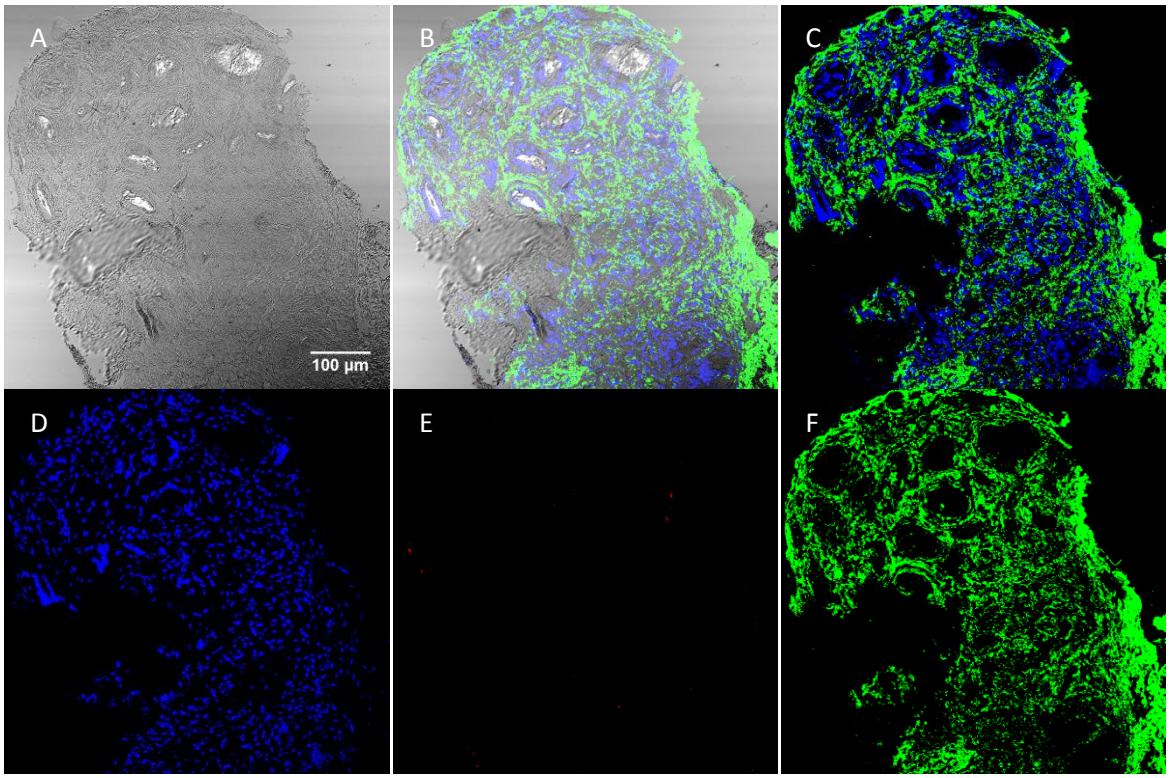

Figure 4.24A-F Collagen-encapsulation of Sculptra® particles. Sculptra® particles are surrounded by capsule tissue visualised in DIC (A) view. Immunofluorescence staining revealed substantial positive collagen type III signals (F) and no collagen type I signal (E). Nuclei (D, blue) were visualised by 4´,6-diamidino-2-phenylindole (DAPI). All channels were merged in B, without DIC in C.

Collagen type III was found in direct proximity of Sculptra® particles (Figure 4.24B; F). Collagen type I was not found to surround these particles (Figure 4.24E). However, collagen type I was found in the periphery of a given granuloma (Figure 4.25).

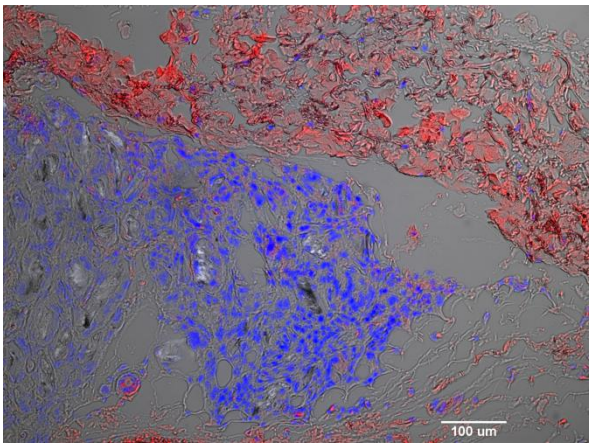

Figure 4.25 Collagen type I staining of Sculptra® granuloma surrounding tissue. Immunofluorescence staining of Sculptra® treated tissue revealed collagen type I positive fibres in capsule periphery. Nuclei (blue) were visualised by 4´,6-diamidino-2-phenylindole (DAPI).

While collagen type I protein is not expressed within a granuloma, mRNA expression analysis shows a strong up-regulation of collagen type I (Figure 4.26) in the biopsies.

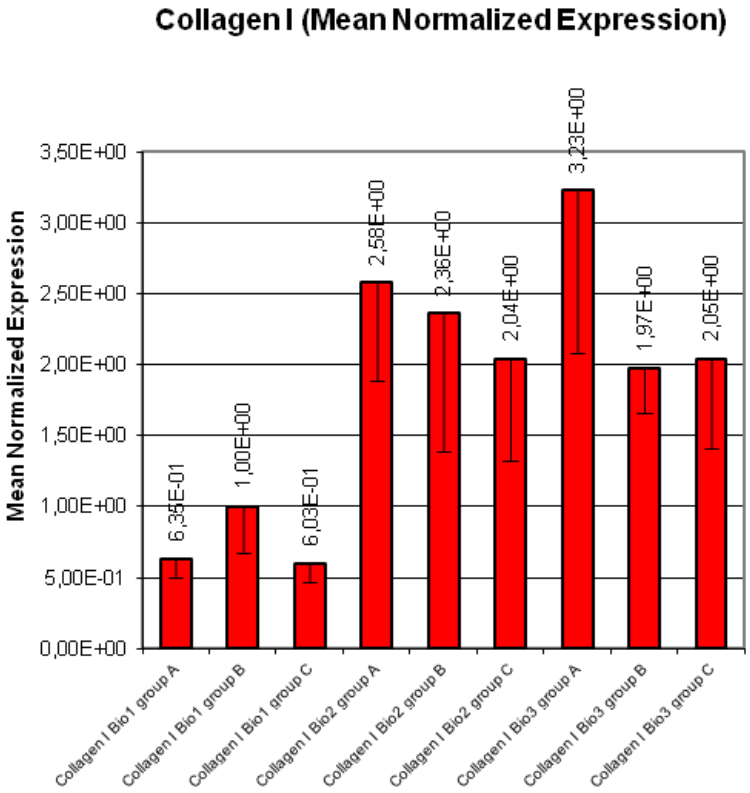

Figure 4.26 Collagen type I mRNA expression increased direcly after the first Sculptra® injection and stayed up regulated until the end of study. The expression of collagen type I mRNA is illustrated during different time points. The first three bars represent the mRNA expression of group A, B and C prior to any Sculptra® injection. Following four bars represent mRNA expressions two weeks after each Sculptra® injections for indicated groups. The second last bar represents mRNA expression 8 month and the last bar for 10 month after the last Sculptra® injection.

The first three bars represent collagen type I mRNA expression of untreated tissue from group A, B and C. The expression varied between 0.64 and 1. Two weeks after the first Sculptra® injection the mRNA expression level increased up to 2.58 in group A. The following three biopsy time points were exactly 2 weeks after the next three Sculptra® injections at three months intervals. The expression varied between 2.04 and 3.25. For long term observation biopsies were taken 8 months (group B) and 10 months (group C) after the last Sculptra® injection. Collagen type I mRNA expression was still elevated (1.97 and 2.05). **In comparison to untreated tissue the collagen type I mRNA expression was increased after the first injection and remained on an elevated level until 10 month after the last injection.**

Furthermore, the mRNA Expression of collagen type III was analysed (Figure 4.27).

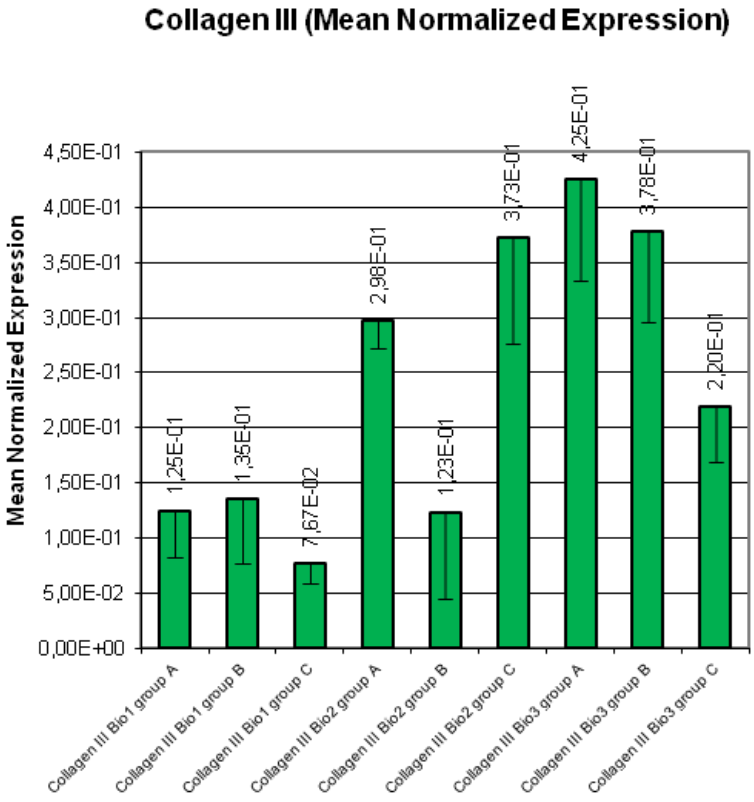

Figure 4.27 Collagen type III mRNA expression increased directly after the first Sculptra® injection and stayed up regulated until the end of study. The expression of collagen type III mRNA is illustrated during different time points. The first three bars represent the mRNA expression of group A, B and C prior to any Sculptra® injection. Following four bars represent mRNA expressions two weeks after each Sculptra® injections for indicated groups. The second last bar represents mRNA expression 8 month and the last bar for 10 month after the last Sculptra® injection.

The first three bars represent collagen type III mRNA expression of untreated tissue from group A, B, C. The expression varies between 0.08 and 0.14. Two weeks after the first Sculptra® injection the mRNA expression level increased to 0.3 in group A. Two weeks after the second Sculptra® injection the mRNA expression level decreased to 0.12 in group B. The following two biopsy time points were exactly two weeks after the next two Sculptra® injections at three months intervals. The expression varied between 0.37 and 0.43. For long term observation biopsies were taken 8 months (group B) 0.38 and 10 months (group C) 0.22 after the last Sculptra® injection. Collagen type III mRNA expression was still elevated. **In comparison to untreated tissue the collagen type III mRNA expression was increased after the first injection, decreased after the second injection in group B, increased after the third injection and remained on an elevated level until 10 month after the last injection.**

Fibroblasts encapsulate Sculptra® particles with collagen typ III, whereas collagen type I is found in the periphery of the tissue reaction. Further, colagen type I and III mRNA expression is up-regulated.

Decorin is a prominent proteoglycan in the human dermis and interacts with collagen. Therefore the mRNA Expression of decorin was analysed (Figure 4.28).

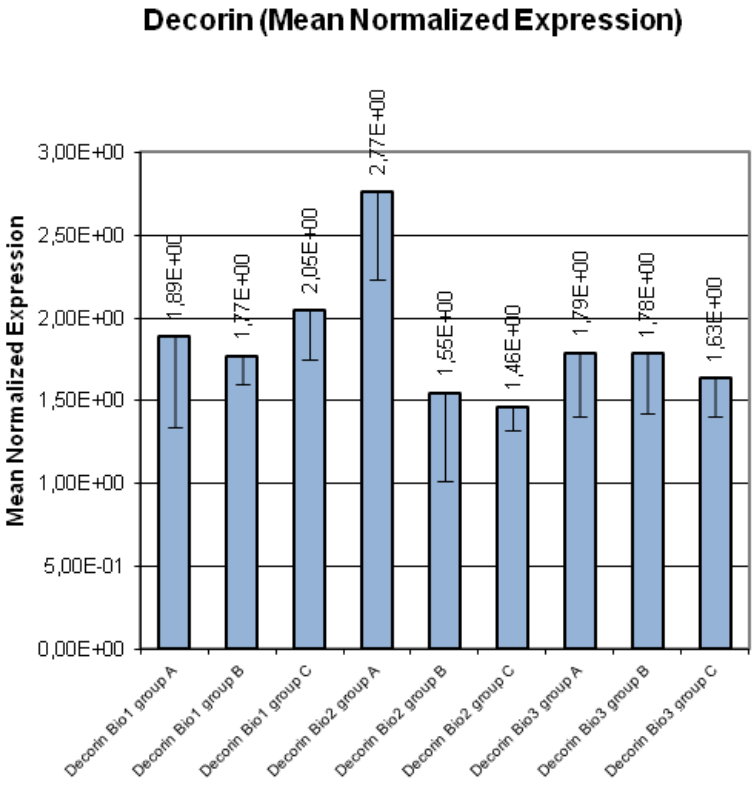

Figure 4.28 Decorin mRNA expression was only increased directly after the first Sculptra® injection, dropped and stayed on the level of the beginning. The expression of decorin mRNA is illustrated during different time points. The first three bars represent the mRNA expression of group A, B and C prior to any Sculptra® injection. Following four bars represent mRNA expressions two weeks after each Sculptra® injections for indicated groups. The second last bar represents mRNA expression 8 month and the last bar for 10 month after the last Sculptra® injection.

The first three bars represent decorin mRNA expression of untreated tissue from group A, B and C. The expression varied between 1.89 and 2.05. Two weeks after the first Sculptra® injection the mRNA expression level increased up to 2.77 in group A. The following three biopsy time points were exactly two weeks after the next three Sculptra® injections at three months intervals. The expression varied between 1.46 and 1.79. For long term observation biopsies were taken 8 months (group B) 1.78 and 10 months (group C) 1.63 after the last Sculptra® injection. **In comparison to untreated tissue the decorin mRNA expression was only elevated after the first Sculptra® injection.**

The activity of MMPs is fine tuned by the TIMPs. Therefore, the mRNA Expression of TIMP was analysed (Figure 4.29).

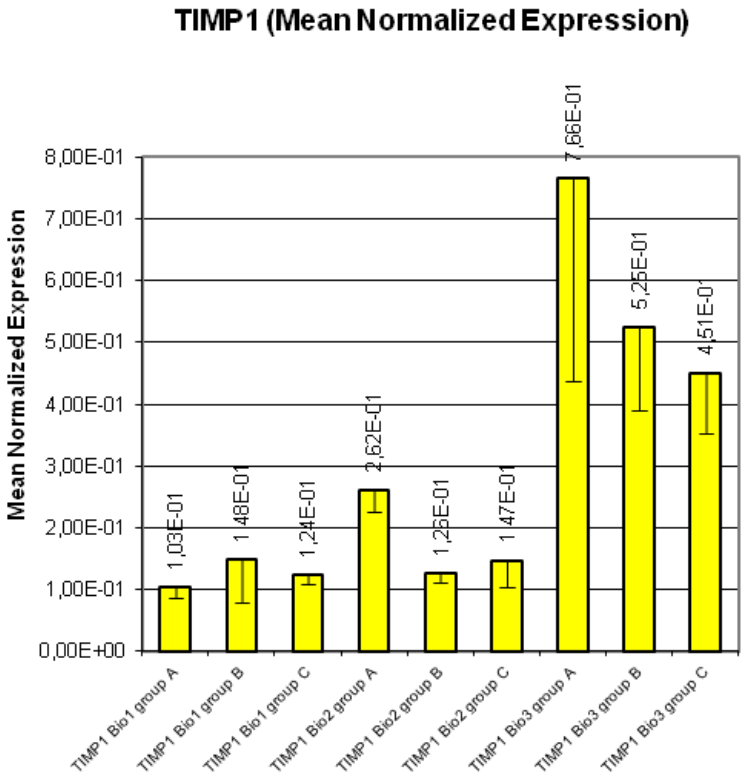

Figure 4.29 TIMP1 mRNA expression increased slightly after the first and massive after the fourth Sculptra® injection and stayed up regulated until the end of study. The expression of TIMP1 mRNA is illustrated during different time points. The first three bars represent the mRNA expression of group A, B and C prior to any Sculptra® injection. Following four bars represent mRNA expressions two weeks after each Sculptra® injections for indicated groups. The second last bar represents mRNA expression 8 month and the last bar for 10 month after the last Sculptra® injection.

The first three bars represent TIMP1 mRNA expression of untreated tissue from group A, B and C. The expression varied between 0.1 and 0.15. Two weeks after the first Sculptra® injection the mRNA expression level increased up to 0.26 in group A. During the following two biopsy time points were exactly two weeks after the next two Sculptra® injections at three months intervals. The expression droped and varied between 0.13 and 0.15. Two weeks after the fourth Sculptra® injection the expression increased massively to 0.77. For long term observation biopsies were taken 8 months (group B) 0.53 and 10 months (group C) 0.45 after the last Sculptra® injection. **In comparison to untreated tissue the TIMP1 mRNA expression increased slightly after the first Sculptra® injection, massively after the fourth injection and was still elevated until the end of the study.**

4.7 mRNA expression of growth factors

Several growth factors and cytokines are responsible for the recruitment, proliferation, differentiation and activity of cells. Therefore mRNA expression of collagen metabolism related TGFß1 (Figure 4.30), PDGFB (Figure 4.31) and CTGF (Figure 4.32) were analysed.

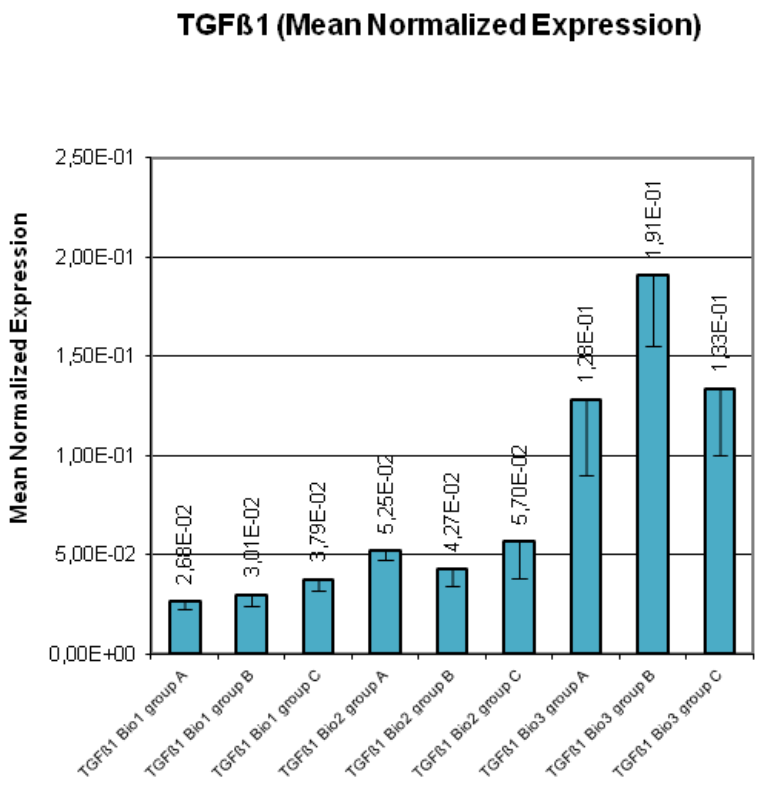

Figure 4.30 TGFß1 mRNA expression increased slightly after the first Sculptra® injection and is remarkable enhanced till the end of the study. The expression of TGFß1 mRNA is illustrated during different time points. The first three bars represent the mRNA expression of group A, B and C prior to any Sculptra® injection. Following four bars represent mRNA expressions two weeks after each Sculptra® injections for indicated groups. The second last bar represents mRNA expression 8 month and the last bar for 10 month after the last Sculptra® injection.

The first three bars represent TGFß1 mRNA expression of untreated tissue from group A, B and C. The expression varied between 0.027 and 0.038. Two weeks after the first Sculptra® injection the mRNA expression level increased slightly up to 0.053 in group A. During the following two biopsy time points were exactly two weeks after the next two Sculptra® injections at three months intervals. The expression varied between 0.043 and 0.057. Two weeks after the fourth Sculptra® injection the expression increased massively to 0.128. For long term observation biopsies were taken 8 months (group B) 0.191 and 10 months (group C) 0.133 after the last Sculptra® injection. **In comparison to untreated tissue the TGFß1 mRNA expression increased slightly after the first Sculptra® injection, massively after the fourth injection and was still elevated until the end of the study.**

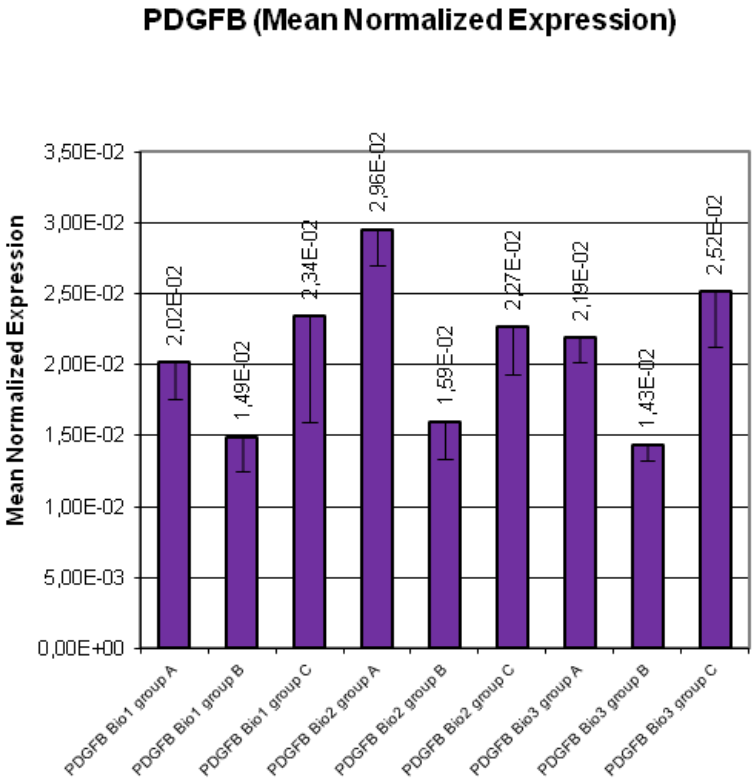

Figure 4.31 PDGFB mRNA expression increased slightly after the first Sculptra® injection and is remarkable enhanced till the end of the study. The expression of PDGFB mRNA is illustrated during different time points. The first three bars represent the mRNA expression of group A, B and C prior to any Sculptra® injection. Following four bars represent mRNA expressions two weeks after each Sculptra® injections for indicated groups. The second last bar represents mRNA expression 8 month and the last bar for 10 month after the last Sculptra® injection.

The first three bars represent PDGFB mRNA expression of untreated tissue from group A, B and C. The expression varied between 0.015 and 0.023. Two weeks after the first Sculptra® injection the mRNA expression level increased to 0.03 in group A. The following three biopsy time points were exactly two weeks after the next three Sculptra® injections at three months intervals. The expression varied between 0.016 and 0.023. For long term observation biopsies were taken 8 months (group B) 0.014 and 10 months (group C) 0.025 after the last Sculptra® injection. **In comparison to untreated tissue the PDGFB mRNA expression was up-regulated two weeks after the first injection, dropped after the second injection, increased after the third injection, decreased after 8 month after the last injection and was enhanced 10 month after the last injection.**

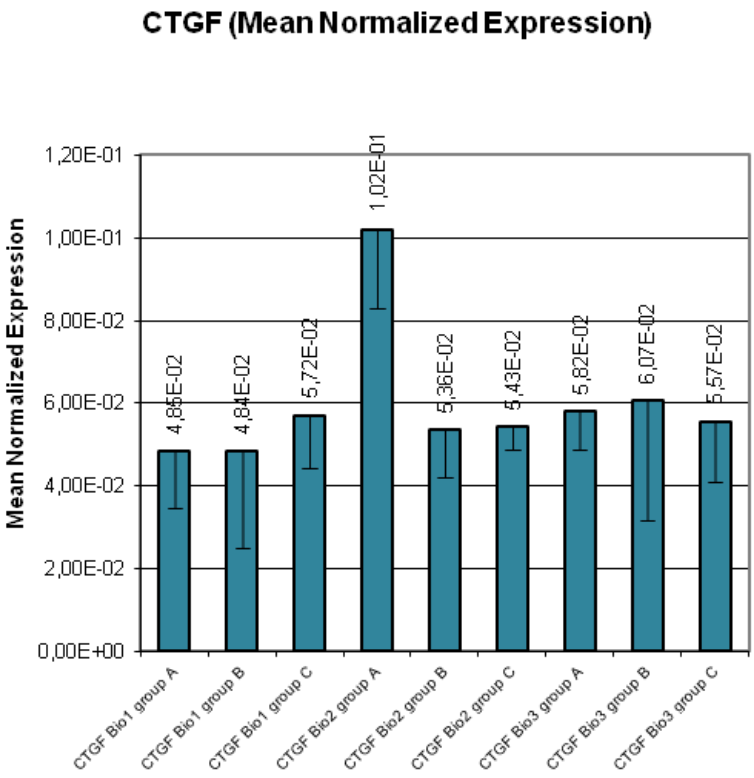

Figure 4.32 CTGF mRNA expression was only increased directly after the first Sculptra® injection, dropped and stayed on the level of the beginning. The expression of CTGF mRNA is illustrated during different time points. The first three bars represent the mRNA expression of group A, B and C prior to any Sculptra® injection. Following four bars represent mRNA expressions two weeks after each Sculptra® injections for indicated groups. The second last bar represents mRNA expression 8 month and the last bar for 10 month after the last Sculptra® injection.

The first three bars represent CTGF mRNA expression of untreated tissue from group A, B and C. The expression varied between 0.048 and 0.057. Two weeks after the first Sculptra® injection the mRNA expression level increased up to 0.102 in group A. The following three biopsy time points were exactly two weeks after the next three Sculptra® injections at three months intervals. The expression varied between 0.054 and 0.058. For long term observation biopsies were taken 8 months (group B) 0.061 and 10 months (group C) 0.056 after the last Sculptra® injection. **In comparison to untreated tissue the CTGF mRNA expression was up regulated two weeks after the first injection and dropped after the second injection on the level of untreated tissue.**

Supplement to privous expression analysis:

Pior to real-time PCR it was essential to find spicific primer pairs for the genes of interest. Here, an exemplary agarose gel is displayed after separating DNA fragments synthesised in a PCR with designed TGFß1 or Col1A1 primer pairs (Figure 4.33). Red marked bands were cut out, DNA extracted and sequenced by Seqlab (Göttingen). Sequenced DNA segments coincide with the corresponding sequences published by NCBI (Figure 7.1;7.2).

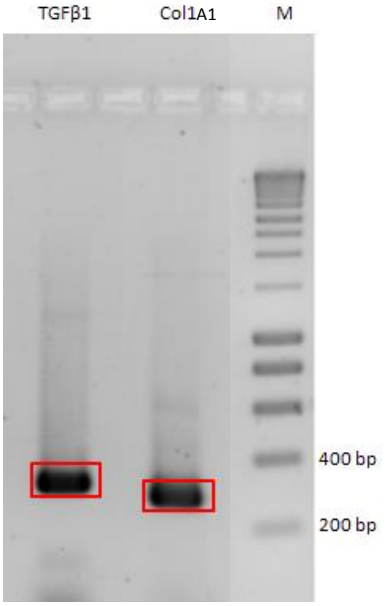

Figure 4.33 Designed primer pairs were employed to synthesise specific PCR products. PCR products (TGFß1 and Col1A1) were mixed with gel loading buffer and subsequently DNA fragments were separated by agarose gel electrophoresis. DNA fragments were stained by ethidium bromide, visualised and documented by VersaDoc.

PCR products, synthesised during real-time PCR, were checked by melting curve analysis (7.3). Thus melting curves were single peaked at relevant melting temperatures, PCR products were judged to be specific.

4.8 Sculptra® does not impair collagenase activity

A possible effect of Sculptra® on collagenase activity was determined *in vitro*. Collagenase activity was calculated at 0.843 U/ml and the specific activity at 0.337 U/mg. In the presence of Sculptra® collagenase specific activity slightly dropped to 0.324 U/mg. **Sculptra® does not exert a crucial inhibitory effect on collagenase activity.**

5. Discussion

5.1 Upper arm augmentation

Facial rejuvenation with Sculptra® has been approved for many years and clinical studies have demonstrated successful augmentation [74-77]. A few publications have reported successful extrafacial rejuvenation of the dorsal hand, intercostal spaces, *stria distensae*, chest wall deformities after breast reconstruction, buttocks and the neck and chest [81-84]. Postmenopausal women tend to suffer from upper arm sagging. Besides a genetic predisposition for dysmorphism, the course of aging and atrophy of musculature and fascia systems are responsible for these alterations [61]. The attempt to use Sculptra® for rejuvenation of the aged upper arm is understandable. However, in contrast to facial augmentation and the above-mentioned examples of the successful extrafacial use of Sculptra®, before and after photos of treated upper arms in the present study revealed no changes in shape or structure during the study course (compare Figure 4.1A, B with 4.2A, B). The lack of visible augmentation may be due to the total amount of material injected. Each upper arm of the 21 volunteers was injected four times at three month intervals with 150 mg PLLA in a 10 ml dilution (total 600 mg PLLA/upper arm). The application of at least two vials of Sculptra® (300 mg PLLA) per cheek (about 50 cm^2) is recommended, distributed over 3-4 visits to augment the face. Throughout the present study, four vials of Sculptra® (600 mg PLLA) were injected into each upper arm (about 190 cm^2). Extrapolating the amounts of Sculptra® applied per cm^2 upper arm, it can be suggested that, compared to the face, only half of the amount was injected into each upper arm. The disposition of Sculptra® was limited by the initial sponsor of the study. Schulman *et al.* 2008 administered a total of 8x150 mg PLLA (2 vials Sculptra®/visit in four one month intervals) to correct a chest wall deformity after breast reconstruction [83]. Lorenc (2012) augmented buttocks during two treatments using 150 mg PLLA in 12 ml dilutions per buttock and session [81]. Mazzuco and Hexsel (2009) rejuvenated necks and chests during an average number of 1.8 sessions per patient and an average total dose of 7.13 ml (109.5 mg) 1:10 dilution (range 4-18.5 ml) per patient [84]. Schell (2006) rejuvenated a dorsal hand with two treatments with a one-quarter vial of Sculptra® (1:10) 75 mg PLLA, intercostal and peristernal depression with one vial of Sculptra® (1:10) 150 mg PLLA [82]. Taken together, various parts of the integument have been augmented with PLLA. However, a systematic study is not available so far. Despite the previously mentioned studies, describing successful extrafacial Sculptra® augmentation, it is not possible to approximate the amount of PLLA necessary for upper arm augmentation Taking the dimension of volume to be augmented into consideration, the study of Schulman *et al.* 2008 might be the most suitable. Furthermore, in general, smaller amounts of Sculptra® are necessary to augment the face; hence, facial tissue is comprised of fine subcutaneous fat pads distributed in independent anatomical departments [57]. Higher amounts are necessary to augment more prominent volume deficiencies. In comparison to the other mentioned locations, the tissue structure of the upper arm differs. With aging, besides the atrophy of the *facia brachialis* and *retinacula cutis,* the more distinct atrophy of the prominent musculature and fat tissue contributes to the more pronounced arm

deformity. Independent subcutaneous fat pads, as known to exist in the face, are not part of the physiological anatomy of the upper arm. Further, quite a few postmenopausal women gain weight, which contributes to the arm circumference. Non-invasive measures for documentation, such as arm circumference and skin structure, depend very much on the position of the arm and tightening of measuring device and are therefore open to influence. For that reason, these measures have been avoided in the clinical part of the study.

Health-related quality of life has gained substantial interest in most fields of medicine. Several studies have shown that many skin conditions may correlate with a markedly reduced quality of life [190]. To evaluate whether the volunteers' quality of life changes during Sculptra® treatment, FLQA-k questionnaires provided by Prof Augustin were employed. Values of the topics: "hiding the own body", "dissatisfaction of the outer appearance" and "cosmetic efforts" slightly decreased until the end of the study (Figure 4.3). This implies that volunteers had a slightly reduced desire to hide their own body, were less dissatisfied with their outer appearance and spent less effort on cosmetics. The value for the topic "avoiding contact" was slightly increased, revealing that volunteers were less interested in contact. The value for the topic "skin problems" decreased to the end of the study, implying that volunteers were more satisfied with their skin.

In general the subjective well-being of the volunteers, with special focus on their skin and outer appearance, did not really improve. Taking the more objective photo documentation into consideration, Sculptra® treatments of the upper arm did not improve the volunteers' quality of life. The applicability of Sculptra® to augment the upper arms of postmenopausal women could not be documented by employing this particular set up of volunteer selection, treatment course and documentation.

5.2 The development of palpable nodules

The incidence of Sculptra®-evoked palpable nodule formation varies considerably in the literature: Denoted incidences were raised in studies which included individuals with I) different immune statuses, II) different treatment locations, III) different dilutions and IV) different injection techniques. However, over the years in general, the formation of subcutaneous nodules could be roughly limited from formally 44% in 2003 [87] to the present level of 18.15%-2.8% [74, 76-78, 198] by optimising its dilution factor and the injection techniques [199].

Here, one vial (150 mg PLLA) was dissolved in 10 ml dH_2O and xylocaine, which reflects the current recommendation for dilution. In this prospective study on extra-facial tissue augmentation, 28% of PLLA-treated volunteers (6 of 21) developed palpable nodules in the ventral aspect of the upper arm. More precisely, 2 volunteers developed nodules in the first month and 4 volunteers developed late-onset nodules corresponding to former findings [79-80]. No further studies on the employment of Sculptra® to augment upper arms have been published. Therefore, the incidence of nodule formation on upper arm tissue has not been studied so far. Hence, the recommended high dilution of Sculptra® and subcutaneous injections were administered; the incidence of nodule formation seems to be relatively high.

Emphasising that nodule formation not only depends on the applied dilution of Sculptra®, but also on the applied location, injection technique and on the immune status of a given individual, it is indeed difficult at that point to enunciate a recommendation on how to use Sculptra® for augmentation of the upper arm.

5.3 Sculptra® injections lead to sonographic detectable subcutaneous tissue changes

In recent years, sonography has been successfully applied to characterise fillers and filler-treated dermal/subcutaneous tissues. Schelke *et al.* (2010) examined various fillers, including PLLA and HA, employing a 13 MHz probe [86]. Injected HA was less reflective than the surrounding tissue and visible as a fairly distinct hypoechogenic lesion with some hyperechogenic reflections. Wortsman *et al.* (2012) confirmed these findings, reporting about subcutaneous hypoechoic pseudocysts with numerous echoes by using a probe with variable frequencies (7-15 MHz) [200]. Furthermore, they observed progressively smaller filler depots over time, until they were undetectable after 6 months. Grippaudo and Mattei (2010) used a 10-13 MHz probe, attested similar findings and reported about HA, revealing a well-defined regular hypoechoic mass in the subcutaneous tissue without internal echoes, comparable to collagen filler [201]. Sonographic patterns of permanent fillers such as polyacrylamide and polyalkylimide show a hyperechoic mass. Wortsman *et al.* (2012) concluded that synthetic fillers generally generate stronger echoes (hyperechogenicity) and different predominant posterior artefacts; for example, silicone appears to be mostly associated with sound scattering, polymethylmethacrylate with reverberance and calcium hydroxyapatite with shadowing, indicating absorption of the ultrasound waves [200].

Sonography was employed as an objective measure to document the effect of Sculptra® on subcutaneous tissue (Figure 4.5). Upon comparison of baseline (t0) with 20 month (t2) values of either arm, a highly significant decrease of echogenicity was determined. Furthermore, a highly- and significant decrease of echogenicity for the right and left arm from t0 to t1 was found. There was no significant change in echogenicity documented between t1 and t2. Upon comparison of both treated sides, the echogenicity was comparable. The absence of significant changes between t1 and t2 may be due to no further PLLA-injections during that time period or a shorter timespan between the measured points. Taking the results of mRNA expression of collagen type I and III into consideration, both expressions showed their maximum 10 months after the first injection (Bio 3 group A), corresponding to t1 in sonography. Thus most prominent (significant) changes took place prior to this time point.

Heterogeneous echo patterns reflect tissue structures with different sound conduction properties. Homogeneous echo patterns, however, reflect tissue structures with comparable sound conduction properties. The echogenicity of Sculptra®-treated subcutaneous tissue decreased significantly, reflecting a more homogenous echo pattern and thus a more homogeneous subcutaneous tissue. This effect may be due to the increased deposition of collagen type I and III in the treated area.

To my knowledge, this is the first time a 22 MHz probe has been applied to examine Sculptra® treated tissue, and it seems better suited to this kind of investigation of tissue changes, than a 13 MHz probe used for example by Schelke *et al.* (2010) [86] or a multi-frequency 7.5-13 MHz probe by Valantin *et al.* (2003) [87]. Using those probes, no changes in echogenicity patterns could be detected after PLLA application, only the increased distance between the skin and underlying bony surfaces due to its augmenting effect on total cutaneous thickness. Especially in combination with the measuring tool in the DUB software, Sculptra®-induced tissue changes are detectable non-invasively due to a decrease in echogenicity over time, even though these tissue changes might not be obvious at first sight. Furthermore, these measures do not depend on nearby bony surfaces.

At this point, sonography employing a 22 MHz ultrasonic probe might not only allow objective documentation of subcutaneous tissue changes during a long-term treatment course, but will also justify repetitive treatments over a longer time period in patients fostering unrealistic expectations. A 22 MHz ultrasonic probe provides a higher resolution, enabling a more detailed illustration of dermal and subcutaneous structures. The DUB software enables a detailed assessment of the echogenicity in specific areas.

5.4 PLLA particles still present 28 months after the last injection causing FBR

Complete degradation of PLLA particles within 9 months or 30 months after Sculptra® injections has been assumed by Lemperle *et al.* (2003) and Vleggaar and Bauer (2004) [92-93], respectively. In contrast, in the present study, 38% of Sculptra®-treated volunteers revealed PLLA particles in the biopsies taken. Upon polarised light microscopy, every PLLA-positive tissue correlated with the picture of a foreign body reaction (Figure 4.7A-D). Furthermore, even 28 months after the last Sculptra® injection, an abundance of particles was detected in one biopsy (Figure. 4.8A-H). These findings contrast those of Lemperle *et al.* (2003) and Vleggaar and Bauer (2004) [92-93]. Matching particle shapes and sizes in our study at 28 months with those 10 months after the last injection, no significant changes were detectable. Therefore, PLLA-degradation within months is unlikely, at least not in every individual. At this point, it should also be taken into consideration that tissue biopsies may not always meet PLLA-injected depots. In this study, Sculptra®-injections and further biopsies were carried out adjacent to the scar of the initial biopsy of untreated tissue. In spite of that, PLLA particles were found first in biopsies of one individual after the second injection and more often only after the fourth injection in tissues of 8 individuals; the higher the number of injections, the higher the likeliness of finding PLLA-depots by biopsy. Here, in 62% of cases, the biopsies did not contain PLLA. Hence, the biopsies were taken 2 weeks after the injections, and assuming an impossible PLLA-degradation within that time frame, the biopsies most likely did not meet the PLLA depot despite biopsy alignment to the initial scar. Therefore, perhaps neither Lemperle *et al.* (2003) nor Vleggaar and Bauer (2004) [92-93] met a given PLLA depot 9 months or 30 months after the Sculptra® injections, respectively. Reszko *et al.* (2009) confirmed upon light microscopy the presence of PLLA 3 years after the injection in one case report [80]. This finding is in alignment with the present study and allows the assumption that PLLA particles are degraded in a much slower manner

than previously assumed. However, at this point, interindividual metabolic differences must also be taken into consideration; hence, it is unclear whether some individuals degrade PLLA faster than others.

5.5 The biological basis for Poly-L-Lactic acid-induced augmentation

Upon light microscopy, foreign body granulomas with numerous FBGCs were detectable around birefringent PLLA particles. In general, foreign body reactions to foreign material comprise one of three succeeding events; namely I) host protein absorption, II) cell recruitment and III) fibrotic encapsulation [97]. Depending on the host protein absorption, different immune cells are recruited and interact; for instance, macrophages binding *via* integrin receptors. Macrophages release cytokines like TGFß1, CTGF, PDGF and GM-CSF, guiding and activating more cells. Furthermore, macrophages fuse to FBGCs when they fail to phagocytise the foreign body. Attracted through TGFß1 and PDGF, fibroblasts reach the foreign material. Together with CTGF, TGFß1 and PDGF act as mitogens for fibroblasts. Fibroblasts by themselves produce TGFß1 and PDGF. Therefore, macrophages and fibroblasts are under autocrine and paracrine communication. TGFß1 stimulates fibroblasts to produce ECM, especially collagen, and to further differentiate into myofibroblasts. Myofibroblasts are characteristic of granulation tissue [175] and synthesise more collagen type III than type I. Macrophages and fibroblasts also release MMP and TIMP. Both proteins influence the balance of ECM turnover and that of the collagen metabolism. Neo-vascularisation of fibrotic tissue is common. To confirm those foreign body reactions to PLLA, the cell infiltrate of PLLA-treated tissue was characterised by immunofluorescence staining.

Here, $CD68^+$ cells were found to be in direct interaction with PLLA particles and in a second, more distant cell layer, $CD90^+$ cells (Figure 3.16A-F). CD68 and CD90 (Tyr-1) are established markers for macrophages and fibroblasts, respectively, and were tested successfully previously on spleen (Figure 4.9A-D) and fresh scar (Figure 4.12A-E) tissue, serving as positive controls. Both antibodies were additionally applied to untreated skin tissue to estimate the normal staining pattern (Figure 4.10A-C; 4.13A-B). Higgins *et al.* (2009) detected $F4/80^+$ (mouse equivalent to CD68) macrophages, surrounding a first row of nylon meshes in mice [184], while Klinge *et al.* (2014) found more than 80% of $CD68^+$ cells in human explant meshes [185]. Macrophages polarise in response to a given stimulus into different subpopulations with different phenotypes and functions. Song *et al.* (2000) illuminated the difference between TNFα-/IFN-γ- and IL-4-induced subpopulations of macrophages and the regulatory mechanisms controlling fibrogenesis, by performing fibroblast-macrophage co-cultures: IL-4-induced, alternatively activated macrophages stimulate fibroblast and collagen synthesis, whereas LPS/IFN-γ-induced, classically activated macrophages markedly reduce collagen production of fibroblasts [147]. Furthermore, mRNA and protein expression of TGFß1, PDGFAA and PDGFBB were elevated in alternatively activated macrophages. Classically activated macrophages exhibited enhanced mRNA and protein expression of TNFα and MMP-7. Kou and Babensee (2010) summarised different primary polarisation types of macrophages [129]. Macrophages acquire into classically activated macrophages (M1) upon danger signals like microbial component LPS and TH1-

derived cytokine IFN-γ. These macrophages kill pathogens by the release of reactive nitrogen and oxygen species. Furthermore, M1 produce the pro-inflammatory cytokines TNFα, IL-12, IL-1, IL-6 and IL-23. Macrophages, stimulated by Th2-derived cytokines IL-4 and IL-13, polarise into alternatively activated macrophages (M2a). These macrophages produce anti-inflammatory cytokines like IL-10 and collagen precursor polyamine and fuse to FBGCS to encapsulate foreign bodies. Macrophages bound to immune complexes differentiate into the M2b phenotype, synthesising IL-10, pro-inflammatory cytokines, TNFα, IL-1, IL-6 and reactive nitrogen and oxygen species. IL-10 induces the M2c phenotype to produce more IL-10 and TGFß1 induces fibrosis.

Here, CD68-staining revealed an abundance of macrophages in close proximity to PLLA particles (Figure 4.11A-B; 4.16A-F). The macrophage phenotype was not determined; however, according to the current literature, M2a and M2c phenotypes are most likely involved. The transition of the earlier dominant M2a to the later dominant M2c type is most likely. This hypothesis would not only explain the early up-regulation of PDGFB- and CTGF-mRNA expression (only after the first injection), but also the late expression of TGFß1 mRNA in respect to the early and consistent increased collagen type I and type III mRNA expression.

The detection of a myriad of fibroblasts in the neighbourhood of PLLA particles raised the question of whether they also synthesise collagen. Collagen neosynthesis has been assumed in Sculptra®-treated subcutaneous tissue [93]. Here, immunofluorescence staining of PLLA-treated tissue revealed the substantial deposition of collagen type III in proximity to PLLA-particles (Figure 4.24B). A positive collagen type I staining in proximity to PLLA was missing (Figure 4.24E), but fibres in the periphery of the PLLA particles could be stained (Figure 4.25). Hence, collagen type I and III antibodies were successfully tested on untreated tissue; the histopathological picture presented is interpreted to be as such (Figure 4.23A-E). Strongly elevated mRNA expression of collagen type I and III was noted immediately after the first PLLA injection, lasting for up to 10 months after the last treatment (Figure 4.26; 4.27). Therefore, up-regulation of collagen type I and III mRNA expression correlates with collagen type I and III protein staining. However, according to immunofluorescence staining, collagen type I was not detectable within the granulation tissue. Most likely, collagen type I and III proteins are deposited in different areas of PLLA-treated tissue. Coincidently, it must be taken into consideration that the measured mRNA level did not reflect the actual protein abundance. In general, the cellular concentrations of proteins correlate with the abundances of their corresponding mRNA, but not strongly. Several post-transcriptional, translational and protein degradation regulations predict the mRNA derived protein abundance only with a coefficient factor of 0.4 or 0.6 [202-203].

von Recum *et al.* (1993) examined capsule tissue surrounding silastic hydroxyapatite, which stained positive for collagen type III but not for collagen type I [181]. Tan *et al.* (2012) stained tissue capsules formed around titanium oxide and hydroxyapatite in rabbits: collagen type III dominated early and decreased over time, paralled by a successive increase of collagen type I [183]. In contrast, a significant increased mean level of type I collagen was

retrieved in PLLA-treated tissue by Goldberg *et al.* (2013) [94]. This finding contrasts at first sight to ours; however, it is most likely that tissue samples were examined from the periphery of the PLLA encapsulating tissue, meaning that PLLA particles are not visible on presented photomicrographs. That would in turn support our collagen type I mRNA results.

TGFß1 mRNA expression of the key mediator of collagen synthesis increased only after 4 injections in month 10 (Figure 4.30). This late finding did not meet general expectations; hence, a mediator for collagen synthesis should be elevated prior to the mRNA expression of collagen synthesis, comparable to Higgins *et al* (2009) and Li *et al.* (2007a) [156, 184]. However, it must be taken into consideration that the interval between a given PLLA injection and the biopsy, i.e. 2 weeks, might have been too long to document elevated TGFß1 mRNA expression. TGFß1 mRNA might increase within hours after PLLA injection and be decreased 2 weeks later. The elevated TGFß1 mRNA expression 10 months after the initial PLLA injection might reflect PLLA-accumulation and therefore continuous stimulation to synthesise collagen in accordance with the above findings. The late increase of TGFß1 mRNA expression could imply previously discussed macrophage transition from M2a to more M2c macrophages, expressing high amounts of TGFß1.

TGFß1 stimulates fibroblasts to differentiate to myofibroblasts, characterised by αSMA [173]. Staining of αSMA revealed myofibroblasts close to the PLLA particles and smooth muscle cells of vessels in the granulation tissue (Figure 4.18). αSMA mRNA expression was elevated two weeks after the first injection (Figure 4.19). Immunofluorescence staining of capsule tissue formed around polyurethane coated implants in rats elevated the collagen I protein content and αSMA positive vascular structures and myofibroblasts [156]. At day 55, collagen type I staining dominated entirely within the tissue and αSMA was no longer detectable. The findings of αSMA positive vascular structures and myofibroblasts correspond with observations made during this study.

Neovascularisation in PLLA-evoked granulation tissue raised the question of whether blood and lymph vessels can be differentiated. For that purpose, antibodies against CD31, an established blood endothelial marker, and podoplanin, an established lymph endothelial marker [204], were first tested in untreated skin biopsies. Interestingly, CD31- and podoplanin-positive vessel structures were found to be similar in consecutively sectioned dermal tissue samples (compare Figure 4.20A-E with 4.21A-E). Further, Janson *et al.* (2012) described the expression of podoplanin in fibroblasts [205]. Papillary fibroblasts express more podoplanin than reticular fibroblasts in culture and in mammary skin. Braun *et al.* (2011) found podoplanin-positive myofibroblasts [206], calling to mind the fact that the blood vessel is surrounded by myofibroblasts and fibroblasts. These findings explain why CD31- and podoplanin-positive structures resemble each other in consecutively sectioned dermal tissue samples. Hence, CD31-positive endothelia of blood vessels are surrounded by podoplanin-positive (myo)-fibroblasts. This marker pair may not be appropriate to differentiate between blood and lymph vessels in these skin biopsies. Hence (myo)-fibroblasts express podoplanin, CD31 and podoplanin positive blood and lymph endothelia

structures of PLLA-evoked granulation tissue could not be differentiated. Further, CD31 is expressed by macrophages, abundant in the PLLA-treated tissue (Figure 4.11). Therefore, CD31- and podoplanin-staining could not differentiate between vessels and other tissue structures (Figure 4.22A-I). Furthermore, podoplanin staining did not reveal lymph vessel structures, which might be due to the abundance of fibroblasts in the granulation tissue, revealed by CD90 staining. However, these results support by means of a second marker the abundance of macrophages and (myo)-fibroblasts.

PDGF serves as a chemoattractant and together with CTGF and TGFß as a mitogen for fibroblasts [167]. PDGF also promotes myofibroblast proliferation [174]. Kim *et al.* (2014) determined collagen production in human foreskin fibroblast cultures, stimulated by different growth factors and cytokines [207]. PDGF-AA, –BB and TGFß1 were found to be powerful collagen-inducing growth factors showing a more than 2-fold increase in type I collagen production. To verify whether PDGFB and CTGF are up-regulated after PLLA-injection, the mRNA expression was analysed accordingly (Figure 4.31; 4.32). Interestingly, mRNA expression of both cytokines was up-regulated after the first injection. Except for this, neither up- nor down-regulation of PDGFB and/or CTGF mRNA was observed during the course of the study. PDGFB up-regulation after the first Sculptra® injection might be responsible for the early up-regulation of collagen expression in spite of the absence of TGFß1. Ward *et al.* (2008) found an increased amount of CTGF transcripts on days 7, 21, and 48-55 in capsule tissue formed around polyurethane coated implants in rats [133]. Mazaheri *et al.* (2003) reported about reduced capsule formation around an implant using anti-sense CTGF in a rat model [158]. Both observations imply that CTGF is involved in capsule formation, which was observed here. This finding could also imply the interpretation that a transition of M2a to more M2c macrophages took place.

TGFß reduces the expression of MMPs and enhances the production of TIMP [169]. MMPs degrade ECM and their activity can be fine-tuned by TIMPs. The mRNA expression of TIMP1 corresponded to the expression pattern of TGFß1, being up-regulated 10 months after the initial PLLA injection (Figure 4.29). An eventual inhibitory effect of Sculptra® on collagenase could be excluded by an enzymatic test (ch. 4.8). Decorin is a proteoglycan interacting closely with collagen I, and is involved in the maturation of collagen fibrils. Decorin binds to collagen fibrils and inhibits MMP1-mediated collagen fibril cleavage [47]. Additionally, decorin binds to TGFß1 and has been discussed as a natural inhibitor of fibrosis [208]. mRNA expression of decorin (Figure 4.28) was equal to PDGFB and CTGF with consistent progression, except for an up-regulation after the first injection. Ward *et al.* (2008) found increased staining of decorin in capsule tissue [133].

In summary, I draw a hypothetical model of the augmentation embedding the results into the literature: The implementation of Sculptra® into subcutaneous tissue is obligatorily accompanied by injury of the micro-vasculature and tissue, which in turn is associated with histamine release of the local mast cell and platelet release. Host proteins opsonise PLLA-particles, undergoing a conformational change. Histamine release mediates the

inflammatory response. Attracted neutrophils, lymphocytes and macrophages release further chemokines and cytokines and interact with unfolded epitopes of PLLA opsonising host proteins. In particular, Th2 cells might release IL4 and IL-13 polarising macrophages into an M2a phenotype. M2a increase the proliferation and collagen synthesis of fibroblasts and mRNA and protein expression of TGFß1, PDGFAA and PDGFBB *in vitro*. M2a fuse to FBGCs and encapsulate foreign bodies. Here, macrophages and FBGC, elevated fibroblast numbers, myofibroblasts, elevated collagen type I and III, TGFß1 (PDGFBB after the first injection) mRNA, and PLLA encapsulation by collagen type III were retrieved. M2a produce elevated amounts of IL-10 that in turn is capable of polarising macrophages into the M2c type. This type produces elevated amounts of TGFß1, which was especially found in the second part of the study. TGß1 is the key cytokine during fibrosis and serves as chemoattractant for fibroblasts, like PDGF. PDGF, TGFß and CTGF are mitogens for fibroblasts, which could explain the prominent fibroblast abundance. Moreover, TGFß enhances the production TIMP1, which was noticed here. Fibroblasts differentiate under the influence of TGFß1 to myofibroblasts, while PDGF promotes myofibroblast proliferation, which also was observed. To conclude, the augmenting effect of Sculptra® is generated by a complex reaction comprising of many cells, chemokines and cytokines, consequently leading to proliferation of fibroblasts and their differentiation into myofibroblasts, producing an enhanced collagen amount and restoring volume defects of the skin.

The augmenting effect of Sculptra® decreases between 18 and 24 months after the injection in the face [78]. The results of this study imply that PLLA particles are degraded in a much slower way than described previously by Lemperle *et al.* (2003) and Vleggaar and Bauer (2004) [92-93]. The question, therefore, is why does the augmenting effect decrease over time? The half-life of collagen type I and III is estimated to be 15 years [2]. MMP1 expression is normally exceedingly low, near the limit of detection [30]. MMP1 mRNA expression was examined, but could not be detected. Hence, ensuring that MMP1 is not over-expressed, no excessive degradation of collagen should take place.

During all steps of wound healing and skin regeneration, including cell-migration and proliferation, the expression of hyluronan is essential [209-210]. Here, as previously mentioned, PDGFB and TGFß1 mRNA was elevated throughout different time points. Heldin *et al.* (1989) investigated the effect of PDGF-BB, -AA, epidermal growth factor (EGF), basic fibroblastic grows factor (bFGF) and TGFß1 on hyaluronan synthesis in human foreskin fibroblasts [211]. All growth factors were found to stimulate fibroblasts to synthesise hyaluronan; PDGF-BB was the most potent stimulator. Kim *et al.* (2014) quantitated the collagen type I and hyaluronan production of foreskin fibroblast cultures, stimulated by recombinant growth factors and cytokines. PDGF-AA, -BB, EGF, IL-1α and IL-1ß were the most effective hyaluronan-inducing cytokines, while TGFß1 significantly increased hyaluronan production, among others [207]. Li *et al.* (2007) conducted comprehensive studies on hyaluronan synthesis of different cell lines [212]. PDGF-BB stimulated human dermal fibroblasts, obtained from breast reduction surgery, exhibited the highest hyaluronan-synthesising activity in comparison to keloid-, lung- and other fibroblasts.

Moreover, the expression of three hyaluronan synthase (HAS) isoforms and two hyaluronidase (HYAL) isoforms at the mRNA and protein level were determined in human dermal fibroblasts. PDGF-BB treatment induced a 3-fold increase of the already high level of HAS2 mRNA and an increase of HAS1 and HYAL1 mRNA, whereas HAS3 and HYAL2 mRNA levels were not affected. PDGF-BB also increased the amount and activity of the HAS2 protein, but not of the HYAL1 and HYAL2 proteins. In contrast to foreskin fibroblasts, TGFß1 did not stimulate hyaluronan synthesis in dermal fibroblasts, but that of HYALs. Consequently, many studies ensure that PDGF-BB stimulates dermal fibroblasts to synthesise hyaluronan, but the stimulatory effect of TGFß1 seems to be dependent on the cell type.

In the present context, PDGF-BB-stimulated fibroblasts may produce hyaluronan, which may contribute, together with collagen type I and III, to the well documented Sculptra®-mediated augmentation. In contrast to the relatively long half-life of collagen type I and III of about 15 years, the half-life of native hyaluronan is estimated to less than 1-3 days [213-214]. When continuous PDGF-BB-stimulation diminishes, hyaluronan synthesis would decrease and previously synthesised hyaluronan would be degraded in less than 1-3 days. TGFß1 expression accumulated up to the end of the study. According to Li *et al.* (2007), TGFß1 might stimulate HYAL activity, contributing to the late-onset hyaluronan degradation [212]. It has to be further elaborated, whether this hypothesis explains the decrease in PLLA-augmentation after a 1-2-year time span.

Comparable to the current literature about Sculptra®, no further examinations on the biological basis of the augmenting effect of calcium hydroxyapatite are available. Comparing histological findings of calcium hydroxyapatite with those of Sculptra®, comparable features were abundant: FBGC, proliferating fibroblasts and collagen depositions were retrieved [69]. An analogous mechanism to PLLA, as described above, is likely. Therefore, this study could serve as an exemplary model for further investigations on calcium hydroxyapatite-induced augmentation. With respect to the app. 160.000 injections in the USA alone in 2013, further biological examinations are required.

In contrast to Sculptra®- and calcium hydroxyapatite-induced augmentation, the biological basis of cross-linked HA-induced augmentation has been studied in detail. Comparing the results of cross-linked HA studies with the results of this study, it can be seen that there are great differences in initialising the augmentation. Injected cross-liked HA exerts effects on the micro-environment of fibroblasts. Stretched fibroblasts proliferate and increasingly express collagen type I [66]. Sculptra®-induced soft tissue augmentation is mediated by macrophages, recognising Sculptra® particles as foreign bodies. As a consequence, macrophages release cytokines stimulating fibroblasts to produce ECM. Wang *et al.* (2007) found up-regulated mRNA levels of CTGF, TGFß1, -2, -3, TIMP1, -2, and -3 in cross-linked HA treated tissue [65]. In Sculptra®-treated tissue, up-regulated mRNA levels of TGFß1, CTGF and TIMP1 were retrieved. Endothelial cells proliferate more strongly in the micro-environment of HA. Furthermore, the epidermis thickened and keratinocytes showed a stronger proliferation [66].

As far as the elaborated biological examinations on Sculptra®-induced augmentation are concerned, the cells involved were characterised and mRNA expression changes indicated cytokine signalling between those cells. Tissue changes of Sculptra®-treated upper arms were detected by 22 MHz sonography. Thus, the applied sonography set-up can be recommended to investigate other fillers employing an ultrasonic probe with a higher resolution than commonly used so far. Augmentation generated by 600 mg PLLA per upper arm was neither documentable by photography nor subjectively by questionnaires. Further examinations employing larger amounts of PLLA are required to examine the applicability of Sculptra® to augment the upper arms in postmenopausal women. PLLA could even be found 28 months after the last injection and is therefore degraded at a much slower pace in human tissue than previously assumed. The augmenting effect of Sculptra® diminishes within 18-20 months; thus, patients require more injections. This implies the accumulation of large amounts of PLLA within the tissue, which might be thought-provoking. Also, 28 months after Sculptra® injection, the cell infiltrate is still abundant around the particles. Whether other ECM components, for example HA, are synthesised during Sculptra®-treatment needs to be examined further. Hence, the augmenting effect declines over time; a decrease of stimulatory factors may be the rationale, despite the remaining particles. To restore these stimulatory factors for continuous ECM deposition, blood plasma injections, as described by Kawazoe and Kim (2012) may be a thought-provoking path to take in PLLA-treated tissue [215].

6. Literature

Bibliography

[1] Kanitakis J. Anatomy, histology and immunohistochemistry of normal human skin. Eur J Dermatol. 2002;12; 390-399; quiz 400-391.
[2] Verzijl N, DeGroot J, Thorpe SR, Bank RA, Shaw JN, Lyons TJ, et al. Effect of collagen turnover on the accumulation of advanced glycation end products. J Biol Chem. 2000;275; 39027-39031.
[3] Shapiro SD, Endicott SK, Province MA, Pierce JA, Campbell EJ. Marked longevity of human lung parenchymal elastic fibers deduced from prevalence of D-aspartate and nuclear weapons-related radiocarbon. J Clin Invest. 1991;87; 1828-1834.
[4] Zhang M, Pierce RA, Wachi H, Mecham RP, Parks WC. An open reading frame element mediates posttranscriptional regulation of tropoelastin and responsiveness to transforming growth factor beta1. Mol Cell Biol. 1999;19; 7314-7326.
[5] Ruoslahti E. Stretching is good for a cell. Science. 1997;276; 1345-1346.
[6] Fisher GJ, Varani J, Voorhees JJ. Looking older: fibroblast collapse and therapeutic implications. Arch Dermatol. 2008;144; 666-672.
[7] Kerrigan JJ, Mansell JP, Sandy JR. Matrix turnover. J Orthod. 2000;27; 227-233.
[8] Wang J, Dodd C, Shankowsky HA, Scott PG, Tredget EE. Deep dermal fibroblasts contribute to hypertrophic scarring. Lab Invest. 2008;88; 1278-1290.
[9] Kurita M, Okazaki M, Kaminishi-Tanikawa A, Niikura M, Takushima A, Harii K. Differential expression of wound fibrotic factors between facial and trunk dermal fibroblasts. Connect Tissue Res. 2012;53; 349-354.
[10] Kohl E, Steinbauer J, Landthaler M, Szeimies RM. Skin ageing. J Eur Acad Dermatol Venereol. 2011;25; 873-884.
[11] Makrantonaki E, Zouboulis CC. William J. Cunliffe Scientific Awards. Characteristics and pathomechanisms of endogenously aged skin. Dermatology. 2007;214; 352-360.
[12] Gilchrest BA. Photoaging. J Invest Dermatol. 2013;133; E2-6.
[13] Hayflick L. The Limited in Vitro Lifetime of Human Diploid Cell Strains. Exp Cell Res. 1965;37; 614-636.
[14] Gilchrest BA. In vitro assessment of keratinocyte aging. J Invest Dermatol. 1983;81; 184s-189s.
[15] Schneider EL, Mitsui Y. The relationship between in vitro cellular aging and in vivo human age. Proc Natl Acad Sci U S A. 1976;73; 3584-3588.
[16] Cristofalo VJ, Pignolo RJ. Replicative senescence of human fibroblast-like cells in culture. Physiol Rev. 1993;73; 617-638.
[17] Gilchrest BA, Vrabel MA, Flynn E, Szabo G. Selective cultivation of human melanocytes from newborn and adult epidermis. J Invest Dermatol. 1984;83; 370-376.
[18] Harley CB, Futcher AB, Greider CW. Telomeres shorten during ageing of human fibroblasts. Nature. 1990;345; 458-460.
[19] Krunic D, Moshir S, Greulich-Bode KM, Figueroa R, Cerezo A, Stammer H, et al. Tissue context-activated telomerase in human epidermis correlates with little age-dependent telomere loss. Biochim Biophys Acta. 2009;1792; 297-308.
[20] Attia EA, Seada LS, El-Sayed MH, El-Shiemy SM. Study of telomerase reverse transcriptase (hTERT) expression in normal, aged, and photo-aged skin. Int J Dermatol. 2010;49; 886-893.
[21] Beckman KB, Ames BN. The free radical theory of aging matures. Physiol Rev. 1998;78; 547-581.
[22] Jastroch M, Divakaruni AS, Mookerjee S, Treberg JR, Brand MD. Mitochondrial proton and electron leaks. Essays Biochem. 2010;47; 53-67.
[23] Wallace DC. 1994 William Allan Award Address. Mitochondrial DNA variation in human evolution, degenerative disease, and aging. Am J Hum Genet. 1995;57; 201-223.

[24] Sohal RS, Weindruch R. Oxidative stress, caloric restriction, and aging. Science. 1996;273; 59-63.
[25] Hensley K, Floyd RA. Reactive oxygen species and protein oxidation in aging: a look back, a look ahead. Arch Biochem Biophys. 2002;397; 377-383.
[26] Piérard GE, Paquet P, Xhauflaire-Uhoda E, Quatresooz P. Physiological Variations During Aging. In: Farage MA, Miller KM, Maibach HI, editors. Textbook of Aging Skin. Berlin Heidelberg. Springer-Verlag, 2010. 45-54.
[27] Kohen R. Skin antioxidants: their role in aging and in oxidative stress--new approaches for their evaluation. Biomed Pharmacother. 1999;53; 181-192.
[28] Hu HL, Forsey RJ, Blades TJ, Barratt ME, Parmar P, Powell JR. Antioxidants may contribute in the fight against ageing: an in vitro model. Mech Ageing Dev. 2000;121; 217-230.
[29] Sander CS, Chang H, Salzmann S, Muller CS, Ekanayake-Mudiyanselage S, Elsner P, et al. Photoaging is associated with protein oxidation in human skin in vivo. J Invest Dermatol. 2002;118; 618-625.
[30] Fisher GJ, Datta SC, Talwar HS, Wang ZQ, Varani J, Kang S, et al. Molecular basis of sun-induced premature skin ageing and retinoid antagonism. Nature. 1996;379; 335-339.
[31] Raschke C, Elsner P. Skin Aging: A Brief Summary of Characteristic Changes In: Farage MA, Miller KM, Maibach HI, editors. Textbook of Aging Skin. Berlin Heidelberg Springer-Verlag 2010. 37-43.
[32] Chung KY, Agarwal A, Uitto J, Mauviel A. An AP-1 binding sequence is essential for regulation of the human alpha2(I) collagen (COL1A2) promoter activity by transforming growth factor-beta. J Biol Chem. 1996;271; 3272-3278.
[33] Quan T, He T, Voorhees JJ, Fisher GJ. Ultraviolet irradiation induces Smad7 via induction of transcription factor AP-1 in human skin fibroblasts. J Biol Chem. 2005;280; 8079-8085.
[34] He T, Quan T, Shao Y, Voorhees JJ, Fisher GJ. Oxidative exposure impairs TGF-beta pathway via reduction of type II receptor and SMAD3 in human skin fibroblasts. Age (Dordr). 2014.
[35] Hornebeck W. Down-regulation of tissue inhibitor of matrix metalloprotease-1 (TIMP-1) in aged human skin contributes to matrix degradation and impaired cell growth and survival. Pathol Biol (Paris). 2003;51; 569-573.
[36] Lambert Ch A, Nusgens BV, Lapiere Ch M. Mechano-sensing and mechano-reaction of soft connective tissue cells. Adv Space Res. 1998;21; 1081-1091.
[37] Eckes B, Zweers MC, Zhang ZG, Hallinger R, Mauch C, Aumailley M, et al. Mechanical tension and integrin alpha 2 beta 1 regulate fibroblast functions. J Investig Dermatol Symp Proc. 2006;11; 66-72.
[38] Grinnell F. Fibroblast biology in three-dimensional collagen matrices. Trends Cell Biol. 2003;13; 264-269.
[39] Kessler D, Dethlefsen S, Haase I, Plomann M, Hirche F, Krieg T, et al. Fibroblasts in mechanically stressed collagen lattices assume a "synthetic" phenotype. J Biol Chem. 2001;276; 36575-36585.
[40] Varani J, Schuger L, Dame MK, Leonard C, Fligiel SE, Kang S, et al. Reduced fibroblast interaction with intact collagen as a mechanism for depressed collagen synthesis in photodamaged skin. J Invest Dermatol. 2004;122; 1471-1479.
[41] Xia W, Hammerberg C, Li Y, He T, Quan T, Voorhees JJ, et al. Expression of catalytically active matrix metalloproteinase-1 in dermal fibroblasts induces collagen fragmentation and functional alterations that resemble aged human skin. Aging Cell. 2013;12; 661-671.
[42] Imokawa G. Recent advances in characterizing biological mechanisms underlying UV-induced wrinkles: a pivotal role of fibrobrast-derived elastase. Arch Dermatol Res. 2008;300 Suppl 1; S7-20.
[43] Sherratt MJ, Bayley CP, Reilly SM, Gibbs NK, Griffiths CE, Watson RE. Low-dose ultraviolet radiation selectively degrades chromophore-rich extracellular matrix components. J Pathol. 2010;222; 32-40.
[44] Naylor EC, Watson RE, Sherratt MJ. Molecular aspects of skin ageing. Maturitas. 2011;69; 249-256.

[45] Adair-Kirk TL, Senior RM. Fragments of extracellular matrix as mediators of inflammation. Int J Biochem Cell Biol. 2008;40; 1101-1110.
[46] Rijken F, Bruijnzeel PL. The pathogenesis of photoaging: the role of neutrophils and neutrophil-derived enzymes. J Investig Dermatol Symp Proc. 2009;14; 67-72.
[47] Li Y, Xia W, Liu Y, Remmer HA, Voorhees J, Fisher GJ. Solar ultraviolet irradiation induces decorin degradation in human skin likely via neutrophil elastase. PLoS One. 2013;8; e72563.
[48] Fisher GJ, Wang ZQ, Datta SC, Varani J, Kang S, Voorhees JJ. Pathophysiology of premature skin aging induced by ultraviolet light. N Engl J Med. 1997;337; 1419-1428.
[49] Lombard DB, Chua KF, Mostoslavsky R, Franco S, Gostissa M, Alt FW. DNA repair, genome stability, and aging. Cell. 2005;120; 497-512.
[50] Chung JH, Eun HC. Angiogenesis in skin aging and photoaging. J Dermatol. 2007;34; 593-600.
[51] El-Domyati M, Attia S, Saleh F, Brown D, Birk DE, Gasparro F, et al. Intrinsic aging vs. photoaging: a comparative histopathological, immunohistochemical, and ultrastructural study of skin. Exp Dermatol. 2002;11; 398-405.
[52] Timar F, Soos G, Szende B, Horvath A. Interdigitation index - a parameter for differentiating between young and older skin specimens. Skin Res Technol. 2000;6; 17-20.
[53] Ghersetich I, Lotti T, Campanile G, Grappone C, Dini G. Hyaluronic acid in cutaneous intrinsic aging. Int J Dermatol. 1994;33; 119-122.
[54] Craven NM, Watson RE, Jones CJ, Shuttleworth CA, Kielty CM, Griffiths CE. Clinical features of photodamaged human skin are associated with a reduction in collagen VII. Br J Dermatol. 1997;137; 344-350.
[55] Uitto J. The role of elastin and collagen in cutaneous aging: intrinsic aging versus photoexposure. J Drugs Dermatol. 2008;7; s12-16.
[56] Bernstein EF, Underhill CB, Hahn PJ, Brown DB, Uitto J. Chronic sun exposure alters both the content and distribution of dermal glycosaminoglycans. Br J Dermatol. 1996;135; 255-262.
[57] Rohrich RJ, Pessa JE. The fat compartments of the face: anatomy and clinical implications for cosmetic surgery. Plast Reconstr Surg. 2007;119; 2219-2227; discussion 2228-2231.
[58] Rohrich RJ, Pessa JE. The retaining system of the face: histologic evaluation of the septal boundaries of the subcutaneous fat compartments. Plast Reconstr Surg. 2008;121; 1804-1809.
[59] Kligman AM, Zheng P, Lavker RM. The anatomy and pathogenesis of wrinkles. Br J Dermatol. 1985;113; 37-42.
[60] Sharabi SE, Hatef DA, Koshy JC, Hollier LH, Jr., Yaremchuk MJ. Mechanotransduction: the missing link in the facial aging puzzle? Aesthetic Plast Surg. 2010;34; 603-611.
[61] Sandhofer M, Schauer P, Anderhuber F. The aesthetic upper arm: On the anatomy and classification of the lipodysmorphic upper arm. Kosmetische Medizin. 2013;34; 56-61.
[62] Requena L, Requena C, Christensen L, Zimmermann US, Kutzner H, Cerroni L. Adverse reactions to injectable soft tissue fillers. J Am Acad Dermatol. 2011;64; 1-34; quiz 35-36.
[63] Sattler G, Sommer B. Liporecycling: a technique for facial rejuvenation and body contouring. Dermatol Surg. 2000;26; 1140-1144.
[64] Scarborough D, Eickhorst KM, Bisaccia E. Cosmetic Surgery in the Elderly. In: Farage MA, Miller KM, Maibach HI, editors. Textbook of Aging Skin. Berlin Heidelberg. Springer-Verlag, 2010. 1147-1173.
[65] Wang F, Garza LA, Kang S, Varani J, Orringer JS, Fisher GJ, et al. In vivo stimulation of de novo collagen production caused by cross-linked hyaluronic acid dermal filler injections in photodamaged human skin. Arch Dermatol. 2007;143; 155-163.
[66] Quan T, Wang F, Shao Y, Rittie L, Xia W, Orringer JS, et al. Enhancing Structural Support of the Dermal Microenvironment Activates Fibroblasts, Endothelial Cells, and Keratinocytes in Aged Human Skin In Vivo. J Invest Dermatol. 2012.
[67] Pitaru S, Noff M, Blok L, Nir E, Goldlust A, Savion N. Long-term efficacy of a novel ribose-cross-linked collagen dermal filler: a histologic and histomorphometric study in an animal model. Dermatol Surg. 2007;33; 1045-1054; discussion 1054.
[68] Jacovella PF. Use of calcium hydroxylapatite (Radiesse) for facial augmentation. Clin Interv Aging. 2008;3; 161-174.

[69] Marmur ES, Phelps R, Goldberg DJ. Clinical, histologic and electron microscopic findings after injection of a calcium hydroxylapatite filler. J Cosmet Laser Ther. 2004;6; 223-226.
[70] Drobeck HP, Rothstein SS, Gumaer KI, Sherer AD, Slighter RG. Histologic observation of soft tissue responses to implanted, multifaceted particles and discs of hydroxylapatite. J Oral Maxillofac Surg. 1984;42; 143-149.
[71] Misiek DJ, Kent JN, Carr RF. Soft tissue responses to hydroxylapatite particles of different shapes. J Oral Maxillofac Surg. 1984;42; 150-160.
[72] Lemperle G, Romano JJ, Busso M. Soft tissue augmentation with artecoll: 10-year history, indications, techniques, and complications. Dermatol Surg. 2003;29; 573-587; discussion 587.
[73] Lemperle G, Knapp TR, Sadick NS, Lemperle SM. ArteFill permanent injectable for soft tissue augmentation: I. Mechanism of action and injection techniques. Aesthetic Plast Surg. 2010;34; 264-272.
[74] Bartus C, William Hanke C, Daro-Kaftan E. A decade of experience with injectable poly-L-lactic acid: a focus on safety. Dermatol Surg. 2013;39; 698-705.
[75] Fitzgerald R, Vleggaar D. Facial volume restoration of the aging face with poly-l-lactic acid. Dermatol Ther. 2011;24; 2-27.
[76] Palm MD, Woodhall KE, Butterwick KJ, Goldman MP. Cosmetic use of poly-l-lactic acid: a retrospective study of 130 patients. Dermatol Surg. 2010;36; 161-170.
[77] Schierle CF, Casas LA. Nonsurgical rejuvenation of the aging face with injectable poly-L-lactic acid for restoration of soft tissue volume. Aesthet Surg J. 2011;31; 95-109.
[78] Lowe NJ, Maxwell CA, Lowe P, Shah A, Patnaik R. Injectable poly-l-lactic acid: 3 years of aesthetic experience. Dermatol Surg. 2009;35 Suppl 1; 344-349.
[79] Alijotas-Reig J, Garcia-Gimenez V, Vilardell-Tarres M. Late-onset immune-mediated adverse effects after poly-L-lactic acid injection in non-HIV patients: clinical findings and long-term follow-up. Dermatology. 2009;219; 303-308.
[80] Reszko AE, Sadick NS, Magro CM, Farber J. Late-onset subcutaneous nodules after poly-L-lactic acid injection. Dermatol Surg. 2009;35 Suppl 1; 380-384.
[81] Lorenc ZP. Techniques for the optimization of facial and nonfacial volumization with injectable poly-l-lactic acid. Aesthetic Plast Surg. 2012;36; 1222-1229.
[82] Schell BJ. Nonfacial Soft Tissue Restoration With Poly-L-lactic Acid. Cosmetic Dermatology. 2006;19; 25-28.
[83] Schulman MR, Lipper J, Skolnik RA. Correction of chest wall deformity after implant-based breast reconstruction using poly-L-lactic acid (Sculptra). Breast J. 2008;14; 92-96.
[84] Mazzuco R, Hexsel D. Poly-L-lactic acid for neck and chest rejuvenation. Dermatol Surg. 2009;35; 1228-1237.
[85] Beer K. A single-center, open-label study on the use of injectable poly-L-lactic acid for the treatment of moderate to severe scarring from acne or varicella. Dermatol Surg. 2007;33 Suppl 2; S159-167.
[86] Schelke LW, Van Den Elzen HJ, Erkamp PPM, Neumann HAM. Use of ultrasound to provide overall information on facial fillers and surrounding tissue. Dermatol Surg. 2010;36 Suppl 3; 1843-1851.
[87] Valantin MA, Aubron-Olivier C, Ghosn J, Laglenne E, Pauchard M, Schoen H, et al. Polylactic acid implants (New-Fill) to correct facial lipoatrophy in HIV-infected patients: results of the open-label study VEGA. AIDS. 2003;17; 2471-2477.
[88] Cutright DE, Hunsuck EE. Tissue reaction to the biodegradable polylactic acid suture. Oral Surg Oral Med Oral Pathol. 1971;31; 134-139.
[89] Brady JM, Cutright DE, Miller RA, Barristone GC. Resorption rate, route, route of elimination, and ultrastructure of the implant site of polylactic acid in the abdominal wall of the rat. J Biomed Mater Res. 1973;7; 155-166.
[90] Kulkarni RK, Pani KC, Neuman C, Leonard F. Polylactic acid for surgical implants. Arch Surg. 1966;93; 839-843.

[91] Gogolewski S, Jovanovic M, Perren SM, Dillon JG, Hughes MK. Tissue response and in vivo degradation of selected polyhydroxyacids: polylactides (PLA), poly(3-hydroxybutyrate) (PHB), and poly(3-hydroxybutyrate-co-3-hydroxyvalerate) (PHB/VA). J Biomed Mater Res. 1993;27; 1135-1148.
[92] Lemperle G, Morhenn V, Charrier U. Human histology and persistence of various injectable filler substances for soft tissue augmentation. Aesthetic Plast Surg. 2003;27; 354-366; discussion 367.
[93] Vleggaar D, Bauer U. Facial enhancement and the European experience with Sculptra (poly-l-lactic acid). J Drugs Dermatol. 2004;3; 542-547.
[94] Goldberg D, Guana A, Volk A, Daro-Kaftan E. Single-arm study for the characterization of human tissue response to injectable poly-L-lactic acid. Dermatol Surg. 2013;39; 915-922.
[95] Amini AR, Wallace JS, Nukavarapu SP. Short-term and long-term effects of orthopedic biodegradable implants. J Long Term Eff Med Implants. 2011;21; 93-122.
[96] Anderson JM, Rodriguez A, Chang DT. Foreign body reaction to biomaterials. Semin Immunol. 2008;20; 86-100.
[97] Junge K, Binnebosel M, von Trotha KT, Rosch R, Klinge U, U PN, et al. Mesh biocompatibility: effects of cellular inflammation and tissue remodelling. Langenbecks Arch Surg. 2012;397; 255-270.
[98] Luttikhuizen DT, Harmsen MC, Van Luyn MJ. Cellular and molecular dynamics in the foreign body reaction. Tissue Eng. 2006;12; 1955-1970.
[99] Rujitanaroj PO, Jao B, Yang J, Wang F, Anderson JM, Wang J, et al. Controlling fibrous capsule formation through long-term down-regulation of collagen type I (COL1A1) expression by nanofiber-mediated siRNA gene silencing. Acta Biomater. 2013;9; 4513-4524.
[100] Wilson CJ, Clegg RE, Leavesley DI, Pearcy MJ. Mediation of biomaterial-cell interactions by adsorbed proteins: a review. Tissue Eng. 2005;11; 1-18.
[101] Jenney CR, Anderson JM. Adsorbed serum proteins responsible for surface dependent human macrophage behavior. J Biomed Mater Res. 2000;49; 435-447.
[102] Jenney CR, Anderson JM. Adsorbed IgG: a potent adhesive substrate for human macrophages. J Biomed Mater Res. 2000;50; 281-290.
[103] Tang L, Eaton JW. Fibrin(ogen) mediates acute inflammatory responses to biomaterials. J Exp Med. 1993;178; 2147-2156.
[104] Berton G, Lowell CA. Integrin signalling in neutrophils and macrophages. Cell Signal. 1999;11; 621-635.
[105] Hu WJ, Eaton JW, Ugarova TP, Tang L. Molecular basis of biomaterial-mediated foreign body reactions. Blood. 2001;98; 1231-1238.
[106] Zdolsek J, Eaton JW, Tang L. Histamine release and fibrinogen adsorption mediate acute inflammatory responses to biomaterial implants in humans. J Transl Med. 2007;5.
[107] Tang L, Jennings TA, Eaton JW. Mast cells mediate acute inflammatory responses to implanted biomaterials. Proc Natl Acad Sci U S A. 1998;95; 8841-8846.
[108] Luster AD. Chemokines--chemotactic cytokines that mediate inflammation. N Engl J Med. 1998;338; 436-445.
[109] Johnston B, Butcher EC. Chemokines in rapid leukocyte adhesion triggering and migration. Semin Immunol. 2002;14; 83-92.
[110] Ghosh AK, Hirasawa N, Ohtsu H, Watanabe T, Ohuchi K. Defective angiogenesis in the inflammatory granulation tissue in histidine decarboxylase-deficient mice but not in mast cell-deficient mice. J Exp Med. 2002;195; 973-982.
[111] Banks RE, Forbes MA, Kinsey SE, Stanley A, Ingham E, Walters C, et al. Release of the angiogenic cytokine vascular endothelial growth factor (VEGF) from platelets: significance for VEGF measurements and cancer biology. Br J Cancer. 1998;77; 956-964.
[112] Ferrara N, Gerber HP, LeCouter J. The biology of VEGF and its receptors. Nat Med. 2003;9; 669-676.
[113] McCourt M, Wang JH, Sookhai S, Redmond HP. Proinflammatory mediators stimulate neutrophil-directed angiogenesis. Arch Surg. 1999;134; 1325-1331; discussion 1331-1322.
[114] Broughton G, 2nd, Janis JE, Attinger CE. The basic science of wound healing. Plast Reconstr Surg. 2006;117; 12S-34S.

[115] Rhodes NP, Hunt JA, Williams DF. Macrophage subpopulation differentiation by stimulation with biomaterials. J Biomed Mater Res. 1997;37; 481-488.
[116] Charo IF, Ransohoff RM. The many roles of chemokines and chemokine receptors in inflammation. The New England journal of medicine. 2006;354; 610-621.
[117] Weber C, Belge KU, von Hundelshausen P, Draude G, Steppich B, Mack M, et al. Differential chemokine receptor expression and function in human monocyte subpopulations. J Leukoc Biol. 2000;67; 699-704.
[118] Love RJ, Jones KS. The recognition of biomaterials: pattern recognition of medical polymers and their adsorbed biomolecules. J Biomed Mater Res A. 2013;101; 2740-2752.
[119] Chen H, Li P, Yin Y, Cai X, Huang Z, Chen J, et al. The promotion of type 1 T helper cell responses to cationic polymers in vivo via toll-like receptor-4 mediated IL-12 secretion. Biomaterials. 2010;31; 8172-8180.
[120] Peiser L, Mukhopadhyay S, Gordon S. Scavenger receptors in innate immunity. Curr Opin Immunol. 2002;14; 123-128.
[121] Miranti CK, Brugge JS. Sensing the environment: a historical perspective on integrin signal transduction. Nat Cell Biol. 2002;4; E83-90.
[122] Xia Z, Triffitt JT. A review on macrophage responses to biomaterials. Biomed Mater. 2006;1; R1-9.
[123] Huber R, Pietsch D, Gunther J, Welz B, Vogt N, Brand K. Regulation of monocyte differentiation by specific signaling modules and associated transcription factor networks. Cell Mol Life Sci. 2014;71; 63-92.
[124] Palsson-McDermott EM, O'Neill LA. Signal transduction by the lipopolysaccharide receptor, Toll-like receptor-4. Immunology. 2004;113; 153-162.
[125] MacMicking J, Xie QW, Nathan C. Nitric oxide and macrophage function. Annu Rev Immunol. 1997;15; 323-350.
[126] Fang FC. Antimicrobial reactive oxygen and nitrogen species: concepts and controversies. Nat Rev Microbiol. 2004;2; 820-832.
[127] Mantovani A, Sica A, Sozzani S, Allavena P, Vecchi A, Locati M. The chemokine system in diverse forms of macrophage activation and polarization. Trends Immunol. 2004;25; 677-686.
[128] Gordon S, Martinez FO. Alternative activation of macrophages: mechanism and functions. Immunity. 2010;32; 593-604.
[129] Kou PM, Babensee JE. Macrophage and dendritic cell phenotypic diversity in the context of biomaterials. Journal of biomedical materials research Part A. 2010.
[130] Modolell M, Corraliza IM, Link F, Soler G, Eichmann K. Reciprocal regulation of the nitric oxide synthase/arginase balance in mouse bone marrow-derived macrophages by TH1 and TH2 cytokines. Eur J Immunol. 1995;25; 1101-1104.
[131] Stein M, Keshav S, Harris N, Gordon S. Interleukin 4 potently enhances murine macrophage mannose receptor activity: a marker of alternative immunologic macrophage activation. The Journal of experimental medicine. 1992;176; 287-292.
[132] Helming L, Gordon S. Macrophage fusion induced by IL-4 alternative activation is a multistage process involving multiple target molecules. Eur J Immunol. 2007;37; 33-42.
[133] Ward WK, Li AG, Siddiqui Y, Federiuk IF, Wang XJ. Increased expression of Interleukin-13 and connective tissue growth factor, and their potential roles during foreign body encapsulation of subcutaneous implants. J Biomater Sci Polym Ed. 2008;19; 1065-1072.
[134] DeFife KM, Jenney CR, McNally AK, Colton E, Anderson JM. Interleukin-13 induces human monocyte/macrophage fusion and macrophage mannose receptor expression. Journal of immunology (Baltimore, Md : 1950). 1997;158; 3385-3390.
[135] McNally AK, Jones JA, Macewan SR, Colton E, Anderson JM. Vitronectin is a critical protein adhesion substrate for IL-4-induced foreign body giant cell formation. Journal of biomedical materials research Part A. 2008;86; 535-543.
[136] McNally AK, DeFife KM, Anderson JM. Interleukin-4-induced macrophage fusion is prevented by inhibitors of mannose receptor activity. The American journal of pathology. 1996;149; 975-985.

[137] Chiozzi P, Sanz JM, Ferrari D, Falzoni S, Aleotti A, Buell GN, et al. Spontaneous cell fusion in macrophage cultures expressing high levels of the P2Z/P2X7 receptor. J Cell Biol. 1997;138; 697-706.
[138] Yagi M, Miyamoto T, Sawatani Y, Iwamoto K, Hosogane N, Fujita N, et al. DC-STAMP is essential for cell-cell fusion in osteoclasts and foreign body giant cells. J Exp Med. 2005;202; 345-351.
[139] Han X, Sterling H, Chen Y, Saginario C, Brown EJ, Frazier WA, et al. CD47, a ligand for the macrophage fusion receptor, participates in macrophage multinucleation. J Biol Chem. 2000;275; 37984-37992.
[140] Sterling H, Saginario C, Vignery A. CD44 occupancy prevents macrophage multinucleation. J Cell Biol. 1998;143; 837-847.
[141] Vignery A. Osteoclasts and giant cells: macrophage-macrophage fusion mechanism. Int J Exp Pathol. 2000;81; 291-304.
[142] Kyriakides TR, Foster MJ, Keeney GE, Tsai A, Giachelli CM, Clark-Lewis I, et al. The CC chemokine ligand, CCL2/MCP1, participates in macrophage fusion and foreign body giant cell formation. Am J Pathol. 2004;165; 2157-2166.
[143] Jones JA, Chang DT, Meyerson H, Colton E, Kwon IK, Matsuda T, et al. Proteomic analysis and quantification of cytokines and chemokines from biomaterial surface-adherent macrophages and foreign body giant cells. J Biomed Mater Res A. 2007;83; 585-596.
[144] Jones JA, Dadsetan M, Collier TO, Ebert M, Stokes KS, Ward RS, et al. Macrophage behavior on surface-modified polyurethanes. Journal of biomaterials science Polymer edition. 2004;15; 567-584.
[145] Hernandez-Pando R, Bornstein QL, Aguilar Leon D, Orozco EH, Madrigal VK, Martinez Cordero E. Inflammatory cytokine production by immunological and foreign body multinucleated giant cells. Immunology. 2000;100; 352-358.
[146] Luttikhuizen DT, Dankers PY, Harmsen MC, van Luyn MJ. Material dependent differences in inflammatory gene expression by giant cells during the foreign body reaction. Journal of biomedical materials research Part A. 2007;83; 879-886.
[147] Song E, Ouyang N, Horbelt M, Antus B, Wang M, Exton MS. Influence of alternatively and classically activated macrophages on fibrogenic activities of human fibroblasts. Cell Immunol. 2000;204; 19-28.
[148] Reunanen N, Li SP, Ahonen M, Foschi M, Han J, Kahari VM. Activation of p38 alpha MAPK enhances collagenase-1 (matrix metalloproteinase (MMP)-1) and stromelysin-1 (MMP-3) expression by mRNA stabilization. J Biol Chem. 2002;277; 32360-32368.
[149] Dayer JM, Beutler B, Cerami A. Cachectin/tumor necrosis factor stimulates collagenase and prostaglandin E2 production by human synovial cells and dermal fibroblasts. J Exp Med. 1985;162; 2163-2168.
[150] Verrecchia F, Mauviel A. TGF-beta and TNF-alpha: antagonistic cytokines controlling type I collagen gene expression. Cell Signal. 2004;16; 873-880.
[151] Gu L, Zhu YJ, Yang X, Guo ZJ, Xu WB, Tian XL. Effect of TGF-beta/Smad signaling pathway on lung myofibroblast differentiation. Acta Pharmacol Sin. 2007;28; 382-391.
[152] Liu Y. Cellular and molecular mechanisms of renal fibrosis. Nat Rev Nephrol. 2011;7; 684-696.
[153] Wynn TA, Barron L. Macrophages: master regulators of inflammation and fibrosis. Semin Liver Dis. 2010;30; 245-257.
[154] Khan R, Sheppard R. Fibrosis in heart disease: understanding the role of transforming growth factor-beta in cardiomyopathy, valvular disease and arrhythmia. Immunology. 2006;118; 10-24.
[155] Yu Q, Stamenkovic I. Cell surface-localized matrix metalloproteinase-9 proteolytically activates TGF-beta and promotes tumor invasion and angiogenesis. Genes Dev. 2000;14; 163-176.
[156] Li AG, Quinn MJ, Siddiqui Y, Wood MD, Federiuk IF, Duman HM, et al. Elevation of transforming growth factor beta (TGFbeta) and its downstream mediators in subcutaneous foreign body capsule tissue. J Biomed Mater Res A. 2007;82; 498-508.
[157] Flanders KC. Smad3 as a mediator of the fibrotic response. Int J Exp Pathol. 2004;85; 47-64.
[158] Mazaheri MK, Schultz GS, Blalock TD, Caffee HH, Chin GA. Role of connective tissue growth factor in breast implant elastomer capsular formation. Ann Plast Surg. 2003;50; 263-268; discussion 268.

[159] Oriente A, Fedarko NS, Pacocha SE, Huang SK, Lichtenstein LM, Essayan DM. Interleukin-13 modulates collagen homeostasis in human skin and keloid fibroblasts. J Pharmacol Exp Ther. 2000;292; 988-994.
[160] Jinnin M, Ihn H, Yamane K, Tamaki K. Interleukin-13 stimulates the transcription of the human alpha2(I) collagen gene in human dermal fibroblasts. J Biol Chem. 2004;279; 41783-41791.
[161] Kaviratne M, Hesse M, Leusink M, Cheever AW, Davies SJ, McKerrow JH, et al. IL-13 activates a mechanism of tissue fibrosis that is completely TGF-beta independent. J Immunol. 2004;173; 4020-4029.
[162] Assoian RK, Sporn MB. Type beta transforming growth factor in human platelets: release during platelet degranulation and action on vascular smooth muscle cells. J Cell Biol. 1986;102; 1217-1223.
[163] Postlethwaite AE, Keski-Oja J, Moses HL, Kang AH. Stimulation of the chemotactic migration of human fibroblasts by transforming growth factor beta. J Exp Med. 1987;165; 251-256.
[164] Heldin CH, Eriksson U, Ostman A. New members of the platelet-derived growth factor family of mitogens. Arch Biochem Biophys. 2002;398; 284-290.
[165] Grotendorst GR, Okochi H, Hayashi N. A novel transforming growth factor beta response element controls the expression of the connective tissue growth factor gene. Cell Growth Differ. 1996;7; 469-480.
[166] Ashcroft GS. Bidirectional regulation of macrophage function by TGF-beta. Microbes Infect. 1999;1; 1275-1282.
[167] Werner S, Grose R. Regulation of wound healing by growth factors and cytokines. Physiol Rev. 2003;83; 835-870.
[168] Border WA, Noble NA. Transforming growth factor beta in tissue fibrosis. N Engl J Med. 1994;331; 1286-1292.
[169] Hall MC, Young DA, Waters JG, Rowan AD, Chantry A, Edwards DR, et al. The comparative role of activator protein 1 and Smad factors in the regulation of Timp-1 and MMP-1 gene expression by transforming growth factor-beta 1. J Biol Chem. 2003;278; 10304-10313.
[170] Nakatsukasa H, Nagy P, Evarts RP, Hsia CC, Marsden E, Thorgeirsson SS. Cellular distribution of transforming growth factor-beta 1 and procollagen types I, III, and IV transcripts in carbon tetrachloride-induced rat liver fibrosis. J Clin Invest. 1990;85; 1833-1843.
[171] Ignotz RA, Endo T, Massague J. Regulation of fibronectin and type I collagen mRNA levels by transforming growth factor-beta. J Biol Chem. 1987;262; 6443-6446.
[172] Bassols A, Massague J. Transforming growth factor beta regulates the expression and structure of extracellular matrix chondroitin/dermatan sulfate proteoglycans. J Biol Chem. 1988;263; 3039-3045.
[173] Desmouliere A, Geinoz A, Gabbiani F, Gabbiani G. Transforming growth factor-beta 1 induces alpha-smooth muscle actin expression in granulation tissue myofibroblasts and in quiescent and growing cultured fibroblasts. J Cell Biol. 1993;122; 103-111.
[174] Bonner JC. Regulation of PDGF and its receptors in fibrotic diseases. Cytokine Growth Factor Rev. 2004;15; 255-273.
[175] Gabbiani G, Le Lous M, Bailey AJ, Bazin S, Delaunay A. Collagen and myofibroblasts of granulation tissue. A chemical, ultrastructural and immunologic study. Virchows Arch B Cell Pathol. 1976;21; 133-145.
[176] Hagood JS, Prabhakaran P, Kumbla P, Salazar L, MacEwen MW, Barker TH, et al. Loss of fibroblast Thy-1 expression correlates with lung fibrogenesis. Am J Pathol. 2005;167; 365-379.
[177] Sanders YY, Kumbla P, Hagood JS. Enhanced myofibroblastic differentiation and survival in Thy-1(-) lung fibroblasts. Am J Respir Cell Mol Biol. 2007;36; 226-235.
[178] Bucala R, Spiegel LA, Chesney J, Hogan M, Cerami A. Circulating fibrocytes define a new leukocyte subpopulation that mediates tissue repair. Mol Med. 1994;1; 71-81.
[179] Abe R, Donnelly SC, Peng T, Bucala R, Metz CN. Peripheral blood fibrocytes: differentiation pathway and migration to wound sites. J Immunol. 2001;166; 7556-7562.
[180] Kis K, Liu X, Hagood JS. Myofibroblast differentiation and survival in fibrotic disease. Expert Rev Mol Med. 2011;13; e27.

[181] von Recum AF, Opitz H, Wu E. Collagen types I and III at the implant/tissue interface. J Biomed Mater Res. 1993;27; 757-761.
[182] Shannon C, Thull R, von Recum A. Types I and III collagen in the tissue capsules of titanium and stainless-steel implants. J Biomed Mater Res. 1997;34; 401-408.
[183] Tan XW, Beuerman RW, Shi ZL, Neoh KG, Tan D, Khor KA, et al. In vivo evaluation of titanium oxide and hydroxyapatite as an artificial cornea skirt. J Mater Sci Mater Med. 2012;23; 1063-1072.
[184] Higgins DM, Basaraba RJ, Hohnbaum AC, Lee EJ, Grainger DW, Gonzalez-Juarrero M. Localized immunosuppressive environment in the foreign body response to implanted biomaterials. Am J Pathol. 2009;175; 161-170.
[185] Klinge U, Dietz U, Fet N, Klosterhalfen B. Characterisation of the cellular infiltrate in the foreign body granuloma of textile meshes with its impact on collagen deposition. Hernia. 2014.
[186] Kassira N, Glassberg MK, Jones C, Pincus DJ, Elliot SJ, Fritz JR, et al. Estrogen deficiency and tobacco smoke exposure promote matrix metalloproteinase-13 activation in skin of aging B6 mice. Ann Plast Surg. 2009;63; 318-322.
[187] Ghose Roy S, Mishra S, Ghosh G, Bandyopadhyay A. Thyroid hormone induces myocardial matrix degradation by activating matrix metalloproteinase-1. Matrix Biol. 2007;26; 269-279.
[188] Yin L, Morita A, Tsuji T. Alterations of extracellular matrix induced by tobacco smoke extract. Arch Dermatol Res. 2000;292; 188-194.
[189] Vayalil PK, Mittal A, Hara Y, Elmets CA, Katiyar SK. Green tea polyphenols prevent ultraviolet light-induced oxidative damage and matrix metalloproteinases expression in mouse skin. J Invest Dermatol. 2004;122; 1480-1487.
[190] Augustin M, Lange S, Wenninger K, Seidenglanz K, Amon U, Zschocke I. Validation of a comprehensive Freiburg Life Quality Assessment (FLQA) core questionnaire and development of a threshold system. Eur J Dermatol. 2004;14; 107-113.
[191] Kubista M, Andrade JM, Bengtsson M, Forootan A, Jonak J, Lind K, et al. The real-time polymerase chain reaction. Mol Aspects Med. 2006;27; 95-125.
[192] Saiki RK, Gelfand DH, Stoffel S, Scharf SJ, Higuchi R, Horn GT, et al. Primer-directed enzymatic amplification of DNA with a thermostable DNA polymerase. Science. 1988;239; 487-491.
[193] Akamine R, Yamamoto T, Watanabe M, Yamazaki N, Kataoka M, Ishikawa M, et al. Usefulness of the 5' region of the cDNA encoding acidic ribosomal phosphoprotein P0 conserved among rats, mice, and humans as a standard probe for gene expression analysis in different tissues and animal species. J Biochem Biophys Methods. 2007;70; 481-486.
[194] Simon P. Q-Gene: processing quantitative real-time RT-PCR data. Bioinformatics. 2003;19; 1439-1440.
[195] Sambrook J, Fritsch EF, Maniatis T. Molecular cloning : a laboratory manual. Cold Spring Harbor, New York. Cold Spring Harbor Laboratory Press. 1989.
[196] Böhmer F. Zur pathologischen Anatomie der Meningitis cerebromedularis epidemica. Ärztliches Intelligenz-Blatt. 1865;12; 539-550.
[197] Grassmann W, Nordwig A. [Quantitative colorimetric test for collagenase]. Hoppe Seylers Z Physiol Chem. 1960;322; 267-272.
[198] Levy RM, Redbord KP, Hanke CW. Treatment of HIV lipoatrophy and lipoatrophy of aging with poly-L-lactic acid: a prospective 3-year follow-up study. Journal of the American Academy of Dermatology. 2008;59; 923-933.
[199] Lam SM, Azizzadeh B, Graivier M. Injectable poly-L-lactic acid (Sculptra): technical considerations in soft-tissue contouring. Plast Reconstr Surg. 2006;118; 55S-63S.
[200] Wortsman X, Wortsman J, Orlandi C, Cardenas G, Sazunic I, Jemec GB. Ultrasound detection and identification of cosmetic fillers in the skin. J Eur Acad Dermatol Venereol. 2012;26; 292-301.
[201] Grippaudo FR, Mattei M. High-frequency sonography of temporary and permanent dermal fillers. Skin Res Technol. 2010;16; 265-269.
[202] Vogel C, Marcotte EM. Insights into the regulation of protein abundance from proteomic and transcriptomic analyses. Nat Rev Genet. 2012;13; 227-232.
[203] Maier T, Guell M, Serrano L. Correlation of mRNA and protein in complex biological samples. FEBS Lett. 2009;583; 3966-3973.

[204] Breiteneder-Geleff S, Soleiman A, Kowalski H, Horvat R, Amann G, Kriehuber E, et al. Angiosarcomas express mixed endothelial phenotypes of blood and lymphatic capillaries: podoplanin as a specific marker for lymphatic endothelium. Am J Pathol. 1999;154; 385-394.
[205] Janson DG, Saintigny G, van Adrichem A, Mahe C, El Ghalbzouri A. Different gene expression patterns in human papillary and reticular fibroblasts. J Invest Dermatol. 2012;132; 2565-2572.
[206] Braun N, Alscher DM, Fritz P, Edenhofer I, Kimmel M, Gaspert A, et al. Podoplanin-positive cells are a hallmark of encapsulating peritoneal sclerosis. Nephrol Dial Transplant. 2011;26; 1033-1041.
[207] Kim MS, Song HJ, Lee SH, Lee CK. Comparative study of various growth factors and cytokines on type I collagen and hyaluronan production in human dermal fibroblasts. J Cosmet Dermatol. 2014;13; 44-51.
[208] Baghy K, Iozzo RV, Kovalszky I. Decorin-TGFbeta axis in hepatic fibrosis and cirrhosis. J Histochem Cytochem. 2012;60; 262-268.
[209] Anderegg U, Simon JC, Averbeck M. More than just a filler - the role of hyaluronan for skin homeostasis. Exp Dermatol. 2014;23; 295-303.
[210] Chen WY, Abatangelo G. Functions of hyaluronan in wound repair. Wound Repair Regen. 1999;7; 79-89.
[211] Heldin P, Laurent TC, Heldin CH. Effect of growth factors on hyaluronan synthesis in cultured human fibroblasts. Biochem J. 1989;258; 919-922.
[212] Li L, Asteriou T, Bernert B, Heldin CH, Heldin P. Growth factor regulation of hyaluronan synthesis and degradation in human dermal fibroblasts: importance of hyaluronan for the mitogenic response of PDGF-BB. Biochem J. 2007;404; 327-336.
[213] Tammi R, Saamanen AM, Maibach HI, Tammi M. Degradation of newly synthesized high molecular mass hyaluronan in the epidermal and dermal compartments of human skin in organ culture. J Invest Dermatol. 1991;97; 126-130.
[214] Fraser JR, Laurent TC, Laurent UB. Hyaluronan: its nature, distribution, functions and turnover. J Intern Med. 1997;242; 27-33.
[215] Kawazoe T, Kim HH. Tissue augmentation by white blood cell-containing platelet-rich plasma. Cell Transplant. 2012;21; 601-607.

7. Appendix

7.1 Abbreviations

(ICAM)-1	intercellular adhesion molecule
(NF)-kb	nuclear factor κb
(VCAM)-1	vascular cell adhesion molecule
A	adenine
A-, B-scan	amplitude modulation-, brightness scan
ACTA2	gene encoding for alpha smooth muscle actin
Ala	alanine
AP-1	transcriptional factor activator protein 1
BER	base excision repair
BSA	bovine serum albumin
C	cytosine
CCL	C-C chemokine ligand
CCR	C-C chemokine receptor
CD	cluster of differentiation
cDNA	complementary deoxyribonucleic acid
Col1A1	gene encoding for collagen type I pro-alpha 1 chain
Col3A1	gene encoding for collagen type III pro-alpha 1 chain
Cq; Ct	quantification cycle; threshold cycle
CR	complement receptor
CTGF	connective tissue growth factor
Cys	cysteine
DAPI	4´,6-Diamidino-2-phenylindole
DC-STAMP	dendritic cell-specific transmembrane protein
DEJ	dermoepidermal junction
DIC	differential interference contrast
DN	gene encoding for decorin
DNA	deoxyribonucleic acid
dNTP	deoxyribose nucleoside triphosphate
ECM	extracellular matrix
EDTA	ethylenediaminetetraacetic acid
EGF	epidermal growth factor
FBC	foreign body capsule
FBGC	foreign body giant cell
FBR	foreign body reaction
FDA	Food and Drug Administration
G	guanine
G-CSF	granulocyte-colony stimulating factor
Gly	glycine

GM-CSF	granulocyte macrophage colony-stimulating factor
H&E	haematoxylin and eosin
HA	hyaluronic acid
HAS	hyaluronic acid synthase
His	histidine
HIV	human immunodeficiency virus
HYAL	hyaluronidase
IFN-γ	interferon γ
IgG	immunoglobulin G
IL	interleukin
LM	carrier material
LPS	lipopolysaccharide
Mac-1	macrophage-1 antigen
MCP-1	monocytic chemotactic protein 1
MHz	megahertz
MMP	matrix metalloproteinase
mRNA	messenger ribonucleic acid
NaAC	sodium acetate
NCBI	National Center for Biotechnology Information
NER	nucleotide excision repair
NHEJ	non-homologous end-joining
PBS(T)	phosphate buffered saline (Triton X-100)
PCR	polymerase chain reaction
PDGF	platelet-derived growth factor
Phe	phenylalanine
PLLA	poly-L-lactic acid
PMN	polymorphonuclear cells
RNA	ribonucleic acid
ROS	reactive oxygen species
RPLP0	ribosomal protein large P0
rpm	rounds per minute
SD	standard deviation
siRNA	small interfering ribonucleic acid
T	thymine
TAE	Tris acetate EDTA
TGFß	transforming growth factor ß
TIMP	tissue inhibitor of matrix metalloproteinase
TNFα	tumor necrosis factor α
TRIS	tri(hydroxymethyl)aminomethane
Trp	tryptophan
Tyr	tyrosine
U	units

UV	ultraviolet
V	volt
VEGF	vascular endothelial growth factor
αSMA	alpha smooth muscle actin

7.2 DNA sequence alignment

```
Homology Block:  Percent Matches 98   Score 252   Length 259
                 Mol 1  742 to 1000,  Mol 2  4 to 261

TGFß1          742 gccaccattcatggcatgaaccggcctttcctgcttctcatggccaccccgctggagagg
Seq1             4 gcca-catt-atggcatgaaccggcctttcctgcttctcatggccaccccgctggagagg

TGFß1          802 gcccagcatctgcaaagctcccggcaccgccgagccctggacaccaactattgcttcagc
Seq1            62 gcccagcatctgcaaagctcccggcaccgccgagccctggacaccaactattgcttcagc

TGFß1          862 tccacggagaagaactgctgcgtgcggcagctgtacattgacttccgcaaggacctcggc
Seq1           122 tccacggagaagaactgctgcgtgcggcagctgtacattgacttccgcaaggacctcggc

TGFß1          922 tggaagtggatccacgagcccaagggctaccatgccaacttctgcctcgggccctgcccc
Seq1           182 tggaagtggatccacgagcccaagggctaccatgccaacttctgcctcgggccctgcccc

TGFß1          982 tacatttg-gagcctggaca
Seq1           242 tacatttgaaagcctggaca
```

Figure 7.1 Alignment of TGFß1 sequence and sequence (Seq1) of the PCR product synthesised in the TGFß1 approach (cf. 4.33). Green highligted bases are identical.

```
Homology Block:  Percent Matches 98   Score 229   Length 238
                 Mol 1  3904 to 4141,  Mol 2  7 to 244

Col1A1        3904 cccactcagcccagtgtggcccagaagaactggtacatcagcaagaaccccaaggacaag
Seq2             7 cccacttcg-ccagtgtggcccagaagaactggtacatcagcaagaaccccaaggacaag

Col1A1        3964 aggcatgtctggttcggcgagagcatgaccgatggattccagttcgagtatggcggccag
Seq2            66 aggcatgtctggttcggcgagagcatgaccgatggattccagttcgagtatggcggccag

Col1A1        4024 ggctccgaccctgccgatgtggccatccagctgaccttcctgcgcctgatgtccaccgag
Seq2           126 ggctccgaccctgccgatgtggccatccagctgaccttcctgcgcctgatgtccaccgag

Col1A1        4084 gcctcccagaacatcacctaccactgcaagaacagcgtggcctacatgg-accagcaga
Seq2           186 gcctcccagaacatcacctaccactgcaagaacagcgtggcctacatggaaccagcaga
```

Figure 7.2 Alignment of Col1A1 sequence and sequence (Seq2) of the PCR product synthesised in the Col1A1 approach (cf. 4.33). Green highligted bases are identical.

7.3 Melting curves

Exemplary melting curves of real-time PCR using cDNA of volunteer 10 biopsy 2.

αSMA

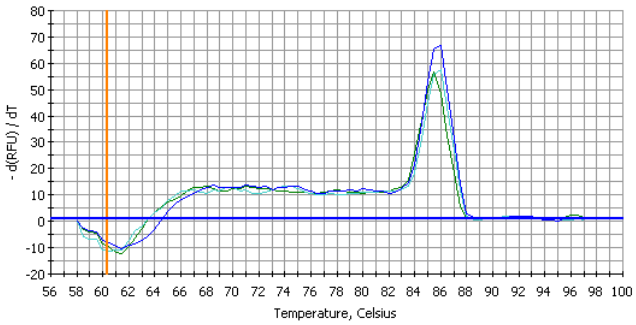

Col1

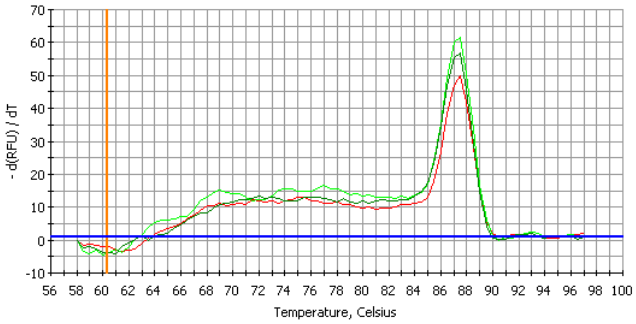

CTGF

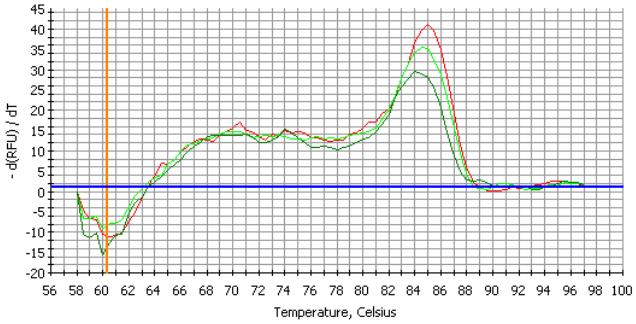

PDGFB

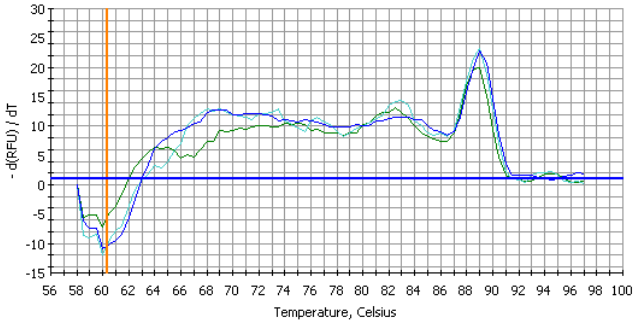

RPLP0

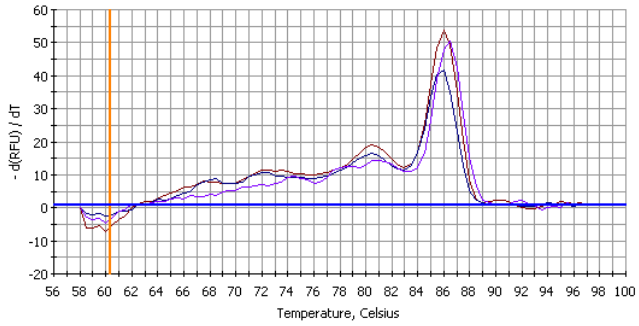

TGFß1

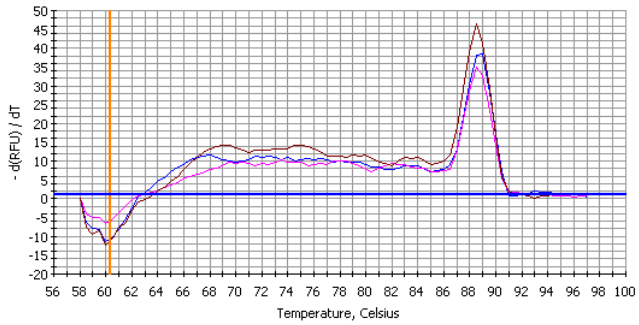

TIMP1

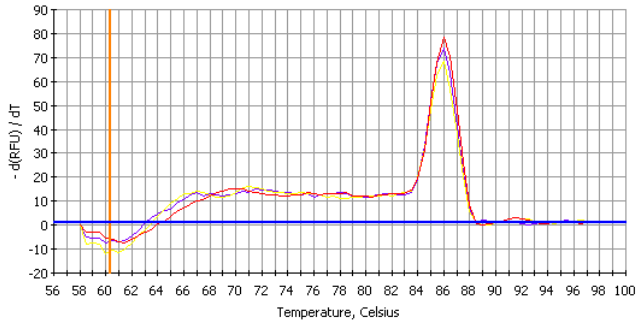

Col3

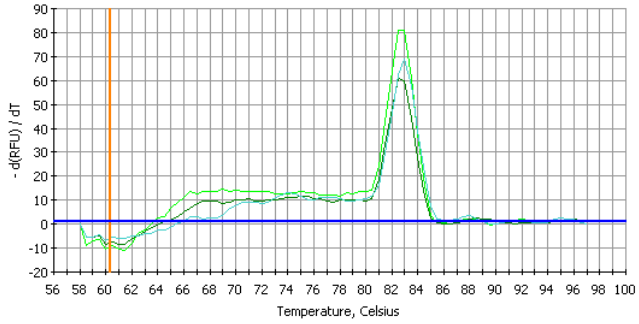

No template control

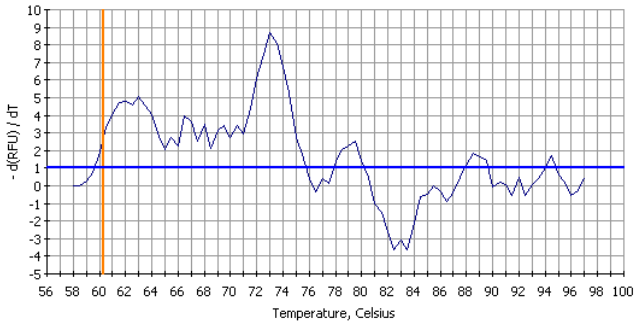

7.4 Informed consent

Probandin:..... Geburtsdatum:.....

(Name, Vorname)

Probanden-Initialen: ..... Probanden-Nummer:.....

„Oberarmaugmentation mit Poly-L-Milchsäure: Klinische, histologische und molekularbiologische Untersuchungen“

Schriftliche Einwilligungserklärung zur Teilnahme an der Studie

Alle Fragen zu dieser vorgesehenen klinischen Studie wurden von Frau Prof. Dr. med. Schürer zu meiner Zufriedenheit beantwortet.

Ich bin über Wesen, Bedeutung und Tragweite dieser klinischen Prüfung aufgeklärt worden, habe die Probandenaufklärung gelesen und verstanden, und hatte genügend Zeit für meine Entscheidung. Ich weiß, dass meine Teilnahme freiwillig erfolgt. Ich kann jederzeit ohne Angabe von Gründen meine Einwilligungserklärung zurückziehen.

Über die Einhaltung der Bestimmungen des Datenschutzes wurde ich aufgeklärt, und ich bin mit der Weitergabe der im Rahmen der klinischen Prüfung erfolgenden Aufzeichnung von Krankheitsdaten und ihrer Weitergabe zur Überprüfung an den Auftraggeber einverstanden.

Eine Kopie der Probandeninformation und dieser Einwilligungserklärung ist mir ausgehändigt worden.

Hiermit willige ich in die Teilnahme an der o.g. Studie ein.
(Datum und Unterschrift sind vom Probanden selbst handschriftlich einzutragen.)

Osnabrück, den _____ _____
Unterschrift des Probanden

Osnabrück, den _____ _____
Unterschrift der aufklärenden Ärztin

7.5 Quality of Life questionnaire

(FLQA-k*) Fragebogen zur Lebensqualität, Haut und Kosmetik

Dieser Fragebogen dient der Beschreibung Ihres Befindens und Ihrer Einstellungen zu Ihrer Haut und dem Äußeren allgemein.

Bitte beantworten Sie die Fragen sorgfältig, aber spontan. Alle Angaben werden streng vertraulich behandelt und anonym ausgewertet.

	Bitte kreuzen Sie in jeder Zeile an, welche Aussage **aktuell** auf Sie zutrifft:	trifft zu: **gar nicht**	**etwas**	**mäßig**	**ziemlich**	**sehr**
1	Ich nehme mir Zeit für Körperpflege.	O	O	O	O	O
2	Ich widme meinem Äußeren viel Aufmerksamkeit.	O	O	O	O	O
3	Ich neige dazu, meinen Körper zu verbergen.	O	O	O	O	O
4	Die äußere Erscheinung sagt viel über einen Menschen aus.	O	O	O	O	O
5	Ich vermeide es, die Blicke anderer auf mein Äußeres zu ziehen.	O	O	O	O	O
6	Ich schaue häufig in den Spiegel.	O	O	O	O	O
7	Ich reagiere stark auf die körperliche Ausstrahlung von anderen.	O	O	O	O	O
8	Ich wünsche mir einen anderen Körper.	O	O	O	O	O
9	Ich betrachte mich gern.	O	O	O	O	O
10	Ich bin mit meinem Aussehen zufrieden.	O	O	O	O	O
11	Ich lasse mich gern berühren.	O	O	O	O	O
12	Es verunsichert mich, wenn irgend etwas an meinem Äußeren nicht so ist, wie es sein sollte.	O	O	O	O	O
13	Mein Aussehen macht mir Kummer.	O	O	O	O	O
14	Ich bin wegen meiner äußeren Erscheinung weniger attraktiv als die meisten anderen Menschen.	O	O	O	O	O
15	Es gibt Situationen, die ich wegen meines Aussehens vermeide.	O	O	O	O	O
16	Ich achte auf die Haut anderer Menschen.	O	O	O	O	O
17	Ich könnte meine Haut noch sorgfältiger als bisher pflegen.	O	O	O	O	O
18	Ich vermeide Sauna oder Schwimmbad, weil andere Leute mich anstarren könnten.	O	O	O	O	O
19	Ich habe das Gefühl, die Leute starren auf meine äußere Erscheinung.	O	O	O	O	O
20	Mein Äußeres schränkt mich generell in meinem Leben ein.	O	O	O	O	O

Bitte kreuzen Sie in jeder Zeile an, welche Aussage trifft zu:

aktuell auf Sie zutrifft:

		gar nicht	**etwas**	**mäßig**	**ziemlich**	**sehr**
21	Wenn ich in den Spiegel schaue, betrachte ich vor allem meine Haut.	O	O	O	O	O
22	Ich mache mir Gedanken darüber, was andere Menschen über mein Äußeres denken.	O	O	O	O	O
23	Ich bin mit meinen Geschlechtsmerkmalen zufrieden.	O	O	O	O	O
24	Ein gutes Aussehen ist mir wichtig.	O	O	O	O	O
25	Für mein Äußeres gebe ich viel Geld aus.	O	O	O	O	O
26	Der Zustand meiner Haut ist mir unangenehm.	O	O	O	O	O
27	Ich fühle mich äußerlich nicht mehr attraktiv.	O	O	O	O	O
28	Ich möchte gerne mehr für meine Schönheit tun.	O	O	O	O	O
29	Am liebsten hätte ich eine andere Haut.	O	O	O	O	O
30	Ich habe keine Hoffnung, mein Äußeres wieder zu mögen.	O	O	O	O	O
31	Die Vorstellung, andere sehen mich nackt, bereitet mir Unbehagen.	O	O	O	O	O
32	Mein Aussehen beeinträchtigt manchmal meine Freizeitaktivitäten.	O	O	O	O	O
33	Durch meine Haut fühle ich mich eher alt.	O	O	O	O	O
34	Ich beneide andere um ihr gutes Aussehen.	O	O	O	O	O
35	Ich fühle mich äußerlich attraktiv.	O	O	O	O	O
36	Mich schön zu machen, bereitet mir Spaß.	O	O	O	O	O
37	Manchmal vermeide ich wegen meines Aussehens Treffen mit anderen.	O	O	O	O	O
38	Ich versuche mich so zu kleiden, daß mein Äußeres möglichst wenig auffällt.	O	O	O	O	O
39	Es fällt mir schwer, zu meinem Aussehen zu stehen.	O	O	O	O	O
40	Mein Äußeres hindert mich daran, von mir aus Kontakt mit anderen aufzunehmen.	O	O	O	O	O
41	Ich befürchte, daß ich mit zunehmendem Alter immer unattraktiver werde.	O	O	O	O	O
42	Ich fühle mich in meiner Haut wohl.	O	O	O	O	O
43	Ein schönes Aussehen gibt mir ein sicheres Gefühl.	O	O	O	O	O
44	Heutzutage zählt nur das Äußere.	O	O	O	O	O

7.6 Erklärung über die Eigenständigkeit der erbrachten wissenschaftlichen Leistung

Ich erkläre hiermit, dass ich die vorliegende Arbeit ohne unzulässige Hilfe Dritter und ohne Benutzung anderer als der angegebenen Hilfsmittel angefertigt habe. Die aus anderen Quellen direkt oder indirekt übernommenen Daten und Konzepte sind unter der Angabe der Quelle gekennzeichnet.

Bei der Auswahl und Auswertung folgenden Materials haben mir die nachstehend aufgeführten Personen in der jeweils beschriebenen Weise entgeltlich/ unentgeltlich geholfen.

1. Das histopathologische Labor von Prof. Kind (Offenbach) fertigte Gewebeschnitte und H&E Färbungen an, die für diese Arbeit verwandt wurden.

Weitere Personen waren an der inhaltlichen materiellen Erstellung der vorliegenden Arbeit nicht beteiligt. Insbesondere habe ich hierfür nicht die entgeltliche Hilfe von Vermittlungs- bzw. Beratungsdiensten (Promotionsberater oder andere Personen) in Anspruch genommen. Niemand hat von mir unmittelbar oder mittelbar geldwerte Leistungen für Arbeiten erhalten, die im Zusammenhang mit dem Inhalt der vorgelegten Dissertation stehen.

Die Arbeit wurde bisher weder im In- noch im Ausland in gleicher oder ähnlicher Form einer anderen Prüfungsbehörde vorgelegt.

…….. ……..

(Ort, Datum) (Unterschrift)

8. Acknowledgement

Bedanken möchte ich mich bei allen, die mich während meiner Promotionszeit unterstützt haben.

An erster Stelle bedanke ich mich bei Frau apl. Prof. Dr. Nanna Y. Schürer für die Möglichkeit meiner Promotion mit einem interdisziplinären Thema, dass verschiedene naturwissenschaftliche und medizinische Aspekte in sich vereint.

Für die Übernahme des Zweitgutachtens und für die Nutzung seines Labors danke ich besonders ausdrücklich Herrn Prof. Dr. Helmut Wieczorek.

Darüber hinaus danke ich Frau Dr. Olga Vitavska für die Betreuung des biologischen Teils meiner Arbeit.

Den Mitarbeitern der Arbeitsgruppe Tierphysiologie, Dr. Felix Tiburcy, Katharina Tabke, Dr. Christin Osteresch, Dr. Svenja Bockelmann, Rabea Bartölke, Dr. Gunnar Bröhan, Marco Kelkenberg, Daniela Heine, Simon Gohlke, Prof. Dr. Hans Merzendorfer, Dr. Thomas Krüppel, Dr. Markus Huss, Harald Mikoleit, Martin Dransmann, Sabine Heuer, Margret Düvel, Gundula Key danke ich für die nette Aufnahme und eine schöne Zeit.

Dr. Ralph Klose möchte ich für den wissenschaftlichen Rat, Markus Staufenbiel für die Einweisung am LSM bedanken.

Dr. Jürgen Blaak, Dr. Olaf Kaup, Olga Kukshausen, sowie den Mitarbeiterinnen der Arbeitsgruppe der medizinischen Mikrobiologie möchte ich für die nette Zusammenarbeit bedanken.

Mein Dank gilt auch den Probandinnen, ohne deren freiwillige Teilnahme die Grundlage für diese Arbeit gefehlt hätte.

Außerdem möchte ich allen Freunden außerhalb der Universität für das Leben abseits der Arbeit danken.

Ebenso möchte ich mich von ganzem Herzen bei meiner Familie bedanken, die mir das Studium ermöglicht hat.